20.10.2016

Dear Dr. Stenke,

we are submitting the revised version of the manuscript „Solar Forcing for CMIP6“ together with a detailed point-by-point response to the reviewer comments and a version of the manuscript with tracked changes.

We list here the most important changes to figures and text which might be not obvious.

1. Figure 1: a comment was added that the CMIP5 recommended TSI forcing which stopped at 2010 was extended with the NRLSSI1 dataset until 2015.
2. Figure 3: was restricted to the satellite era and a few other SSI observations have been added.
3. Figure 4 is now based on 81-day averages.
4. Figure 5: new figure which shows the EUV part of our dataset, all other figures are therefore shifted by one number
5. Figure 26 presents the updated variable pi control experiment.
6. The text with respect to the updated variable pi control experiment has been adapted.
7. A new Appendix (A) to describe the reconstruction of the SSI in the EUV, all other appendices are moved therefore.

We hope that this version of the manuscript satisfies the reviewers and think that the manuscript improved significantly.

All changes have been made in accordance with the other co-authors.

Many thanks and we hope that the manuscript is acceptable for you now.

Katja Matthes and Bernd Funke

Review by M. Snow

This manuscript gives a very understandable overview of how the recommended solar forcing is determined. The topic is very technical, but the authors have done a great job in making the content accessible to a wide range of scientists. My comments are primarily on the radiative sections, and all of them are minor.

Dear Marty,

thank you very much for your suggestions and comments. We specify in our point-by-point response below how we plan to include them into the revised version of the paper.

Katja and Bernd on behalf of all authors

P3 L29: The text mentions uncertainties in the irradiance measurements, and there is no question that these uncertainties can be sometimes larger than solar variability at some wavelengths. There is a brief discussion that uncertainties in models are sometimes difficult to assess. Measurements only go back a few solar cycles, and both irradiance models are based on interpretation of those measurements. Extrapolating these proxy models to the past and future requires several assumptions about proxy relationships remaining invariant. For example, the numerical relationship between sunspot number (or area) and the sunspot blocking function in NRLSSI2 could change if the sunspot contrast evolves over time. So it is not automatically true that we understand proxy relationships well enough over long timescales. Model development will continue to improve as we continue to make better measurements. State of the art model reconstructions as described in this manuscript are the best we currently have, but their uncertainties are also still significant.

Reply: We fully agree that all models (whether empirical or semi-empirical) most likely underestimate the SSI when moving away from the space age. You are right in pointing that out, and this will be emphasized more strongly in the text.

P9 L14: Averaging two quantities that disagree produces a result that is also not likely to be correct. Calling this "the most reasonable approach" is perhaps controversial. Maybe calling it "a reasonable approach" would be more appropriate.

Reply: This approach has indeed been met by some skepticism. We have here two models that have been derived almost independently, and as of today there are no objective criteria allowing us to prefer one to the other. In that context, from a statistical point of view, there is one clear and sound solution: just average the two. This solution is also what is advocated by the IPCC when combining GCM model predictions, see for example [D. Smith el al., Real-time multi-model climate predictions, Climate Dynamics 41 (2013), http://adsabs.harvard.edu/abs/2013ClDy...41.2875S]. We shall update our text to insist more heavily on this sound justification for averaging the two SSI models. We will also follow the reviewers suggestion and call our approach “a reasonable” one.

P9 L30: The comment that F10.7 was a good proxy for EUV at one time, but "this may not be true anymore" reinforces my discussion about page 3 above. It is an assumption that proxy relationships do not change over time, and this assumption must factor into the estimation of model uncertainties.

Reply: You are correct, and this is something that we should clarify in the text. We are working on it in SOLID, but as you may imagine, it is difficult too to provide realistic confidence intervals for such long-term variations.

Overall, I think this manuscript does an excellent job in describing the recommended solar forcing for the climate community.

Reply: Thank you!

Anonymous Referee #2

This is an important paper as it is meant to be a standard reference for the climate models taking part in the CMIP6 exercise. It is rather comprehensive, covering many topics. Some parts are well written, easy to understand and, as far as I can see, are internally consistent. However, other parts are inconsistent or unclear. Below I list the points where the paper could be improved. Many of these are minor issues such as typos etc. that should be easy to take care of, but there are a few points that are more fundamental and which the authors must deal with carefully. They might require bigger changes to the manuscript.

Dear reviewer,

thank you very much for your thorough and detailed review which clearly helps to improve the clarity of the manuscript. Please find below our detailed point-by-point response to your concerns which we all hope to address satisfactorily.

Katja Matthes and Bernd Funke on behalf of all coauthors

1) page 1, line 10 (abstract): "The TSI and SSI time series are defined as averages of two (semi-) empirical solar irradiance models, namely the NRLTSI2/NRLSSI2 and SATIRE-TS." Two comments: a) NRLTSI2/NRLSSI2 are empirical, not semi-empirical models. This is correctly explained later in the text of the manuscript but the statement in the abstract is misleading. b) More importantly, could the authors describe why they have taken recourse to this unusual step of averaging two independent models? Both models are constructed differently, and both have to some extent been tested against data. What the authors do is to provide a new model that is largely untested with regard to solar data. More comments on this aspect will be made later.

Reply:

a) We shall clarify the text accordingly.
b) You are not the first one to object against this averaging (see e.g. also the first reviewers comment), which, however, is actually statistically rooted and well-justified. As of today, there is no community consensus (established by independent means) on which of the two SSI models provides a more accurate description of the SSI. For that reason we have no objective means for preferring one model to the other, or for assigning different weights to them. Meanwhile, these two models have - as you say - been constructed independently, and this precisely what gives us a strong statistical justification for just taking their average. This solution is also what is advocated by the IPCC when combining GCM model predictions, see for example [D. Smith el al., Real-time multi-model climate predictions, Climate Dynamics 41 (2013), http://adsabs.harvard.edu/abs/2013ClDy...41.2875S]. We shall update our text to insist more heavily on this sound justification for averaging the two SSI models. We will also follow the reviewers suggestion and call our approach "a reasonable" one.

2) page 2, lines 1-2: "The slight negative trend in TSI during the last three solar cycles in CMIP6 is statistically indistinguishable from available observations". What do the authors mean by this? Different TSI composites indicate different trends. There are implicit assumptions underlying this statement that need to be spelt out and the reasoning clarified.

Reply: This result is indeed quite recent, and is detailed in an article that is about to be submitted. In this article, we demonstrate that the latest TSI composite, when made with realistic confidence intervals, makes it very difficult, if not impossible to conclude about the existence of a downward trend. We shall cite this reference in the revised manuscript.

3) page 2, line 5: CMIP6 cannot be tested against CMIP 5. It can only be compared to CMIP5.

Reply: You are correct, we shall clarify the text.

4) page 2, line 6: The expression "background SSI" is neither clear nor used in the literature.

Reply: You are correct, we shall clarify the text.

5) page3, line 5: "Because of its prominent 11-year cycle, solar variability may offer a degree of predictability for regional climate and could therefore help reduce uncertainties in decadal climate predictions." However, the solar cycle itself is notoriously hard to predict and predictions of upcoming solar minima have not been particularly successful, so that the statement does seem too optimistic. But possibly the authors are not concerned with such niceties here?

Reply: Indeed, as you pointed out, we are dealing here with decadal time scales, ignoring the more subtle dynamics of sub-solar-cycle variations, which can be appropriately considered as a modulation of approximately 11-years.

6) page 3, lines 23-24: "The quantitative assessment of radiative solar forcing has been systematically hampered so far by the large uncertainties and the instrumental artifacts that plague TSI and SSI observations" The TSI observations are signiïňˇA¸cantly more precise than those of SSI (especially SSI in the near UV and visible spectral domains). This makes the quoted sentence misleading.

Reply: We shall clarify the text to distinguish the relatively better shape of the TSI.

7) page 3, line 28: The IAU resolution (Mamajek et al. 2015) adopted the result of Kopp & Lean (2011). The latter is a well-known and well-cited paper in a refereed journal, while the former is not a scientific paper at all, is not properly published, and the text in the reference is not really useful. Please replace the reference to IAU resolution with the Kopp & Lean paper everywhere in the text.

Reply: A new and peer-reviewed publication (Prsa et al. (2016), http://adsabs.harvard.edu/abs/2016AJ....152...41P) now replaces the one by Mamajek et al.

(2015). In contrast to the article by Kopp and Lean (2011), which focuses on the scientific background, the two articles on the IAU resolution explain what is exactly meant by a nominal TSI and hence are important too.

8) page 3, line 29: The proxy reconstructions of the TSI do not exhibit "occasional phases of unusually low nor high activity", the Sun does. Also, Usoskin et al. 2014 did not mention TSI reconstructions at all.

Reply: We shall rewrite the sentence accordingly.

*9) page 3, line 32: "There is growing evidence for the Sun to enter a phase of low activity near 2050, after a grand maximum that peaked during the 20th century." The authors should explain what they base this claim on. The solar dynamo is chaotic, possibly even stochastic and it is even difficult to predict the next solar cycle much before the previous minimum. Going beyond the next cycle is even tougher. See e.g. * J. Jiang, R.H. Cameron, M. Schüssler, 2015: The cause of the weak solar cycle 24; ApJL 808 L28 * Cameron et al. 2013: Limits to solar cycle predictability: Cross- equatorial flux plumes, A&A 557, A141*

Reply: Several recent studies (excluding here the more speculative ones) have suggested that the Sun may be entering a phase of low activity, and this issue was recently addressed at ISSI by a VarSITI forum. This will be clarified in the text.

Regarding predictions of the solar cycle, we explicitly state that "As of today, even predicting the cycle amplitude one cycle ahead remains a major challenge (Pesnell, 2012).", so we don't seem to disagree, do we ?

Fortunately, since we focus on multi-decadal time scales only, this complexity of solar cycle prediction is beyond the scope of our study.

10) page 4, line 12: " . . . with respect to the CMIP5 solar forcing recommendation." Is the CMIP5 paper supplying the solar input cited? At least so far "CMIP5" is not associated with such a paper.

Reply: CMIP5 provides annually-resolved TSI since 1610, and monthly-resolved since 1882, see http://solarisheppa.geomar.de/cmip5. You are right, there is no paper associated with CMIP5 solar forcing recommendation, it is just described on the indicated website.

10a) page 4, line 20: "Lockwood et al., 2019" This is likely "Lockwood et al., 2010"; also to be corrected on page 74

Reply: Thank you for pointing this out.

11) page 6, line 15: " . . . and one observational estimate (SOLID), . . ." Is this correct? From the evidence given in the paper, SOLID is not an "observational estimate" but an empirical model (see below).

Reply: The SOLID composite, built by statistical means, and entirely based on SSI observations only, includes a few proxies to help fill the gaps. We call it an observational composite, and not en empirical model, because it is truly different from models such as NRLSSI2, which involve physical assumptions. As described below this will be better explained in the revised manuscript.

12) page 6, lines 26-27: The sentence simplifies things too much. Faculae are not "the Mg II index" and dark sunspots are not "sunspot area". These proxies are used to represent the contributions from faculae and sunspots to the irradiance. This should be written more carefully to reflect the actual relationships.

Reply: We shall rewrite the text as you suggest.

13) page 7, line 8: ". . ..SORCE SSI observations Lean and DeLand (2012) the wavelength dependent scaling coefficients ..." Change to: "....SORCE SSI observations (Lean and DeLand, 2012) the wavelength dependent scaling coefficients . . ."

Reply: Thank you for pointing this out.

14) page 7, lines 5-15: The description of the adjustments in the NRLSSI2 model is not clear. The authors should explain better how the adjustments are done.

Reply: As you propose, we will expand the NRLSSI2 model adjustments better in the revised manuscript.

15) page 7, line 19: What is SATIRE-TS? It does not become clear from reading the paper, as references are given only to SATIRE-T and SATIRE-S. TS is used multiple times, so that it cannot be a typo. Is TS some combination of the two models? What kind of combination?

Reply: The SATIRE model we use is indeed a blend of SATIRE-S and a SATIRE-T that has been run with the sunspot data we had specifically provided for CMIP6, and thus differs from the official SATIRE-T. We shall rephrase that in the text, and replace SATIRE-TS by SATIRE to avoid ambiguities.

16) page 7, line 28: The reconstruction made by Dasi-Espuig et al. (2014) is not based on to expectations.

Reply: We'll remove that citation.

17) page 8, line 3: "In NRLSSI2, this internal consistency also applies to the integral of the facular and sunspot contributions to SSI to their respective counterparts in TSI (see Coddington et al. (2015) for more details). Why are the authors stressing this point? This sounds rather trivial. Doesn't every model that distinguishes between spots and faculae do that? Or are they implying that SATIRE does not fulfil such internal consistency? They should either explain why this is such an achievement and is unique to NRLSSI, or they should remove this unnecessary sentence.

Reply: We'll remove lines 3 and 4.

18) page 9, lines 5-6: "The controversial out-of-phase behavior of SORCE/SIM observations in that band (Harder et al., 2009) are likely to be an instrumental artefact (Lean and DeLand, 2012; Ermolli et al., 2013) but this has not yet been corrected in the SOLID composite." If SORCE is wrong, is then the SOLID composite the best one to use to test the SSI models? If models are chosen by how close they are to SOLID, this could have unwanted effects for the atmospheric chemistry and finally climate modelling. As shown by Haigh et al. (2010, An influence of solar spectral variations on radiative forcing of climate, Nature, 467, 696), the SSI variability found by SORCE has a major effect on atmospheric ozone, changing its concentration in a way contrary to expectations.

Reply: You are right, the text in its current form is misleading. The SOLID team has decided to deliver a first version of the SOLID observational composite that is totally devoid of model assumptions, and does not rely on nudged data. This raw composite can then be tested against SSI models, and from there onwards we may decide if some of the original datasets should be corrected (or rather, if their confidence intervals should be increased to reflect our understanding of the data). The description of the SOLID database is now extended in the paper (see answer to comment 31) which will hopefully also clarify this point.

*19) page 8, line 14 "In NRLSSI2, the proxy index for sunspot darkening is the sunspot area as recorded by ground-based observatories in white light images since 1882 (Lean et al., 1998). Values prior to that are estimated from the sunspot number." Does not also the SATIRE model rely on sunspot areas over the period of time covered by Greenwich observatory? It seems to according to * Krivova et al. 2010: Reconstruction of solar spectral irradiance since the Maunder minimum; JGRA, DOI: 10.1029/2010JA015431 Please comment.*

Reply: The referee is right, SATIRE relies on sunspot areas and then sunspot number to expand the model in time. We shall modify the text accordingly.

20) Sect. SOLID composite After reading this section the exact nature of the SOLID composite is still very unclear. A single paper (Schöll et al., 2016) is cited, which explains only the preprocessing of the data. As long as SOLID is not properly documented, it is important to make the description here sufficiently clear so that readers who don't know the nitty gritty of the SOLID approach can follow and, if necessary make their own judgement. So far, this composite *(if it is really a composite at all and not an empirical model, see below) is not widely-known or established in the solar community.*

Reply: Please see our detailed answer to comment 31 below.

21) page 9, line14: "..., the most reasonable approach consists in averaging both reconstructions, weighted by their uncertainty. But this means that yet another model is produced, one that is untested, except for the rudimentary tests briefly discussed in the paper. It is not clear why this is "the most reasonable approach"

Reply: As already explained above, the averaging is well justified. As of today we do not see a better approach and call our approach "a reasonable" one. Obviously, the outcome can be considered as another model, or rather meta-model, but for obvious reasons it is premature to expect the outcome to be thoroughly tested against observations. Having said that, we do provide some comparisons in Fig. 3 during the satellite era. We rely on SATIRE and NRLSSI precisely because these have been tested extensively against observational data by their respective teams.

22) page 9, line 17: "... SATIRE-TS (Yeo et al., 2014)." What is SATIRE-TS? Is it a typo or a combination of SATIRE-T and SATIRE-S? Please define it. In Yeo et al. (2014) I could find a description of SATIRE-S, but no mention of SATIRE-TS, so that this reference seems not to be relevant (unless TS is a combination of T and S).

Reply: Please see answer to comment 15.

23) page 9, line 24: "The EUV band (10-121 nm) is required for CMIP6 but is ab- sent from NRLSSI and SATIRE. We added it with spectral bins from 10.5-114.5 nm by using a nonlinear regression from the SSI in the 115.5-188.5 nm band, trained with TIMED/SEE data from 2002 to 2009." Indeed, this is a difficult situation and the au- thors have done the reasonable thing and somehow modelled this wavelength region themselves. The procedure chosen may be fine and may produce a good result, but without being shown anything it is hard for the reader to judge. Please provide a figure and some more explanation.

Reply: We'll add a figure on the EUV band.

24) page 9, line 29: "Let us note that while the F10.7 index is a good proxy for EUV variability on daily to yearly time scales, this may not be true anymore on multi-decadal time scales." This is a good point.

Reply: Thank you!

25) page 10, line 3: ". . . observed composite from PMOD" This sounds strange since the composite was not observed. Rather it is based on a set of observations of TSI.

Reply: This should indeed be “observational composite”.

26) page 10, line 7: “All TSI records agree well on daily to yearly time scales, and in some cases (e.g. NRLTSI1 and NRLTSI2) they match as well on multi-decadal time scales.” Aren’t both models part of the same model family and are founded on the same proxies? I am not sure what is remarkable about them being consistent with each other? The authors can leave this – it is not an important point – but I would like to understand why they stress this agreement, which I would have naively thought to be trivial.

Reply: NRLTSI1 and NRLTSI2 are based on the same method and proxy, but were trained with different datasets: NRLTSI1 were trained with a previous version of the PMOD composite while NRLTSI2 was trained with SORCE/TIM observations. Even if not remarkable, it is worth mentioning it.

27) page 11, Figure 1: The orange curve described as CMIP5 goes till 2015. What exactly is plotted? Are these extrapolated CMIP5 data? Or are the plotted CMIP5 data regularly updated and are available up to 2015?

Reply: Plotted are the extended NRLTSI1 data that have been the basis for CMIP5 (from 1882 until 2010). We will adopt the plot and the figure caption to make this clear.

28) page 11, line 12: “The major difference come from SATIRE-TS ..” “The major difference comes from SATIRE-TS ..”

Reply: Has been corrected.

29) page 12, Figure 2, bottom left diagram Why is NRLSSI2 producing such strange cycles between ∼1940 and 1960? These certainly do not look realistic. How come, these strange cycle shapes are restricted mainly to the visible (although there may be some sign of similar behavior in the IR)? Should not also the UV cycles behave strangely in order to compensate for the behavior in the visible and produce a reasonable TSI? Has the TSI produced by NRLSSI2 been compared with measured time series? Also, something seems to be going wrong right at the start of the time series. How do the authors explain and compensate for these problems?

Reply: We have sought clarification from the NRL team. The rather modest solar cycle variation in the visible radiation in the new NRLSSI2 model is thought to be related to the scaling of the two sunspot area data bases, the Royal Greenwich Observatory (RGO) sunspot areas (before 1976) and the areas in the SOON (USAF) database, which have to be combined. This scaling affects the relative roles of sunspots and faculae before (and including) 1976. Apparently, there is quite bit of debate about how these two datasets relate - with scaling factors ranging from the RGO being 20% to 50% larger than SOON areas. NRLSSI2 uses a scaling factor of 0.67, in which the GW sunspot areas are assumed to be 1/0.67 = 1.5 times larger than SOON.

The problem at the beginning and end of the time series is caused by smoothing of the data taken between 1882 and 2010. We will update the plot and take the longer timeseries (available on an annual basis before 1882) in order to avoid this smoothing problem.

30) page 12, line 4: " ... and higher-quality data from the SORCE mission on the rotational timescale in NRLSSI2, . . ." But isn't SORCE giving wrong trends for SSI? This is what the authors claim multiply elsewhere in the paper.

Reply: Yes indeed, but rotational time scales (<81 days) used to train the NRLSSI2 model are not affected by long-term drifts of the SORCE instrument.

31) page 13, Figure 3: Fig. 3 is confusing and does not agree with the text of the paper, mainly regarding SOLID. Earlier it was said that SOLID is based entirely on observed data (page 8, line 20: "More specifically it is derived as the weighted mean of all available SSI observations in the satellite era.") If that were true, then the green curve should be a lot closer to the plotted observations. Thus, it is not clear why The SOLID composite departs so strongly from SORCE at a time when that is the only data set used (according to the authors)? Or are other data sets also used after all? The SSI variations shown by SOLID seem to be smaller than of all the instrumental records, except maybe UARS SOLSTICE (it is hard to see - there are too many light colors in this plot). Anyway, SOLSTICE shows a behavior completely inconsistent with an SSI composite of the observations. This is a serious problem that points to a fundamental inconsistency in the paper. Another strange feature of this plot is that SOLID covers also the 1950s and 1960s when there were no SSI data available. How does SOLID produce something at those times if it is purely based on SSI data? The description given in the paper is totally inadequate and obviously seriously misleading. However, Fig. 3 very strongly suggests that the SOLID "composite" uses either a proxy (possibly something like 10.7 cm flux?) or makes really strong changes to the data while processing them. In either case, I would strongly oppose calling it a composite of SSI observations. Rather Fig. 3 clearly shows that it is an empirical model. If the authors want to maintain that SOLID is a composite of observed SSI, then they should provide a detailed explanation that goes far beyond the inadequate one in the current version of the paper. This should include a list of all data sets that enter into the SOLID "com- posite" and all the steps that are undertaken to produce it. Also, they should provide a convincing explanation why SOLID differs so strongly from the observational data. Fig. 3 raises an issue regarding fairness and bias in the paper. If SOLID is indeed an empirical model, and I have seen no evidence to counter this in the paper, I see no advantage in using SOLID to "test" the other two models. Indeed, if SOLID is a model (and an unpublished one at that), why is it being discussed ahead of the nu- merous other (published!) models in the literature. I see only two paths that that the authors can follow: a) Either remove SOLID completely from the publication and in- stead compare the averaged model that the authors have produced more rigorously with the observations directly, b) or discuss SOLID on an equal footing with the other SSI models that the authors simply ignore in this version of the paper. Irrespective of which of these paths the authors follow, I strongly urge them to use the original SSI ob- servations to test the new model data set obtained by averaging NRLSSI2 and SATIRE (-TS?).

Reply: Let us answer stepwise:

i) Earlier it was said that SOLID is based entirely on observed data (page 8, line 20: "More specifically it is derived as the weighted mean of all available SSI observations in the satellite era.") If that were true, then the green curve should be a lot closer to the plotted observations.

The previous version of Fig. 3 did not include all observational datasets going into SOLID. Figure 3, right panel, has been revised and now also includes the scaled SORCE/SOLSTICE observations which were not shown in the previous plot as the dataset does not cover the full spectral range from 200-400nm. In addition a table with all observational estimates used in the SOLID composite has been added to the SOLID description. Also, Fig. 3 has been restricted now to the satellite era and starts only in 1980.

ii) Thus, it is not clear why The SOLID composite departs so strongly from SORCE at a time when that is the only data set used (according to the authors)?

For the spectral range (200 - 400nm) shown in Fig. 3 apart from SORCE/SIM many other observations are available, such as NIMBUS, NOAA9, NOAA11, UARS/SOLSTICE, UARS/SUSIM. Moreover, SORCE/SOLSTICE also enters the SOLID composite for the spectral range 200-320nm. SORCE/SOLSTICE has a relatively low uncertainty (compared to the other instruments) and as such a relatively high weight in the composite. Therefore, it is plausible that the integrated SSI from 200-400nm deviates from the SORCE/SIM dataset. Note, SORCE/SOLSTICE was not shown in Fig 3 as it does not cover the full spectral range of the figure. It has now been added so that the influence of the various datasets is visible. Some text to explain this will be added to the paper.

iii) Another strange feature of this plot is that SOLID covers also the 1950s and 1960s when there were no SSI data available. How does SOLID produce something at those times if it is purely based on SSI data? The description given in the paper is totally inadequate and obviously seriously misleading. However, Fig. 3 very strongly suggests that the SOLID "composite" uses either a proxy (possibly something like 10.7 cm flux?) or makes really strong changes to the data while processing them.

We thank the reviewer for pointing this out. One technicality to derive the SOLID composite is that in order to apply the same scale-wise decomposition, all datasets have to cover the full time interval under consideration. This means for some dataset gaps have to be filled or the datasets have to be extended in time. To achieve this we use (observed) proxy data and the "maximization expectation" technique which makes use of the original signal in the data. This technique also allows us to cover the times before observations are available, e.g. 1959-1960. We agree with the reviewer that more details need to be given in the paper and will add those. However to avoid confusion, we will restrict the figure to the satellite era as already explained above.

iv) In either case, I would strongly oppose calling it a composite of SSI observations. Rather Fig. 3 clearly shows that it is an empirical model. If the authors want to maintain that SOLID is a composite of observed SSI, then they should provide a detailed explanation that goes far beyond the inadequate one in the current version of the paper. This should include a list of all data sets that enter into the SOLID "composite" and all the steps that are undertaken to produce it. Also, they should provide a convincing explanation why SOLID differs so strongly from the observational data.

The SOLID composite is produced using a statistical framework in a maximum-likelihood sense and no physical assumptions go into it. More details will be given in the revised SOLID section including information on the individual data sources used in the composite as well as their statistical combination.

v) Fig. 3 raises an issue regarding fairness and bias in the paper. If SOLID is indeed an empirical model, and I have seen no evidence to counter this in the paper, I see no advantage in using SOLID to "test" the other two models. Indeed, if SOLID is a model (and an unpublished one at that), why is it being discussed ahead of the numerous other (published!) models in the literature.

As already stated above, in our view the SOLID composite is not an empirical model as no physical assumptions go into it. We use the composite as an independent source of (observed) information, and as such it is a very valid dataset to which the recommended CMIP6 dataset is compared to.

vi) I see only two paths that that the authors can follow: Either remove SOLID completely from the publication and instead compare the averaged model that the authors have produced more rigorously with the observations directly, b) or discuss SOLID on an equal footing with the other SSI models that the authors simply ignore in this version of the paper.

To follow option b) more details will be given in the SOLID section including information on the individual data sources used in the composite as well as their statistical combination.

vi) Irrespective of which of these paths the authors follow, I strongly urge them to use the original SSI observations to test the new model data set obtained by averaging NRLSSI2 and SATIRE (-TS?).

In Fig. 3 we do compare the CMIP6 recommended SSI model data with the SSI observations, along with the SOLID composite.

32) page 13, Figure 4 and its discussion in the text: Averaging over one month at activity maximum and minimum does not allow eliminating the rotational cycle in solar variability, so that this ïn˘A ̧gure mixes information on shorter timescales into the solar cycle variability that the authors want to show. The figure should be redone using at least 81-day averaging. Why are *the comparisons in Figures 3 and 4 being done in such broad, seemingly arbitrary wavelength bands, rather than broken up according to the important molecular band listed in Table 1? What is the advantage for the climate community of following the bands used by Ermolli et al. (2013). Also, where would the observations lie in Fig. 4 (to the extent available for exactly these times, which is a limitation of the figure)?*

Reply: The referee is correct and Fig.4 now uses a 81-day averaging. This does not change the differences between the reconstruction but the numbers have changed slightly (less cycle variability in general) and we will update the related discussion in the revised manuscript. We think that it is important for the climate community to use the same bins than in Ermolli et al. (2013).

33) page 13, lines 1-2: " . . . the only available measurements are from the SORCE/SIM instrument, which has calibration issues (Lean and DeLand, 2012) . . ." Until now no calibration issues in SORCE/SIM instrument have been reported by the instrumental team. In particular, the paper by Lean & DeLand does not identify any calibration issue.

Reply: You are correct, Lean and Deland do not explicitly evoke calibration issues. These are unofficial. We shall clarify this.

34) page 14, line 5: "In the NIR CMIP6 shows slightly larger variability than CMIP5 and remarkable here is the largest variability in NRLSSI2." Why is this remarkable? Both SATIRE & NRLSSI2 reproduce TSI. NRLSSI2 has a smaller variability in the UV and this must be compensated by NRLSSI2 in the IR. Or is there something more complex at work here that I am missing? Please explain or simplify the text.

Reply: We shall reformulate the text and simply remove the part "...and remarkable here is the largest variability in NRLSSI2".

35) page 17, line 1: "Solar activity and hence spectral irradiance vary between different solar cycles. However, these differences are small compared to the total 11 year solar cycle amplitude . . ." This has been the case in the second half of the 20th century, but the sizes of cycles vary between zero and the very high amplitude of cycle 19. This is only a minor quibble, however.

Reply: You are correct. We shall clarify this.

36) page 19, line 18: "... produces slightly higher SW heating rates than NRLSSI1(CMIP5)" "... produces slightly higher SW heating rate differences than NRLSSI1(CMIP5)"; the diagram shows the differences between heating rates for solar minimum and solar maximum.

Reply: Yes, thank you, we will change the sentence accordingly.

37) page 20, Figure 5: "Impact of solar forcing according . . ." add: for perpetual solar minimum conditions

Reply: We shall add this.

38) page 21, Figure 6: "CMIP6 SSI differences in % for perpetual solar minimum conditions . . ." It may not be immediately clear what differences are actually meant here, i.e. differences in which parameter; add e.g.: "CMIP6 SSI differences of the solar irradiance in % . . ."

Reply: We shall add this.

39) page 21, line 1: "More important for the solar ozone signals seems to be the choice of the CCM (with its specific photolysis scheme, see also Fig. 8), especially for the lower stratosphere (10 hPa and below)." This is true for the lower stratosphere only; above that the dataset-induced differences are larger than the model-induced ones, in particular in the lower Mesosphere.

Reply: Yes, we agree. We will therefore add: "In the lower mesosphere however, the dataset-induced differences are larger than the model-induced ones."

40) page 21, line 12: "Note that statistically significant irradiance differences between CMIP5 and CMIP6-SSI irradiances are particularly observed between 300 and 350nm . . . (Fig. 8)." In Figure 8 differences in the irradiance amplitude between solar minimum and solar maximum are shown. i.e. "irradiance differences" should be replaced by "differences in the irradiance amplitude".

Reply: Will be changed to "difference in irradiance amplitude".

41) page 25, line 19: ". . .for mesospheric OH production Fytterer et al. (2015b), and for . . . ". . . for mesospheric OH production (Fytterer et al., 2015b), and for . . ."

Reply: Thank you for spotting this typo.

42) page 27, Figure 11: SSN scaled by a factor of 0.67 should have larger values (in Figure 13 SSN scaled by a factor of 0.741 has values above 200); a factor of 0.067 appears to be much more reasonable.

Reply: The factor is indeed 0.067. Thank you for spotting this.

43) page 33, Figure 16: There are differences between the caption and the labels in the diagram. caption: 70–90oS (left) and 70–90oN (right); in the diagram: 70–90oS (right); 70–90oN (left) caption: 0.01 hPa (upper panel) and 0.1 hPa (lower panel); in the diagram: 0.1 hPa (upper panel) and 1 hPa (lower panel)

Reply: The caption is wrong: NH is shown on the left and SH on the right. The pressure levels are 0.1 hPa (top) and 1 hPa (bottom).

44) page 36, line 13: "Since fast transient solar energetic particle events often occur at the background of enhanced geomagnetic disturbances, straight-forward computation of the particle trajectories in a realistic geomagnetic field is needed" Why are fast transient solar energetic particle events relevant in this context? This paragraph deals with the penetration of GCRs in the Earth's atmosphere.

Reply: Since the reviewer thinks this is confusing, we can modify this sentence as follows: the text "Since fast transient ... are fully rejected (Cooke et al., 1991)." can be substituted by "This shielding is usually parameterized in the form of the effective geomagnetic rigidity cutoff, so that only particles with rigidity/energy exceeding the cutoff can penetrate to the atmosphere at a given location while less energetic particles are fully rejected (Cooke et al., 1991)."

45) page 38, line 25: The CMIP6 future solar forcing is different from that of CMIP5. However the manuscript does not demonstrate that it is "more realistic". The authors need to provide solid arguments for this realism or remove any such claims.

Reply: The CMIP5 solar forcing recommendation was to simply repeat solar cycle 23. Many climate modeling groups ended up repeating the last four solar cycles because they argued that solar cycle 23 was special. Observations of a wide range of solar activity indices clearly demonstrate significant cycle to cycle variability, and long-term trends [Solanki et al 2000, Usoskin et al 2016]. Therefore the CMIP5 solar forcing recommendation was certainly unrealistic. For CMIP6 we have developed solar forcing **scenarios** which include cycle to cycle variability, and long term trends, both of which are established from observations or reconstructions of solar activity metrics. Therefore, taken purely as a **scenario rather than a prediction**, we fail to see how the CMIP6 future solar forcing recommendation can be less realistic than the CMIP5 solar forcing recommendation.

Solanki S.K., Schussler M., Fligge M.: Evolution of the Sun's Large-Scale Magnetic Field Since the Maunder Minimum. Nature 408 , p. 445-447 (2000).

I.G. Usoskin, G.A. Kovaltsov, M. Lockwood, K. Mursula, M. Owens and S.K. Solanki, A new calibrated sunspot group series since 1749: Statistics of active day fractions, Sol. Phys., p.1-24, doi:10.1007/s11207-015-0838-1, 2016 ADS

46) page 38, lines 29-31: "We ignore scenarios with high levels of solar activity because the Sun just left such an episode (called grand solar maximum), and several studies suggest that it is very unlikely to return to one in the next 300 years". As pointed out above (see point 9 of this report), predictions of anything beyond the next cycle are affected by chance (in the sense that the activity level can be changed significantly by singular events that in turn cannot be predicted). It also seems that statistically, from the record of past solar activity, a grand *minimum is equally unlikely as another grand maximum. According to Solanki and Krivova (2011, Science 334, 916), "Half the grand maxima in (6) were followed by one or more subsequent grand maxima before a grand minimum ïnˇA ̧nally occurred." (The reference (6) in this sentence is to Usoskin et al. 2007, Astron. Astrophys. 471, 301.) Consequently, the authors should revise the above statement and find new arguments for why they choose to concentrate on just low values of solar activity for the coming centuries.*

Reply: There is indeed strong evidence against the occurrence of another Grand Solar Maximum within the 21st century. We say this for several reasons. The first is that runs made with various dynamo models (Charbonneau, private comm.) indicate that after a state of Grand Maximum, the Sun is much more likely to move into a Grand Minimum, rather than into another Grand Maximum (see our detailed discussion to point 47 below). Another piece of evidence comes from the various empirical models that we tested using a Monte-Carlo approach, with various parameters. Among the several hundred reconstructions that we made, not a single one showed a grand maximum in the 21st century.

For this particular study, our prime objective is to provide a likely scenario. As stated in the text, the low activity scenario is much less likely, and is merely given to test climate model sensitivity.

47) "Nonetheless, memory effects associated with these periodic reversals play a major role in determining solar variability on multi-decadal time scales, and to some degree are decoupled from the short-term variability. This is our prime motivation for considering predictions on multi-decadal time scales." As given, this is just a statement without a physical basis. As this is their prime motivation for the predictions, the authors should provide solid evidence for such memory effects and the decoupling of multi-decadal from decadal variability.

Reply: It is certainly the case that we currently do not have a reliable scheme for forecasting of solar activity on centennial timescales, whether empirical (based on data) or physical (based on dynamo models). At the purely empirical level, the low probability of another soon-to-occur Grand Maximum can be argued on the basis of (1) the fact that the sun just exited a Grand Maximum, and that return to something closer to the historical norm appears more likely than the opposite; (2) naive extrapolation of the so-called Gleissberg modulation points to lower-than-average activity in the middle of the twenty-first century; (3) more elaborate reconstruction schemes (such as those cited in the paper), notwithstanding their potential failings and uncertainties, also point towards reduced activity in the 21st century. At the physical level, in the (broad) class of non-kinematic dynamo models which generate Grand Minima through nonlinear backreaction on large-scale flows, periods of much Higher-than-average activity (arguably equivalent to Grand Maxima in such models) are more likely to be followed by a Grand Minimum than another Grand Maximum; this is because, in such models showing intermittency, collapse to the trivial solution often requires a large excursion at the boundary of the attractor associated with "normal" cyclic behavior, such excursions corresponding to periods of higher-than-average cycle amplitudes. Examples include the models presented in Passos et al. (2012, Solar Physics 279, 1).

Moreover, in models that achieve Grand Minimum-like behavior exclusively through magnetically-mediated amplitude/parity modulation (without intermittent behavior), recurring epochs of much-higher-than-average cycle amplitude are typically separated by epochs of much-lower-than-average amplitude often of similar temporal duration. Examples include the models presented in Tobias 1996 (A&A 307, L21) and Moss and Brooke 2000 (MNRAS 315, 521). In the model of Brooke et al. 2002 (A&A 395, 1013), Grand Maxima are always followed by a long period of low amplitude cyclic behavior. "Memory" in these dynamical models results from the time required for the field to dissipate back to "normal" values, and large-scale flow to then re-establish themselves to "normal" magnitude; and depending on parameter values, that "memory" can be much longer than the primary cycle period. The empirical study by Inceoglu et al. (2016) (Solar Phys., 291, 303) claims that a grand maximum is at reduced probability to be followed by another grand maximum on short timescales.

Of course, there also exist classes of dynamo models that enter and exit Grand Minima (and Maxima) primarily through stochastic driving, making any long term prediction truly impossible. Stochastic driving certainly takes place in the sun via the impact of convective turbulence and vaguaries of active region emergence; but nonlinear magnetic backreaction on the inductive flows also certainly takes place; therefore some level of long term memory must remain, unless stochastic effects completely dominate the fluctuating behavior even on multidecadal timescales.

The only tentative conclusion that emerges from all these various models is thus that Grand Maxima appear more likely to be followed by a Grand Minimum than by another Grand Maximum. This is the basis of our choice to restrict our extreme scenario for the 21st century to a Grand Minimum rather than a Grand Maximum. We have modified/expanded the text in section 1 (p 5), section 3 (p 39) and section 6 (p 55) to be more explicit about the rationale underlying this choice. We have also "softened" our statements regarding the specific activity predictions, to avoid giving the impression that they are physically sounder than they really are.

48) Sections 3.1-3.4. I have signiïn˘A ̧cant doubts about the results presented in these sections. Section 3.1 presents three forecast methods, chosen seemingly arbitrarily from all those that have been proposed. As far as I can tell, they are all in one way or another linear. For a strongly non-linear system such as the solar dynamo, I see little value in using linear forecasting methods. I argue that applying inappropriate, but complex sounding forecasting techniques projects a sense of accuracy where none is present in reality. The performance of the techniques is discussed in Sect. 3.3 and Fig. 21c. From Fig. 21a I get the impression that the errors in the Phi forecast are comparable (and over some periods exceed by a factor of 2-3, e.g. around 2080-2090) the values of Phi. Around 2200 various methods give Phi of about 100 to

400, and the forecast error is 150 for all methods. This essentially means the range of 0 to 550 (with 600 being the highest value measured during the modern Grand max). In summary, Fig 21 shows that the three methods often give hugely different results (which is not surprising and simply reinforces that solar activity cannot be reliably predicted using such simple techniques and possibly cannot be predicted at all on these time scales). The authors then consider the mean of these three results, claiming that it represents "the most likely level of solar activity". Such an approach can hardly be called scien- tiïn˘A ̧c and cannot lead to a "more realistic" forecast than CMIP5. Thus, the mean of 3 more or less random numbers is still a more or less random number of little value. The construction of the "extreme" scenario is also difïn˘A ̧cult to follow. A lot of the description is rather opaque. All this seems such a complicated way of computing something that is likely very unreliable anyway and does not provide that much reliable information. For example, the reference scenario seems to be somewhat below present conditions and stays nearly constant at that level, while the extreme scenario drops down to the Maunder minimum and basically stays there. Is that so much different from what was done for CMIP5. I would find it a lot more honest towards the reader to not invoke all these different methods, but rather to make a clear and simple assumption and to show the result it gives. This result may turn out not to be very different from what the authors are proposing now, if the authors make the appropriate assumptions. BTW, what is the meaning of a negative modulation potential (Fig. 21B) and how is it obtained?

Reply: Let us reply pointwise

- Arbitrary: the choice is by no means arbitrary. These techniques are part of the basic set that is advocated for time series prediction e.g. [Brockwell and Davis, Introduction to time series and forecasting. Springer, 2010]. Analogue forecasts have the advantage of not requiring any parametric model. Autoregressive models is by far the most widely used class of models for linear differential equations. And the harmonic model is directly motivated by the evidence for periodicities in the level of solar activity. One could have added analogue neural networks, etc, but then one would be transitioning toward a black box approach. The three models we advocate on the contrary each have their justification.
- Linearity: the analogue forecast does not make linearity assumptions. The harmonic one is linear by construction, but can handle both linear and nonlinear systems. Only the autoregressive model explicitly assumes that the system is described by a linear differential equation.
- Performance: we do not claim that our models are capable of providing good forecasts, especially since their predictive capacity drops within a few decades (but still does better than the persistence scenario that has been recommended for CMIP5). Probably no model ever will. However, we use these model to get the 'best' possible scenarios with the information at hand.
- Taking the mean: the justification is exactly the same as for the averaging of the SSI models: in the absence of objective criteria for preferring one model to the other, the recommendation is to average them all, which provides a mean state of phi. In this particular context, however, since we have prediction skills, we use these to weight the models.
- Negative modulation potential: this is a consequence of the prediction methods being unable to provide positive definite values, except for the analogue forecast. Furthermore,

these negative phi values are also present in the Steinhilber 2012 phi record, resulting from the modulation potential reconstruction techniques. Therefore, although the negative phi values are unphysical, they are not necessarily caused by the forecast techniques. Also Solanki et al. (2004), McCracken et al. (2007) obtained formally negative phi values in their reconstructions, which are however, consistent with zero phi within the uncertainties. Strictly speaking, negative phi is not necessarily a physical nonsense but may be related to a poor knowledge of the low-energy part of the local interstellar spectrum (LIS) of cosmic rays outside the heliosphere, which is not very well known.

49) page 39, line 17: ". . . is certainly presentat some level." ". . . is certainly present at some level."

Reply: Thank you for pointing this out.

50) page 39, line 35: ". . . using the geomagnetic reconstruction of the open solar flux Lockwood et al. (2014)." ". . . using the geomagnetic reconstruction of the open solar flux (Lockwood et al., 2014)."

Reply: Thank you for pointing this out.

51) p. 40, line 11-12: "According to solar dynamo models, the solar-cycle averaged modulation potential (and the sunspot number) cannot be predicted more than a few decades ahead." This statement is not entirely consistent with p. 39, line 7-8 "As of today, even predicting the cycle amplitude one cycle ahead remains a major challenge (Pesnell, 2012)." Which statement do the authors actually support, one cycle ahead or multiple cycles ahead? According to Cameron et al. and Jie et al. (referred to earlier in this report; see point 9), the statement on p. 39 appears to be the valid one and the statement on p. 40 should be changed accordingly.

Reply: The text should indeed say "one solar cycle ahead".

52) page 40, line 12-14: "The observed modulation potential has an autocorrelation function that decays exponentially with a characteristic time of 48 ± 5 years. This quantity can be interpreted as the time beyond which memory is lost." This is weak und unconvincing evidence of memory. Earlier in the same paragraph, the authors state that they are dealing with 22-year averages of the modulation potential Phi. The decay time of 48 years is hence basically the time resolution of the data (based on the Nyquist frequency). I do not see this as evidence for a memory, just that the true resolution of the data is not very high. In addition to this argument, there may well be hidden connections between data points lying close in time, so that they are not entirely independent. This can be the case in cosmogenic isotope data, so that using this as an argument of memory should be done with considerable care. The authors should first convincingly show that individual data points are completely independent, before making claims of memory.

Reply: Regarding the wording "memory", this is conventionally used for the decay time of the autocorrelation function, though the more technical "decorrelation time" is more accurate.

We agree that the measured decay time is indeed not so much longer than the sampling period. We did discuss the way the Steinhilber (2012) record has been made and found no evidence for a smoothing that may artificially increase the correlation between samples. Note that the relatively larger value of the decay time is also confirmed by the duration of the grand minima/maxima, which always take a finite time to start and to recover.

53) Page 40, line 15-16: "To the best of our knowledge, no existing method has been able to meaningfully predict solar activity more than 60 years ahead." This seems to imply that there are methods that can predict up to 60 years ahead. I would like to hear more about these. E.g. how do the authors know that they work up to 60 years ahead, without waiting for another 60 years to find out? Unless, of course, they are referring to methods that are at least 60 years old and that I seem to have missed. I have seen many so-called predictions tuned to reproduce past data exceptionally well, but then do rather less well when predicting even the next cycle. This statement also is not consistent with p. 39, line 7-8 and other work.

Reply: We should indeed rephrase this more carefully. As of today, very few models are able to shed light on horizons beyond the 22-year timeline. What we meant to say, is that to the best of our knowledge, that no single realistic approach has gone beyond 60 years.

As you probably know, few of the more elaborate methods have been tested against observations because they rely on space age data.

54) Page 45, line 1: "The resulting SSN time series of both future scenarios have then be used" "The resulting SSN time series of both future scenarios have then been used"

Reply: Thank you for pointing this out.

55) page 53, line 5: NRLTSI2/NRLSSI2 are empirical models not semi-empirical ones.

Reply: This has been corrected.

56) page 54, lines 8-10: the statement is not clear (see above);

Reply: Please see reply to comment 2.

57) page 54, line 13: The statement is too ambiguous. Which satellite measurements are meant?

Reply: This refers to the observations used in the SOLID composite. We shall update the text accordingly.

Solar Forcing for CMIP6 (v3~~.1~~.2)

Katja Matthes[1,2], Bernd Funke[3], Monika E. Andersson[18], Luke Barnard[4], Jürg Beer[5], Paul Charbonneau[6], Mark A. Clilverd[7], Thierry Dudok de Wit[8], Margit Haberreiter[9], Aaron Hendry[14], Charles H. Jackman[10], Matthieu Kretzschmar[8], Tim Kruschke[1], Markus Kunze[11], Ulrike Langematz[11], Daniel R. Marsh[19], Amanda Maycock[12], Stergios Misios[13], Craig J. Rodger[14], Adam A. Scaife[15], Annika Seppälä[18], Ming Shangguan[1], Miriam Sinnhuber[16], Kleareti Tourpali[13], Ilya Usoskin[17], Max van de Kamp[18], Pekka T. Verronen[18], and Stefan Versick[16]

[1]GEOMAR Helmholtz Centre for Ocean Research Kiel, Kiel, Germany
[2]Christian-Albrechts Universität zu Kiel, Kiel, Germany
[3]Instituto de Astrofísica de Andalucía (CSIC), Granada, Spain
[4]University of Reading, Reading, United Kingdom
[5]EAWAG, Dübendorf, Switzerland
[6]University of Montreal, Canada
[7]British Antarctic Survey (NERC), Cambridge, UK
[8]LPC2E, CNRS and University of Orléans, France
[9]Physikalisch-Meteorologisches Observatorium Davos/World Radiation Center, Davos, Switzerland
[10]Emeritus, NASA Goddard Space Flight Center, Greenbelt, MD, U.S.A.
[11]Freie Universität Berlin, Berlin, Germany
[12]University of Leeds, Leeds, UK
[13]Laboratory of Atmospheric Physics, Aristotle University of Thessaloniki, Thessaloniki, Greece
[14]Department of Physics, University of Otago, Dunedin, New Zealand
[15]Met Office Hadley Centre, Fitz Roy Road, Exeter, Devon, UK
[16]Karlsruhe Institute of Technology, Karlsruhe, Germany
[17]ReSoLVE Centre of Excellence and Sodankylä Geophysical Observatory, University of Oulu, Finland
[18]Finnish Meteorological Institute, Helsinki, Finland
[19]National Center for Atmospheric Research, Boulder, CO, USA

Correspondence to: Katja Matthes (kmatthes@geomar.de)

Abstract. This paper describes the solar forcing dataset for CMIP6 and highlights ~~in particular~~ changes with respect to the CMIP5 recommendation. The solar forcing is provided for radiative properties, ~~i.e.~~namely, total solar irradiance (TSI)~~and~~ , solar spectral irradiance (SSI), ~~and~~ the F10.7 ~~cm radio flux~~index, as well as particle forcing, ~~i.e.,~~ with geomagnetic indices Ap and Kp, and ionisation rates to account for effects of solar protons, electrons and galactic cosmic rays. This is the first time that a recommendation for solar-driven particle forcing is provided for a CMIP exercise. The solar forcing ~~dataset is~~ datasets are provided at daily and monthly resolution separately for the CMIP6 ~~Historical Simulation~~ historical (1850–2014) ~~, for the~~ and future (2015–2300) ~~, including~~ simulations. The datasets include an additional extreme Maunder ~~Minimum-like~~ minimum-like sensitivity scenario, as well as ~~for~~ a constant and a time-varying forcing for the preindustrial control simulation. ~~The paper not only~~ This paper describes the forcing ~~dataset, but~~ datasets and also provides detailed recommendations ~~for how to implement~~ as to their implementation in the different forcing components in climate models.

The TSI and SSI time series are defined as ~~averages of two (semi-) empirical~~ the average of two solar irradiance models~~,~~ ~~namely the~~ : an empirical one (NRLTSI2 / NRLSSI2~~and SATIRE-TS~~) and a semi-empirical one (SATIRE). A new and lower TSI value is recommended: the contemporary solar cycle-average is now 1361.0 W/m^2. The slight negative trend in TSI during the last three solar cycles in CMIP6 is statistically indistinguishable from available observations and only leads to a small global radiative forcing of -0.04 W/m^2. In the 200–400 nm range, which is also important for ozone photochemistry, CMIP6 shows a larger solar cycle variability contribution to TSI than CMIP5 (50% as compared to 35%).

~~The~~ We compare the CMIP6 dataset ~~is tested and compared~~ to its CMIP5 predecessor by using timeslice experiments of two chemistry-climate models and a reference radiative transfer model. The changes in the ~~background~~ long-term evolution of the SSI in the CMIP6 dataset, as compared to CMIP5, impact on climatological stratospheric conditions (lower shortwave heating rates (-0.35 K/day at the stratopause), cooler stratospheric temperatures (-1.5 K in the upper stratosphere), lower ozone abundances in the lower stratosphere (-3%), and higher ozone abundances (+1.5% in the upper stratosphere and lower mesosphere). Between the maximum and minimum phases of the 11-year solar cycle, there is an increase in shortwave heating rates (+0.2 K/day at the stratopause), temperatures ($\sim$1 K at the stratopause), and ozone (+2.5% in the upper stratosphere) in the tropical upper stratosphere using the CMIP6 forcing dataset. This solar cycle response is slightly larger, but not statistically significantly different from that for the CMIP5 forcing dataset.

CMIP6 models with a well-resolved shortwave radiation scheme are encouraged to use SSI, as well as solar-induced ozone signals, in order to better represent solar climate variability compared to models that only prescribe TSI and/or exclude the solar-ozone response. Monthly mean solar-induced ozone variations will also be incorporated into the CCMI CMIP6 Ozone Database for climate models that do not calculate ozone interactively. CMIP6 models with interactive chemistry are encouraged to use the particle forcing which will allow the potential long-term effect of particles to be addressed for the first time. The consideration of particle forcing has been shown to significantly improve the representation of reactive nitrogen and ozone variability in the polar middle atmosphere, eventually resulting in further improvements of the representation of solar climate variability.

1 Introduction

Solar variability affects the Earth's atmosphere in numerous, and often intricate ways through changes in the radiative and energetic particle forcing (Lilensten et al., 2015). For many years, the role of the Sun in climate model simulations was reduced to its sole total radiative output, named Total Solar Irradiance (TSI), and this situation prevailed in the assessment reports of the IPCC until 2007 (Alley et al., 2007). However, there has been growing evidence for other aspects of solar variability to be major players for climate, in particular Solar Spectral Irradiance (SSI) variations and, more recently, Energetic Particle Precipitation (EPP).

For about a decade, studies involving stratospheric resolving (chemistry) climate models have included SSI variations (e.g., Haigh, 1996; Matthes et al., 2003, 2006; Austin et al., 2008; Gray et al., 2010). Whereas relative TSI variations in the 11-year solar cycle are small, about 0.1%, SSI changes are wavelength dependent, and may vary by up to 10% at 200 nm in the ultraviolet (UV) wavelength range (Lean, 1997). Variations in UV radiation over the solar cycle have significant impacts on the radiative heating and ozone budget of the middle atmosphere (Haigh, 1994).

Through dynamical feedback mechanisms solar forcing can also influence the lower atmosphere and the ocean (e.g., Gray et al., 2010). Therefore, its importance is becoming increasingly evident, in particular for regional climate variability ~~is becoming increasingly evident~~ (e.g., Gray et al., 2010; Seppälä et al., 2014). Together with volcanic activity, solar variability is an important external source of natural climate variability. Because of its prominent 11-year cycle, solar variability on time scales of years, and beyond may offer a degree of predictability for regional climate and could therefore help reduce uncertainties in decadal climate predictions.

However, there are still uncertainties in the observed atmospheric signals of solar variability (Mitchell et al., 2015a) and its transfer mechanism(s) to the surface. Proposed transfer mechanisms include changes in TSI and SSI, as well as in solar-driven energetic particles (e.g., Seppälä et al., 2014). In addition, recent work suggests a lagged response in the North Atlantic/European sector due to atmosphere-ocean coupling (e.g., Gray et al., 2013; Scaife et al., 2013), as well as a synchronisation of decadal variability in the North Atlantic Oscillation (NAO) by the solar cycle (Thieblemont et al., 2015). Lagged responses have been also attributed to particle effects (Seppälä and Clilverd, 2014) and hence the observed solar surface signal could be a combination of top-down solar UV and particle as well as bottom-up atmosphere-ocean mechanisms.

Since some of the climate models run under the previous fifth Coupled Model Intercomparison Project (CMIP5) included the stratosphere and the mesosphere for the first time, and were thus able to capture the so-called "top-down" mechanism for solar-climate coupling, both TSI and SSI variations were recommended by the WCRP/SPARC SOLARIS-HEPPA activity (http://solarisheppa.geomar.de/cmip5). Recent modeling efforts have made progress in defining the pre-requisites to simulate solar influence on regional climate more realistically (e.g., Gray et al., 2013; Scaife et al., 2013; Thieblemont et al., 2015), but the lessons learned from CMIP5 show that a more process based analysis of climate models within CMIP6 is required to better understand the differences in model responses to solar forcing (e.g., Mitchell et al., 2015b; Misios et al., 2016; Hood et al., 2015). In particular, the role of solar-induced ozone changes and the need for a suitable resolution of climate model radiation schemes to capture SSI variations is becoming increasingly evident, and will be touched upon in this paper. In addition we will for the first time provide the solar-driven energetic particle forcing together and consistent with the radiative forcing.

The quantitative assessment of radiative solar forcing has been systematically hampered so far by the large uncertainties and the instrumental artifacts that plague ~~TSI and SSI observations(e.g., Ermolli et al., 2013; Solanki et al., 2013), and also by~~ SSI observations, and to a lesser degree TSI observations (e.g., Ermolli et al., 2013; Solanki et al., 2013). Another problem is the sparsity of the observations, which started in the late 1970s only with the satellite era. These problems have deprived us of the hindsight that is needed to properly assess variations on time scales that are relevant for climate studies. Another issue is the uncertainty regarding their absolute level. Since CMIP5, the nominal TSI has been reduced to 1361.0 $\pm$ 0.5 W/m^2~~(Mamajek et al., 2015)~~, see (Prša et al., 2016), and also (Kopp and Lean, 2011). This adjustment has inevitable implications for understanding the Earth's radiation budget.

On multi-decadal time scales, proxy reconstructions of the TSI ~~exhibit~~ reveal occasional phases of unusually low or high solar activity, which are respectively called grand solar minima and maxima (Usoskin et al., 2014). Of particular interest in this regard is the future evolution of long-term solar activity. ~~There is growing evidence for the Sun to enter~~ Solar activity reached unusually high levels in the second half of the twentieth century, so that one could expect subsequent activity to fall back to levels closer to the historical mean, an expectation buttressed by the low amplitude of current activity cycle 24. Moreover, some recent empirical long-term forecast even predict a phase of ~~low activity near 2050, after a grand maximum that peaked during the 20th century~~ very low activity in the second half of the twenty-first century – perhaps akin to the 1645-1715 Maunder Minimum (Abreu et al., 2008; Barnard et al., 2011; Steinhilber et al., 2012). However, how deep and how long ~~this new~~ such phase of low solar activity ~~is likely to~~ would be is still ~~uncertain (Abreu et al., 2008; Barnard et al., 2011; Steinhilber et al., 2012)~~largely uncertain. Recent studies have investigated the climate impacts of a large reduction in solar forcing over the 21st century, revealing only a small impact on a global scale (Feulner and Rahmstorf, 2010; Anet et al., 2013; Meehl et al., 2013). However, a systematic assessment of the regional impacts of a more realistic future solar forcing is still to be done. For example, on regional scales, a future grand solar minimum could potentially reduce Arctic amplification (Chiodo et al., 2016) and reduce long-term warming trends over western Europe (Ineson et al., 2015).

The above-mentioned uncertainty in the SSI is particularly challenging in the UV band (Ermolli et al., 2013). All climate model intercomparison studies relied so far on the NRLSSI1 dataset (Lean, 2000). However, it is becoming increasingly evident that its solar cycle variability in the UV part of the spectrum may be too low as compared to updated and more recent SSI reconstructions by models such as NRLSSI2 ~~(?) and SATIRE-TS~~ (Coddington et al., 2016) and SATIRE (Yeo et al., 2014). Recent studies have emphasized the sensitivity to UV forcing changes due to top down effects (Ermolli et al., 2013; Langematz et al., 2013; Ineson et al., 2015; Thieblemont et al., 2015; Maycock et al., 2015; Ball et al., 2016), thereby stressing the need for a state-of-the-art representation of the SSI, and in particular the UV band, in the CMIP6 solar forcing recommendation. For that reason, we will ~~in particular~~ focus on the SSI uncertainty and possible impacts of the higher SSI variability in CMIP6 with respect to the CMIP5 solar forcing recommendation ~~.~~ (http://solarisheppa.geomar.de/cmip5).

Analysis of model simulations and observations have shown a response of global surface temperature to TSI variations over the 11-year solar cycle of about 0.1 K (Lean and Rind, 2008; Misios et al., 2016). However, the observed lag and the spatial pattern of the solar cycle response are poorly represented in CMIP5 models (e.g., Mitchell et al., 2015b; Misios et al., 2016; Hood et al., 2015).

In addition, (Gray et al., 2010) report that previous long-term variations in solar forcing used in some experiments (Alley et al., 2007) may be too weak due to an unfortunate choice of epoch (around 1750) for the preindustrial solar forcing, as this was a period of relatively high solar activity.

More recently, it has become better established that there is a solar response in the Arctic Oscillation (AO) and NAO from the top-down mechanism (Shindell et al., 2001; Kodera, 2002; Matthes et al., 2006; Woollings et al., 2010; Lockwood et al., 2010; Ineson et al., 2011; Langematz et al., 2013; Ineson et al., 2015; Maycock et al., 2015; Thieblemont et al., 2015). Earlier models often employed a lower vertical domain, missing key physical processes by which solar signals in the stratosphere couple to surface winter climate. However, some of the more recent studies using stratosphere resolving (chemistry) climate models confirm a stratospheric downward influence on the NAO from solar variability, in particular associated with changes in UV radiation and possibly through interaction with stratospheric ozone (e.g., Matthes et al., 2006; Rind et al., 2008; Ineson et al., 2011; Chiodo et al., 2012; Langematz et al., 2013; Thieblemont et al., 2015; Ineson et al., 2015). Some of these studies also suggest weaker model responses than are apparent in observations, although with large uncertainty (e.g., Gray et al., 2013; Scaife et al., 2013).

Another very important solar forcing mechanism after electromagnetic radiation is energetic particle precipitation (Gray et al., 2010; Lilensten et al., 2015). Although the impact of EPP on the atmosphere is well documented, it had been ignored in solar forcing recommendations for earlier phases of CMIP. The term EPP encompasses particles with very different origins: solar, magnetospheric, and from beyond the solar system. These particles are mainly protons and electrons, and occasionally α–particles, and heavier ions.

Solar protons with energies of 1 MeV to several hundreds of MeV are accelerated in interplanetary space during large solar perturbations called coronal mass ejections (Reames, 1999; Richardson and Cane, 2010). These sporadic events, also known as solar proton events (SPEs), are associated with the presence of complex sunspots, and are therefore more frequent during solar maximum.

Auroral electrons originate from the Earth's magnetosphere, and are accelerated to energies of 1-30 keV during auroral substorms (Fang et al., 2008). Sudden enhancements of their flux occurs during geomagnetic active periods, which are more frequent 1-2 years after peak of the 11-year solar cycle. Medium-energy electrons are accelerated to energies of a few hundred keV during geomagnetic storms in the terrestrial radiation belts (Horne et al., 2009). Precipitation of middle energy electrons can be triggered both by solar coronal mass ejections, and high-speed solar wind streams, leading to more frequent events near solar maximum and during the declining phase of the solar cycle. Particle precipitation, regardless of its origin, is thus modulated by solar activity, and varies with the solar cycle. However, these intermittent variations take place on different timescales, and at different altitude regions. Their sources and variability have recently been reviewed by Mironova et al. (2015).

EPP affects the ionisation levels in the polar middle and upper atmosphere, leading to significant changes of the chemical composition. In particular, the production of odd nitrogen and odd hydrogen species causes changes in ozone abundances via catalytic cycles, potentially affecting temperature and winds (see, e.g., the review by Sinnhuber et al., 2012). Recent model studies and the analysis of meteorological data have provided evidence for a dynamical coupling of this signal to the lower atmosphere, leading to particle-induced surface climate variations on a regional scale (e.g., Seppälä et al., 2009; Baumgaertner et al., 2011; Rozanov et al., 2012; Maliniemi et al., 2014).

The third, and most energetic components of EPP is represented by galactic cosmic rays (GCR), which mainly consist of protons with energies from hundreds of MeV to TeV. This continuous flux of particles is the main source of ionisation in the troposphere and lower stratosphere. GCRs are deflected by the solar magnetic field, and hence their flux is anti-correlated with the solar cycle. Laboratory-based studies have confirmed the existence of ion-mediated aerosol formation and growth rates; however, the connection between GCR ionization and cloud production, and therefore convection, is still under debate. Meanwhile, the chemical impact via ozone-depleting catalytic cycles and subsequent dynamical forcing is rather well understood (Calisto et al., 2011; Rozanov et al., 2012).

The effect of various components of EPP on surface climate is an emerging research topic. However, the particle impact on regional climate may be comparable to that of the UV forcing (Seppälä and Clilverd, 2014). One of the major challenges here is to quantify the long-term climate impact of such local and mostly intermittent particle precipitations.

The uncertainties in the solar forcing itself are compounded by possible errors in the simulated climate response to this forcing in models (e.g., Stott et al., 2003; Scaife et al., 2013). Possible errors in climate model responses could be related to biases in the representation of dynamical processes and dynamical variability, the inability of model radiation schemes to properly resolve SSI changes (Forster et al., 2011), or to the missing or inadequate representation of UV and particle-induced ozone signals (Hood et al., 2015). Any comparison of climate model simulations with observations could be affected by a combination of these possible sources of error. In addition, the comparison of models with observations is inhibited by the insufficient length of the observational records, and in some cases model simulations.

This paper will provide the first complete overview on solar forcing (radiative, particle and ozone forcing) recommendations for CMIP6 from preindustrial times to the future and provides in this respect an advance to earlier MIPs (CMIP5, CCMVal, CCMI) as it gives a complete and state-of-the-art overview on our current understanding of solar variability and provides the dataset in a user-friendly way.

Section 2 presents the historical to present-day solar forcing dataset with individual subsections on solar irradiance (Section 2.1) and particle forcing (Section 2.2). Section 3 provides a description of the future solar forcing recommendation, section 4 on the pre-industrial control forcing and section 5 finally a description of the solar induced ozone signal. A summary with respect to differences to the CMIP5 recommendation is given in section 6.

2 Historical (to Present) Forcing Data (1850-2014)

In this section we first describe the solar irradiance dataset (including the TSI, the F10.7 decimetric radio index, and the SSI, see Sec. 2.1), and subsequently address the energetic particle datasets (including solar protons, auroral electrons, medium-energy electrons, and and galactic cosmic rays, see Sec. 2.2).

2.1 Solar Irradiance (TSI, SSI, and F10.7)

This subsection starts with a description of the available TSI and SSI datasets from two different solar irradiance models (NRLSSI and SATIRE), and one observational estimate (SOLID), before introducing the CMIP6 recommendation. Afterwards a recommendation on how to implement the solar irradiance forcing in CMIP6 models is provided. An evaluation of the comparison between different SSI forcing datasets with a focus on CMIP5 and CMIP6 solar irradiance recommendations in a line-by-line model and two state-of-the-art CCMs, i.e. CESM1(WACCM) and EMAC, is performed at the end to highlight the effects of solar irradiance variability on the atmosphere, and possible effects on atmospheric dynamics all the way to the ocean.

2.1.1 Description of Solar Irradiance Datasets

NRLTSI2 and NRLSSI2

The Naval Research Laboratory (NRL) family of SSI models (Lean, 2000; Lean et al., 2011) is based on the premise that changes in solar irradiance from background quiet Sun conditions can be described by a balance between bright facular, and dark sunspot features on the solar disk. These two contributions are determined by linear regression between solar proxies, and direct observations of TSI and SSI by satellite missions such as SORCE (Rottman, 2005). These models are thus empirical.

Both the TSI and the SSI consist of a baseline solar contribution, with a wavelength-dependent contributionfrom bright faculae (i. e., the Mg II index, see below) and dark sunspots (i.e., sunspot area, see below). The Magnesium (MgII) index, for example, represents the contribution of bright faculae, whereas the sunspot area represents the contribution of sunspots. The time dependency in TSI and SSI thus emerges from the temporal variability in the solar proxies. SORCE measurements at solar minimum conditions are the basis for the adopted quiet Sun irradiance (Kopp and Lean, 2011) in NRLSSI2.

The recently updated version of the NRL models, named NRLTSI2 (for TSI only) and NRLSSI2, have been transitioned to the National Centers for Environmental Information (NCEI) as part of their Climate Data Record (CDR) Program (see http://www.ngdc.noaa.gov), and operational updates are provided on a near quarterly basis. ? Coddington et al. (2016) describe the model algorithm, the uncertainty estimation approach, and comparisons to observations in detail.

In NRLSSI2, a multiple linear regression approach of solar proxy inputs with observations of TSI from SORCE/TIM (Kopp et al., 2005), and observations of SSI from the SORCE/SOLSTICE (McClintock et al., 2005) and SORCE/SIM (Harder et al., 2005) instruments is used to determine the scaling coefficients that convert the proxy indices to irradiance variability. Because of concerns regarding Concerns for the long-term stability of the SORCE SSI observations Lean and DeLand (2012) the (Lean and DeLand, 2012) that are not shared with regard to the SORCE TSI record mean the wavelength-dependent scaling coefficients used in the NRLSSI2 are derived from model are derived for solar rotation time scales (i.e. , the SSI observations and the proxy indices are detrended with an 81-day running mean). A separate adjustment is made However, because regression coefficients derived from detrended SSI time series differ from those developed from non-detrended SSI time series, a further adjustment is required to extend the SSI variability from solar rotational to solar cycle time scales. In NRLSSI2, this adjustment is made by a linear scaling that is constrained by the TSI variability. This adjustment is made in the separate facular and sunspot proxy records and the magnitude of the adjustment is smaller than the assumed uncertainty in the proxy indices themselves. In this approach, the integral of the SSI tracks the TSI; however, the relative facular and sunspot contributions at any given wavelength are not constrained to match their specific TSI contributions.

The NRLTSI2 and NRLSSI2 irradiances also include a speculated long-term facular contribution that produces a secular (i.e., underlying the solar activity cycle) net increase in irradiance from a small accumulation of total magnetic flux. This secular impact is specific to historical time scales (i.e., prior to 1950) and is consistent with simulations from a magnetic flux transport model (Wang et al., 2005).

SATIRE-TSSATIRE

The SATIRE (Spectral And Total Irradiance REconstruction) family of semi-empirical models assumes that the changes in the solar spectral irradiance are driven by the evolution of the photospheric magnetic field (Fligge et al., 2000; Krivova et al., 2003, 2011). The model makes use of the calculated intensity spectra of the quiet Sun, faculae and sunspots generated from model solar atmospheres with a radiative transfer code (Unruh et al., 1999). SSI at a particular time is given the sum of these spectra, weighted by the fractional solar surface that is covered by faculae and sunspots, as apparent in solar observations.

The implementation of SATIRE employing solar images in visible light, and solar magnetograms (magnetic field intensity and polarity) is termed SATIRE-S (Wenzler et al., 2005; Ball et al., 2012; Yeo et al., 2014), and that based on the sunspot number is SATIRE-T (Krivova et al., 2010; Dasi-Espuig et al., 2014)(Krivova et al., 2010). Individual records are accessible at http://www2.mps.mpg.de/projects/sun-climate/. The dataset we consider here is a combination of SATIRE-S for observations between 1974 and 2014, where full-disc magnetograms are available, and a reconstruction based on In order to guarantee the homogeneity of our past and future SSI reconstructions, we use here SATIRE-Tfrom 1850 to 1974, and from 2014 onwards. SATIRE-S has been demonstrated to be consistent with SSI measurements where the latter are reliable, see Yeo et al. (2015), driven by the same sunspot number record. On decadal to centennial time scales, SATIRE reproduces observations such as: the composite of the Lyman-α line at 121.5 nm (since 1947, Woods et al., 2000), the measured solar photospheric magnetic flux (since 1967), the empirically reconstructed solar open magnetic flux (since 1845, Lockwood et al., 2014), and the ^{44}Ti activity in stony meteorites (Krivova et al., 2010; Vieira et al., 2011; Yeo et al., 2014).

Let us stress that SATIRE-TS SATIRE and NRLSSI2 are internally consistent, in the sense that the integral of the modeled spectral irradiance equals the TSI. In NRLSSI2, this internal consistency also applies to the integral of the facular and sunspot contributions to SSI to their respective counterparts in TSI (see **?** for more details)These are among the best model reconstructions we currently have. Note, however, that both models reconstruct the SSI prior to the space age by assuming the relationship between sunspot number and SSI to be time-invariant. The model-uncertainty associated with this assumption is difficult to quantify. For that reason, it is not included in the uncertainties that are provided with the model datasets, which might therefore be underestimated.

Proxies Used

Both NRLSSI2 and SATIRE-TS SATIRE rely on the sunspot number when no other solar proxies are available. For the CMIP6 composite, we decided to rely on version 1.0 of the international sunspot number (from http://www.sidc.be/silso/versionarchive), even though a newer version 2.0 recently came out (Clette et al., 2014). Indeed, SSI models have not yet been thoroughly trained and tested with this new sunspot number. Recent results by Kopp et al. (2016) suggest that this revision has little impact after 1885, and leads to greater solar-cycle fluctuations prior.

In NRLSSI2 the proxy index for facular brightening is the composite Magnesium (Mg) II MgII index from the University of Bremen. The Mg II MgII index (Viereck et al., 2001) is a disk-integrated ratio of the core to the wings of the Mg II MgII emission line at 280 nm, and used by many models as a UV proxy. The ~~Mg II~~ MgII index is available from 1978 onwards; values prior to that are estimated from the sunspot number.

In NRLSSI2 and in SATIRE, the proxy index for sunspot darkening is the sunspot area as recorded by ground-based observatories in white light images since 1882 (Lean et al., 1998). ~~Values prior to that are~~ The sunspot darkening prior to 1882 is estimated from the sunspot number.

SOLID Composite

The task at hand – to determine the most likely temporal variation in SSI – is challenged by the paucity of direct SSI observations, ~~which, in addition, suffer from~~ and the numerous instrumental artefacts that affect these observations. Recently, this task has been addressed by an international consortium~~to produce~~ , which has produced an observational SSI composite ~~. The~~ (Haberreiter et al., 2017). This SOLID[1] ~~SSI~~ composite is the first of its kind ~~in the sense that it is based on a probabilistic approach. More specifically it is derived as the weighted mean of all available SSI observationsin the satellite era. This approach leads to a new observational SSI composite that serves here~~ to include a large ensemble of observations, which are listed in Table 1. These observations are combined by using a probabilistic approach, without any model input. We consider this observational composite here mainly as an independent ~~data set to validate the SSI reconstruction models described above. However, the observations are restricted to the satellite era and the extension using proxies is limited back to 1950. Thus the SOLID composite cannot be employed for the CMIP6 solar forcing recommendation time period~~means for comparing the SSI reconstructions. While it is premature to use this composite as a benchmark for testing the models, it definitely represents the most comprehensive description to date of SSI observations.

The making of ~~such a~~ this composite involves several steps~~: first, the raw data are preprocessed (Schöll et al., 2016). Next, each individual~~ . First, the SSI datasets as provided by the instrument teams (see the list of instruments in Table 1) are pre-processed, e.g., corrected for outliers and aligned in time. Furthermore, the short-term and long-term uncertainties of the SSI time series are determined. These steps are detailed in (Schöll et al., 2016).

Second, for each individual dataset all data gaps are filled by expectation-maximization (Dudok de Wit, 2011). This approach makes use of observed proxies representing the SSI variation of different wavelength ranges in the solar spectrum, as listed in Table 2. We emphasize here that the gap-filling is a purely statistical method, as no physical assumption goes into it. Third, each individual time series is decomposed ~~into different time scales (typically, from daily to annual~~by wavelet transform into 13 time scales $a = 2^j$, with j being the level of the scale. These scales go from 1 day (Level 0) to 11.2 years (Level 12). For each time scale, ~~their uncertainty is estimated. All these records are then merged scale-wise, by computing their average, weighted by their~~ the uncertainty is determined by taking into account the short-term and long-term uncertainties. Fourth, the recomposed records are recombined by calculating the weighted average for each scale thereby taking into account the scale-dependent and wavelength-dependent uncertainties. Finally, the SSI composite is obtained by adding up the ~~average obtained for each time scale~~averaged temporal scales. Additionally, the time-dependent and wavelength-dependent uncertainties are also summed-up.

[1]FP7 SPACE Project *First European SOLar Irradiance Data Exploitation (SOLID)*; http://projects.pmodwrc.ch/solid/

Table 1. SSI datasets used for the SOLID composite. The first column gives the instrument, the second column the spectral band, and the third column the temporal coverage of the observations.

Name of the instrument	Wavelength range [nm]	Observation Period
GOES13/EUVS	11.7–123.2	07/2006–10/2014
GOES14/EUVS	11.7–123.2	07/2009–11/2012
GOES15/EUVS	11.7–123.2	04/2010–10/2014
ISS/SolACES	16.5–57.5	01/2011–03/2014
NIMBUS7/SBUV	170.0–399.0	11/1978–10/1986
NOAA9/SBUV2	170.0–399.0	03/1985–05/1997
NOAA11/SBUV2	170.0–399.0	12/1988–10/1994
NOAA16/SBUV2	170.0–406.2	10/2000–04/2003
SDO/EVE	5.8–106.2	04/2010–10/2014
SME/UV	115.5–302.5	10/1981–04/1989
SNOE/SXP	4.5	03/1998–09/2000
SOHO/CDS	31.4–62.0	04/1998–06/2010
SOHO/SEM	25.0–30.0	01/1996–06/2014
SORCE/SIM	240.0–2412.3	04/2003–05/2015
SORCE/SOLSTICE	115.0–309.0	04/2003–05/2015
SORCE/XPS	0.5–39.5	04/2003–05/2015
TIMED/SEE-EGS	27.1–189.8	02/2002–02/2013
TIMED/SEE-XPS	1.0–9.0	01/2002–11/2014
UARS/SOLSTICE	119.5–419.5	10/1991–09/2001
UARS/SUSIM	115.5–410.5	10/1991–08/2005

The SOLID composite is currently available for the time frame of November 8, 1978 to December 31, 2014; for further details see (Haberreiter et al., 2017).

Let us stress that the foremost aim has been to keep the observations, and ultimately the

Our aim was to keep this composite fully independent from existing models. This means that no SSI models have been used to correct the observational data, which were are taken at their face value, without any correction.

One challenge of this - as with any statistical - approach is its dependence reliance on the number of independent datasets. While for the past decades several missions were dedicated to measuring the UV band of the solar spectrum, the picture becomes more bleak when it comes to the visible part bleaker when considering recent observations in the visible and near-UV parts of the spectrum. In that band, only observations After 2003, the only remaining observations are from SORCE/SIMare available. Clearly, this means , whose out-of-phase behavior (Harder et al., 2009) is controversial (Lean and DeLand, 2012; Ermolli et al., 2 Let us therefore stress that the SOLID composite relies entirely on the SORCE/SIM dataset in this spectral region. The

Table 2. Proxies used in addition to the original SSI data in order to fill in data gaps.

Name of proxy	Origin (Observatory)	relevant for
30.0 cm radio flux	Nobeyama/Toyokawa	UV
15.0 cm radio flux	Nobeyama/Toyokawa	UV
10.7 cm radio flux	Penticton/Ottawa	UV
8.2 cm radio flux	Nobeyama/Toyokawa	UV
3.2 cm radio flux	Nobeyama/Toyokawa	UV
sunspot darkening	Greenwich/SOON netw.	VIS

controversial out-of-phase behavior of SORCE/SIM observations in that band (Harder et al., 2009) are likely to be an instrumental artefact (Lean and DeLand, 2012; Ermolli et al., 2013) but this has not yet been corrected in the SOLID compositeis based on observations only, and will necessarily undergo revisions as new physical constraints are incorporated, or new versions of the datasets are released.

2.1.2 CMIP6 Recommended Solar Irradiance Forcing

NRLSSI and SATIRE are not the only available models for reconstructing the SSI (Ermolli et al., 2013). However, they are the only ones that have been widely tested, and can easily cover the 1850–2300 time span for CMIP6 with one single and continuous record. The resulting homogeneity in time is a major asset of our reconstructions, and a necessary condition for obtaining a realistic solar forcing.

NRLSSI and SATIRE agree well on time scales of days to months, but exhibit more pronounced differences on longer time scales, which have fueled a debate (e.g. Yeo et al., 2015) that is unlikely to settle soon. The two models have been derived independently, and as of today there is no consensus regarding their relative performance. In this context, and until additional information may help us better constrain long-term variabilityfor the time being, the most reasonable approach (in a maximum likelihood sense) consists in averaging both their reconstructions, weighted by their uncertainty. However, since Since in addition we are lacking uncertainties that can be meaningfully compared, our current recommendation is an to simply take the arithmetic mean of the two model datasets: (i) the empirical model NRLTSI2 and NRLSSI2 (?)(Coddington et al., 2016), and (ii) the semi-empirical model SATIRE-TS (Yeo et al., 2014). Clearly, this solution can be improved in the future as better reconstructions and observational composites (including SOLID) will become availableSATIRE (Yeo et al., 2014). Note that multi-model averaging is a widely-used practice in climate modelling (e.g Smith et al., 2013).

For historical data (Jan 1, 1850 – Dec 31, 2014) both models rely, as described above, on one or several of: the international sunspot number V1.0, sunspot area distribution (after 1882), solar photospheric magnetic field (after 1974), and the Mg II MgII index (after 1978). Since NRLSSI2 and NRLTSI2 have yearly averages only before 1882, we reconstructed sub-yearly variations by using an ARMAX (AutoRegressive Moving Average with eXogeneous input) model (Box et al., 2015) with that uses the sunspot number as input.

The EUV band (10-121 nm) is required for CMIP6 but is ~~absent from NRLSSI and SATIRE. We~~ not provided by NRLSSI2 and SATIRE, whose shortest wavelength is 115.5 nm. We thus added it with spectral bins from 10.5-114.5 nm by using a nonlinear regression from the SSI in the 115.5~~-188.5~~–123.5 nm band, trained with TIMED/SEE data from 2002 to ~~2009.~~ 2011. This is further detailed in Appendix A.

In some climate models the EUV flux is parameterised as a function of the F10.7 index, which is the daily radio flux at 10.7 cm from Penticton Observatory, adjusted to 1 AU, and measured daily since 1947 (Tapping, 2013). For practical purposes, we also provide this index. Values prior to 1947 are obtained by multi-linear regression to the first 20 principal components of the SSI and application of minor non-linear adjustments. Let us note that while the F10.7 index is a good proxy for EUV variability on daily to yearly time scales, this may not be true anymore on multi-decadal time scales. As of today, the lack of direct EUV observations does not allow us to constrain its long-term evolution, whereas the F10.7 index at solar minimum has not significantly varied since 1947, when its first measurements started.

The dataset, together with a technical description, and a routine for how to read and integrate the SSI data to the radiation bands used in climate models can be found at http://solarisheppa.geomar.de/cmip6. In addition, a recommendation on how to implement the SSI changes in the models is provided in the Appendix B. A detailed description of the CMIP6 solar irradiance forcing in TSI and SSI, and a comparison to the CMIP5 recommendation is presented in the following.

Total Solar Irradiance (TSI)

Figure 1 presents time series of the TSI from the CMIP5, CMIP6, and the original NRLTSI2 and ~~SATIRE-TS~~ SATIRE datasets, along with one ~~observed~~ observational composite from PMOD (version 42.64.1508)~~()~~[2]. We stress that all the data are taken at their face value, using their latest version, without any adjustments or scaling, except for NRLTSI1, whose value we uniformly reduced by 5 W/m^2 to account for the new recommendation for average TSI (see below).

All TSI records agree well on daily to yearly time scales, and in some cases (e.g. NRLTSI1 and NRLTSI2) they match as well on multi-decadal time scales. The major difference arises in the long-term behaviour of ~~SATIRE-TS~~ SATIRE and NRLTSI2, which impacts the CMIP6 composite, and leads to a weaker trend as compared to the CMIP5 recommendation (which was based on NRLTSI1 only). In both models, the historical reconstructions are sensitive to the assumptions made when constraining them to direct (satellite era) observations that suffer from large uncertainties. This mainly explains why these models differ before 1990 by an offset. There is no consensus yet as to which one better represents long-term solar variability, and this is what motivated us to average them for making the CMIP6 composite.

More subtle differences between the different TSI datasets arise in the satellite era, especially with the unusually deep solar minimum that occurred in 2008-2010: the NRLTSI2 model has a weak negative trend between successive solar minima, whereas the ~~SATIRE-TS~~ SATIRE reconstruction exhibits a larger one. The resulting trend in the CMIP6 composite is comparable to the observational TSI composite from PMOD (grey area). Figure 1 does not show any model uncertainties, because these are either absent or difficult to compare. We do provide uncertainties, however, for the observational PMOD composite, based on an instrument-independent approach that is described in ~~Dudok de Wit et al. (2016b)~~(Dudok de Wit et al., 2016a).

[2] https://www.pmodwrc.ch/pmod.php?topic=tsi/composite/SolarConstant

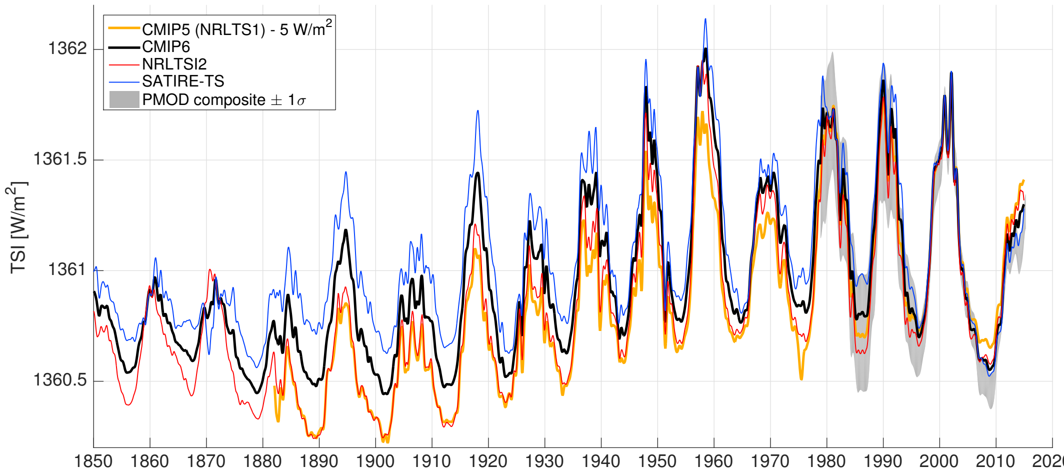

Figure 1. Comparison of several TSI reconstructions, showing 6-month running averages of: the NRLTSI1 record (reference for CMIP5, and thus continuing after the 2010 end date of CMIP5), the CMIP6 composite, and the reconstructions from the NRLTSI2, and SATIRE-TS SATIRE models. Also shown is the observational composite from PMOD (version 42.64.1508) with a $\pm 1\sigma$ confidence interval. A negative offset of -5 W/m^2 has been applied to the NRLTSI1 record to account for the change in average TSI that occurred between CMIP5 and CMIP6.

Note that both models are mostly within the $\pm 1\sigma$ confidence interval, which highlights how delicate it is to constrain them by observational data.

After CMIP5, the recommended value of the average TSI during solar minimum was reduced from 1365.4 ± 1.3 W/m^2 to a lower value of 1360.8 ± 0.5 W/m^2 after reexamination by Kopp and Lean (2011), later confirmed independently by Schmutz et al. (2013). Based on this, the International Astronomical Union recently recommended 1361.0 ± 0.5 W/m^2 as the nominal value of the TSI, averaged over solar cycle 23(, which lasted from 1996 to 2008) (Mamajek et al., 2015)(Prša et al., 2016). Our CMIP6 composite complies with this recommendation.

To summarise for the TSI: the CMIP6 and CMIP5 recommendations are comparable on decadal and sub-decadal time scales. They differ, however, by a weaker secular trend in CMIP6. Between 1980 and 1880, the difference TSI(CMIP6)-TSI(CMIP5) progressively increases from 0.1 to 0.4 W/m^2 (after correcting the aforementioned 5 W/m^2 offset in CMIP5). This results in a weaker change in solar forcing, which will be detailed in Sec. 2.1.3.

To estimate the impact of these different trends on the radiative forcing (RF), we have conducted a high spectral resolution calculation using a single profile with a line-by-line radiative transfer code (libradtran) described in more detail below. This indicated an instantaneous change in downward solar flux of -0.16 W/m^2 over the 1986-2009 period for the combined CMIP6 dataset. A crude estimate of the global mean forcing from this change is -0.04 W/m^2, which is relatively small in comparison to other forcings over this period.

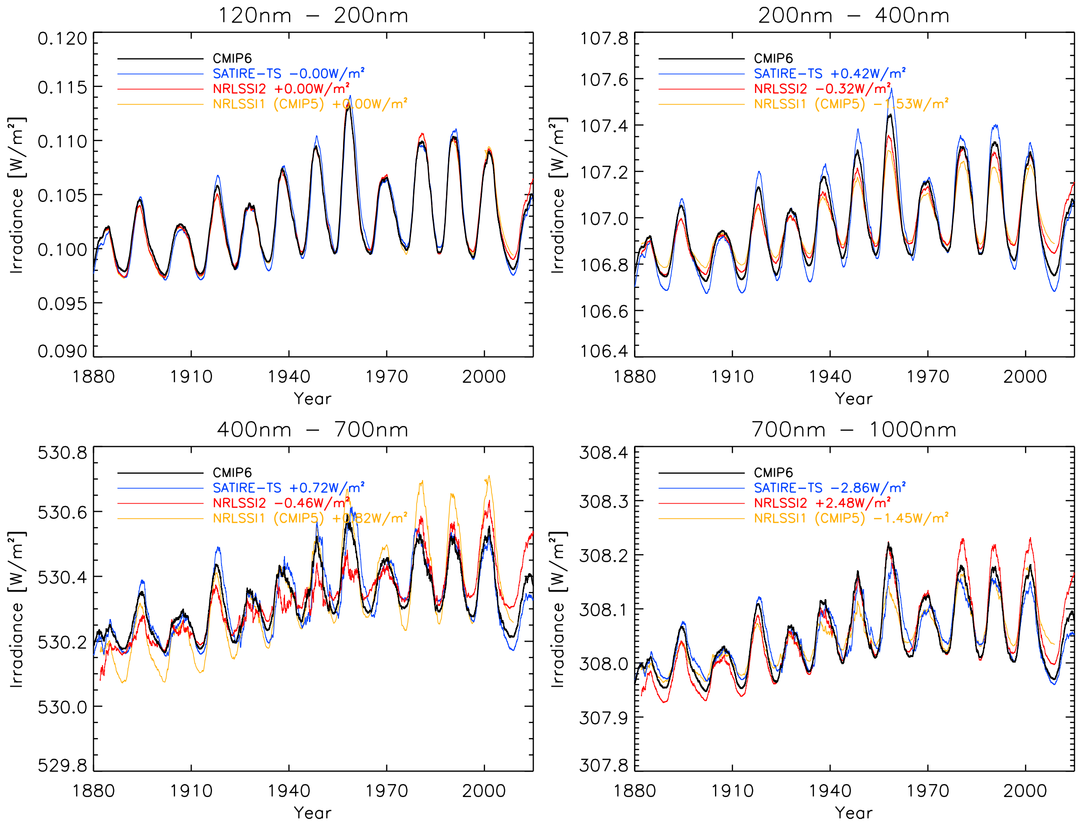

Figure 2. SSI time series from 1882 to 2014, integrated over following wavelength ranges: 120-200 nm (top left), 200-400 nm (top right), 400-700 nm (bottom left), and 700-1000 nm (bottom right). An offset, indicated in the legend, has been added to each time series, to ease visualisation. All time series are running averages over 2 years.

Solar Spectral Irradiance (SSI)

To investigate differences and similarities between the SSI datasets, following Ermolli et al. (2013), we concentrate on four specific wavelength ranges, 120–200 nm (UV1), 200–400 nm (UV2), 400–700 nm (VIS), and 700–1000 nm (NIR), with special emphasis on the CMIP5 (i.e NRLSSI1) and the CMIP6 (~~(~~average of NRLSSI2 ~~+SATIRE-TS) /2)~~ and SATIRE) datasets. These ranges are relevant for climate studies, see for example Table 3 below. Figure 2 shows the SSI time series from 1880 through 2014. Note that we added vertical offsets by adjusting the mean values to facilitate their comparison, using ~~the~~ CMIP6 as a reference. We note that:

– The long-term increase from 1880 to 1980 is similar in all datasets (NRLSSI1 might appear to have larger long-term increase in the VIS but this is mostly caused by different solar cycle amplitudes). ~~SATIRE-TS~~ SATIRE predicts a slightly larger increase in the UV2 (+0.03 W/m^2 with respect to NRLSSI2) from 1880 to 1930 compensated by a smaller increase in the VIS. NRLSSI2 has a larger but still small increase (+0.07 5W/m^2 with respect to ~~SATIRE-TS~~SATIRE) in the NIR

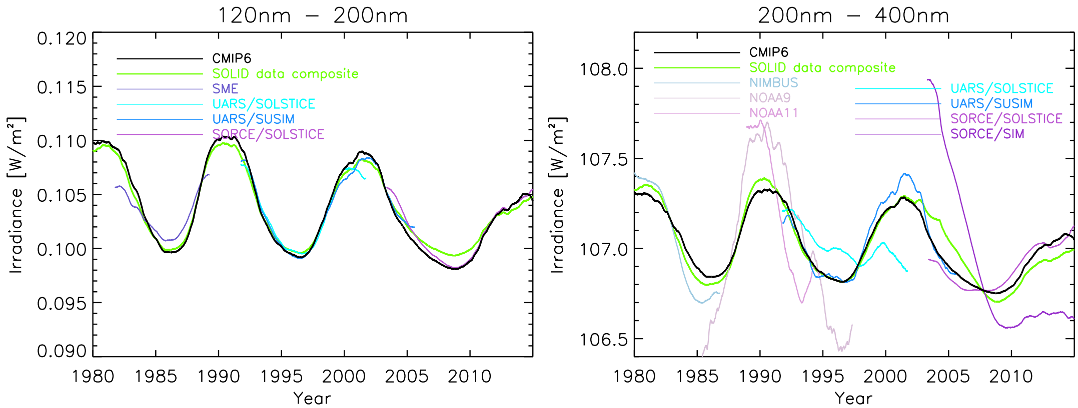

~~CMIP6 recommended SSI time series (black) from 1950 to 2015 together with the SOLID data composite (green) and relevant instrument observations for the following wavelength bins: 120nm–200nm (left), 200nm–400nm (right). The SOLID and instrument time series have been adjusted to match the average level of the CMIP6 time series. All time series are running averages over 2 years.~~

Figure 3. CMIP6 recommended SSI time series (black) from 1980 to 2015 together with the SOLID data composite (green) and relevant instrument observations for the following wavelength bins: 120nm–200nm (left), 200nm–400nm (right). The SOLID and instrument time series have been adjusted to match the average level of the CMIP6 time series. Note that SORCE/SOSLTICE only covers 200nm-309nm and SORCE/SIM only 240nm-400nm. All time series are running averages over 2 years.

from 1880 to present, which was also present in NRLSSI1 (CMIP5). Before 1970, NRLSSI2 shows less smoothed cycles with respect to the other models in the visible. The major difference ~~come from SATIRE-TS~~ on the long-term trend comes from SATIRE after 1985 (see below).

– As already described for the TSI behaviour above (Fig. 1), ~~SATIRE-TS~~ SATIRE predicts a significant downward trend of the baseline for the last three solar cycles, as can be seen by comparing the SSI at solar minima between cycles 21 & 22 (1985), 22 & 23 (1995), and 23 & 24 (2008). NRLSSI2 does not predict significant variations and therefore the recommended CMIP6 time series has a slower downward trend than ~~SATIRE-TS~~ SATIRE in the recent cycles. This trend was not apparent in the dataset recommended for CMIP5.

– The solar cycle variability in CMIP6 exceeds that of CMIP5, particularly in the UV2 and NIR ranges, while it is approximately the inverse in the VIS. The change in the NRLSSI model can be explained by the use of new, and higher-quality data from the SORCE mission on the rotational timescale in NRLSSI2, while NRLSSI1 was based on data from older satellite missions. In the UV2, ~~SATIRE-TS~~ SATIRE predicts larger solar cycle amplitudes, which can be explained by a larger weight of the network at these wavelengths.

In Figure 2, the apparently less regular solar cycle reconstruction by NRLSSI2 between 1940 and 1960 is most likely caused by the transition from one sunspot record to another in that model, (see Coddington et al., 2016).

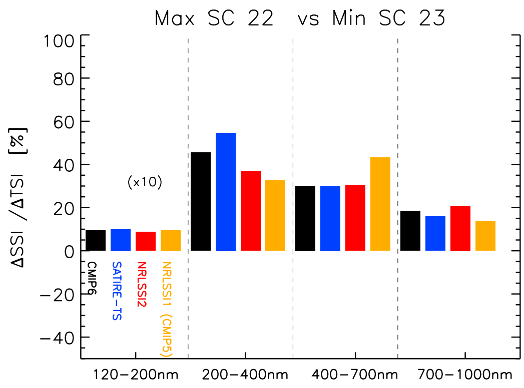

Figure 4. Contribution in percent of various wavelength ranges to the TSI variability between the maximum of cycle 22 and the minimum between cycles 22 and 23. Contributions between 120 nm and 200 nm have been multiplied by 10 for improved visibility. Maximum and minimum values have been taken over an 81-day period centered on November 1989 and on November 1994, respectively.

Figure 3 compares our CMIP6 dataset with the observational SOLID composite (see description above) and some direct SSI satellite observations. Generally speaking, the observations and observation-based composite agree very well with each other, and the CMIP6 dataset up to 200 nm. Larger cycle variations than in the CMIP6 SSI occur above about 200 nm in the observations. Such discrepancies are inherent to the observation of small variations over eleven years. On the right panel of Fig. 3, one can notice the different influence of the various datasets on the SOLID composite, as a consequence of their uncertainty at different scales. For example, the SORCE/SIM data have only a minor (but significant) effect on the long-term variations of the composite. In the VIS and NIR part of the spectrum, the only available measurements are from the SORCE/SIM instrument, ~~which has calibration issues~~ whose solar-cycle variation is controversial (Lean and DeLand, 2012) and hence ~~cannot be meaningfully compared to the modeled SSI datasets.~~ should be considered with great caution.

Figure 4 shows the contribution of the different wavelength ranges to TSI variations between solar maximum on November 1989 (solar cycle 22) and solar minimum on November 1994 (between cycles 22 and 23) for the different solar irradiance models. ~~A similar figure can be found in Ermolli et al. (2013) except that its dates belong~~ Both extrema are averaged over 81 days. We use the same spectral bands and color coding as in Fig. 2 of the review by Ermolli et al. (2013). The latter figure, though, applies to the next solar cycle, when SORCE/SIM ~~was~~ is operating. Our dates coincide with the ones chosen in the CCM timeslice experiments, see Section 2.1.3.

Both SSI models agree very well for the 120-200 nm wavelength range. Discrepancies arise for wavelengths longward of 200 nm, as already discussed in Fig. 2. In the 200-400 nm range, the ~~SATIRE-TS~~ SATIRE model shows the largest variability, followed by NRLSSI2, and NRLSSI1. This results in a CMIP6 variability that is larger than for CMIP5, ~~50~~45% as compared to ~~35~~32% (Fig. 4). In the VIS range this reverses, CMIP6 shows a smaller variability than CMIP5 (~~25~~30% as compared to 40%). Remarkable is also the very good agreement between NRLSSI2 and ~~SATIRE-TS~~SATIRE. In the NIR CMIP6 shows

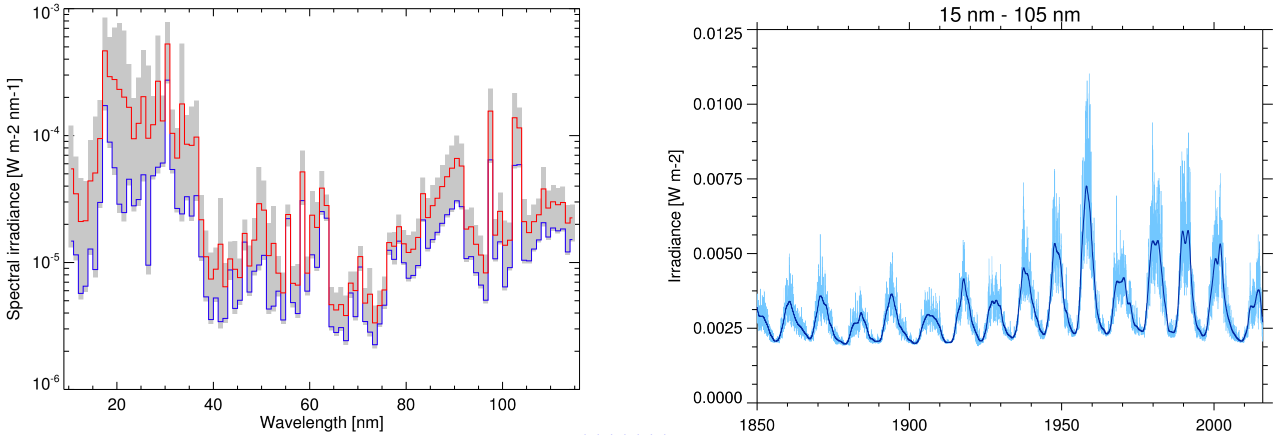

Figure 5. Left: EUV spectra for 20 November 2008 (corresponding to low solar activity conditions, in blue) and 8 February 2002 (corresponding to high solar activity conditions, in red). The full spectral variability range during 1850–2015 is grey-shaded. Right: Time series of the EUV irradiance integrated from 15–105 nm. The thick blue line corresponds to annual averages.

slightly larger variability than CMIP5~~and remarkable here is the largest variability in NRLSSI2~~. The implications of these different spectral variabilities on the atmospheric heating and ozone chemistry and subsequent thermal and dynamical effects with respect to both, climatological differences between CMIP5 and CMIP6 as well as the solar cycle signals in CMIP5 and CMIP6 will be discussed in section 2.1.3.

Figure 5 illustrates the reconstruction of the EUV band by comparing spectra obtained at high and low levels of solar activity, and by showing the historical reconstruction of the band-integrated flux. As explained in Section 2.1.2, we estimate the EUV flux by nonlinear regression from the SSI at longer UV wavelengths, using the first seven years of observations from TIMED/SEE. Not surprisingly, this reconstruction agrees well with the observations from TIMED/SEE. However, by lack of other long-duration EUV observations that are of sufficient radiometric quality, it is very difficult to assess the quality of our reconstruction. For the same reason, multi-decadal variations are poorly constrained, and in particular, the presence of trends remains largely unknown. Note that wavelengths below 28 nm require more caution, since they rely on TIMED/XPS observations that were partly degraded (Woods et al., 2005). One future improvement of our dataset involves reconstructions of the EUV band that are based more advanced models such as NRLEUV2 (Lean et al., 2011).

2.1.3 Evaluation of SSI Datasets in Climate Models

Providing a first assessment of implications employing the SSI recommended for CMIP6 in comparison to CMIP5, we present results of two state-of-the-art chemistry climate models (CCM): – the Whole Atmosphere Community Climate Model (CESM1(WACCM); Marsh et al., 2013) – and the ECHAM/MESSy Atmospheric Chemistry model (EMAC; Jöckel et al., 2010, 2016). Additionally, we include results of single-profile radiative transfer calculations performed with the line-by-line radiative transfer code *libradtran* (Mayer and Kylling, 2005). We use the latter to present estimates of direct SW radiative heating impacts neglecting the ozone chemistry feedback which is included in the CCM results.

Chemistry-Climate Model Descriptions

WACCM: The Whole Atmosphere Community Climate Model (version 4; Marsh et al., 2013) is an integrative part of the *Community Earth System Model* suite (version 1.0.6; Hurrell et al., 2013). CESM1(WACCM) is a "high-top" CCM covering an altitude range from the surface to the lower thermosphere, i.e. up to 5×10^{-6} hPa equivalent to approx. 140 km. It is an extension of the *Community Atmospheric Model* (CAM4; Neale et al., 2013) with all its physical parametrisations. For this study the model is integrated with a horizontal resolution of 1.9°lat×2.5°lon and 66 levels in the vertical. CESM1(WACCM) contains a middle atmosphere chemistry module based on the Model for Ozone and Related Chemical Tracers (MOZART3; Kinnison et al., 2007). It contains all members of the O_X, NO_X, HO_X, ClO_X, and BrO_X chemical groups as well as tropospheric source species N_2O, H_2O, CH_4, CFCs and other halogen components (59 species and 217 gas-phase chemical reactions in total). Its photolysis scheme resolves 100 spectral bands in the UV and VIS range (121-750 nm) (see also Tab. 3). The SW radiation module is a combination of different parametrisations. Above approx. 70 km the spectral resolution is identical to the photolysis scheme (plus the parametrisation of Solomon and Qian, 2005, based on F10.7cm solar radio flux to account for EUV irradiances). Below approx. 60 km the SW radiation of CAM4 is retained, employing 19 spectral bands between 200 and 5,000 nm (Collins, 1998). For the transition zone (60-70 km) SW heating rates are calculated as weighted averages of the two approaches. Tab. 3 contains an overview of the SW radiation and photolysis schemes in comparison to EMAC, the second CCM utilized for this study. CESM1(WACCM) features relaxation of stratospheric equatorial winds to an observed or idealized Quasi-Biennial Oscillation (QBO; Matthes et al., 2010).

EMAC: The ECHAM/MESSy Atmospheric Chemistry (EMAC) model is a CCM that includes sub-models describing tropospheric and middle atmospheric processes and their interaction with oceans, land and human influences (Jöckel et al., 2010). It uses the second version of the Modular Earth Submodel System (MESSy2) to link multi-institutional computer codes. The core atmospheric model is the 5th generation European Centre Hamburg general circulation model (ECHAM5, Roeckner et al., 2006). For the present study we applied EMAC (ECHAM5 version 5.3.02, MESSy version 2.51, Jöckel et al., 2016) in the T42L47MA-resolution, i.e. with a spherical truncation of T42 (corresponding to a quadratic Gaussian grid of approx. 2.8 by 2.8 degrees in latitude and longitude) with 47 hybrid pressure levels up to 0.01 hPa ($\sim$80 km). The applied model setup comprises, among others, the submodels: MECCA, JVAL, RAD/RAD-FUBRAD, and QBO. MECCA (Module Efficiently Calculating the Chemistry of the Atmosphere) (Sander et al., 2011a) provides the atmospheric chemistry model. JVAL (Sander et al., 2014) provides photolysis rate coefficients based on updated rate coefficients recommended by JPL (Sander et al., 2011b). RAD/RAD-FUBRAD (Dietmüller et al., 2016) provides the parameterisation of radiative transfer based on Fouquart and Bonnel (1980) and Roeckner et al. (2003) (RAD). For a better resolution of the UV-VIS spectral band RAD-FUBRAD is used for pressures lower than 70 hPa, increasing the spectral resolution in the UV-VIS from one band to 106 bands (Nissen et al., 2007; Kunze et al., 2014). Tab. 3 presents more details of the SW radiation and photolysis schemes in comparison to WACCM. The

Table 3. Summary of spectral resolution of the SW radiation and photolysis schemes in EMAC and CESM1(WACCM). Boundaries of spectral intervals and further refinement in brackets when larger than one.

Spectral region	Gases	CESM1(WACCM)	EMAC
SW radiation[*, +]			
Lyman-α	O_2		[121-122]
Schumann-Runge continuum	O_2		[125-175] (3)
Schumann-Runge bands	O_2		[175-205]
Herzberg cont./Hartley bands	O_2, O_3	[200-245]	[206.5-243.5] (15)
Hartley bands	O_3	[245-275] (2)	[243.5-277.5] (10)
Huggins bands	O_3	[275-350] (4)	[277.5-362.5] (18)
UV-A/Chappuis bands	O_3	[350-700] (2)	[362.5-690] (58)
Near Infrared/Infrared	O_2, O_3, CO_2, H_2O	[700-5000] (10)	[690-4000] (3)
Photolysis			
Lyman-α		[121-122]	[121-122]
Schumann-Runge continuum		[122-178.6] (20)	
Schumann-Runge bands		[178.6-200] (12)	[178.6-202]
Herzberg cont./Hartley bands		[200-241] (15)	[202-241]
Hartley bands		[241-291] (14)	[241-289.9]
Huggins bands		[291-305.5] (4)	[289.9-305.5]
UV-B		[305.5-314.5] (3)	[305.5-313.5]
UV-B/UV-A		[314.5-337.5] (5)	[313.5-337.5]
UV-A/Chappuis bands		[337.5-420] (17)	[337.5-422.5]
Chappuis bands		[420-700] (9)	[422.5-682.5]

[*]Note that given bands for CESM1(WACCM) apply below ∼65 km only. The resolution of the SW radiation code above ∼65 km corresponds to the resolution of the photolysis scheme. [+]Note that given bands from 121–690 nm for EMAC apply at pressures lower than 70 hPa only. At pressures larger than 70 hPa there is one band extending from 250–690 nm.

submodel QBO is used to relax the zonal wind near the equator towards the observed zonal wind in the lower stratosphere (Giorgetta and Bengtsson, 1999).

CCM Experimental Design

The CCM simulations with CESM1(WACCM) and EMAC are identically conducted in atmosphere-only timeslice configuration. This means, the external forcings such as the solar and the anthropogenic forcing are fixed for the whole simulation period, that is 45 model years plus spin-up (~5 years for EMAC, ~3 years for CESM1(WACCM)). Concentrations of greenhouse gases (GHGs) and ozone-depleting substances (ODS) are set to constant conditions representative for the year 2000. The lower-boundary forcing is specified by the mean annual cycle of SSTs and sea-ice of the decade 1995-2004 derived from the *HadISST1.1*-dataset (Rayner et al., 2003). All simulations are nudged towards an observed (EMAC) or idealized 28-months varying (CESM1(WACCM)) QBO. The only difference between the simulations is in the solar forcing. Four simulations for each of the following SSI datasets have been performed with EMAC and WACCM: CMIP6-SSI, its constituent datasets NRLSSI2 (?) and SATIRE-TS (Coddington et al., 2016) and SATIRE (Krivova et al., 2010; Yeo et al., 2014), as well as NRLSSI1 (Lean, 2000). The latter was recommended as solar forcing for CMIP5 including a uniform scaling of the spectrum to match TSI measurements of the *Total Irradiance Monitor* (TIM) instrument. As one emphasis of this study is to highlight differences to the previous phase of CMIP we employed NRLSSI1 including this scaling and refer to it as NRLSSI1(CMIP5) in the following. Runs for each of the four dataset have been performed with both CCMs for a solar minimum timeslice and a solar maximum timeslice, respectively. For solar maximum timeslices, SSIs averaged over Nov. 1989 are used (maximum of solar cycle 22) while for the solar minimum timeslices averages over Nov. 1994 are chosen. The latter does not match the absolute minimum of solar cycle 21/22 (Jun. 1996). However, solar activity in Nov. 1994 was already close to the minimum. The differences in solar activity between our solar minimum and solar maximum timeslices for the respective datasets are within a range of 0.988 W/m^2 for NRLSSI1(CMIP5) to 1.057 W/m^2 for NRLSSI2.

It should be noted that these experiments will illustrate only one part of solar influence on climate. Given the atmosphere-only set-up of the runs, oceanic absorption of (mainly visible) solar irradiance and subsequent heating and feedbacks to the atmosphere – the so-called bottom-up mechanism (see Gray et al., 2010, and references therein) – is not represented in our simulations. Therefore we focus only on stratospheric signals and "top-down" dynamically induced responses in the troposphere. A second constraint of this study's experimental set-up is the choice of one solar cycle. Solar activity and hence spectral irradiance vary between different solar cycles. However, these differences are small compared to the total 11 year relatively small as compared to a typical solar cycle amplitude and will probably not affect the main results of this study. It should also be noted that the timeslice simulations were designed as a sensitivity study to test the impact of the different solar input datasets. They do not represent the full feedbacks of transient CMIP6 simulations.

Radiative Transfer Model libradtran

Radiatiative transfer calculations were performed with the high resolution model libradtran (Mayer and Kylling, 2005), which is a library of radiative transfer equation solvers widely used for UV and heating rate calculations (www.libradtran.org). Libradtran was configured with the pseudo-spherical approximation of the DISORT solver, which accounts for the sphericity of the atmosphere, running in a six-streams mode. Calculations pertain to a cloud- and aerosol-free tropical atmosphere (0.56°N), the surface reflectivity is set to a constant value of 0.1 and effects of Rayleigh scattering are enabled. The atmosphere is portioned into 80 layers extending from the surface to 80km. The model output is annual averages of spectral heating rates from 120 nm to 700 nm in 1 nm spectral resolution, calculated according to the recommendations for the Radiation Intercomparison of the Chemistry-Climate Model Validation Activity (CCMVal) (Forster et al., 2011). As for the CCM simulations described above, calculations of the heating rates were performed for CMIP6-SSI, SATIRE-TSSATIRE, NRLSSI2 and NRLSSI1(CMIP5). The same climatological ozone profile is specified for both solar maximum and minimum conditions in order to assess the direct effects in atmospheric heating by SSI variations only. As such, the line-by-line calculations do not take into account the positive ozone feedback with the solar cycle and SW heating rate changes are expected to be weaker compared to the signatures in the two CCM simulations.

Methods

The analyses presented in the following consist of differences between climatologies derived from the various simulations. Given the timeslice configuration of the CCM runs with all external forcings equal except for the SSI dataset, we assume that statistically significant differences of two climatologies are the result of the differing solar irradiance forcings. Confidence intervals (95%) as presented in Figs. 6 and 8 as well as statistical significances ($p<5\%$) as marked in Figs. 10 and 11 are based on 1000-fold bootstrapping. Confidence intervals in Figs. 6 and 8 are only given for the CCM-results related to CMIP6 SSI.

Climatological Differences to CMIP5

Although all solar irradiance reconstructions subject to this analysis agree fairly well in TSI (see Fig. 1), they disagree significantly with respect to the spectral distribution of energy input, i.e. the shape of the solar spectrum. This is obvious from the offsets noted in Fig. 2 for the different spectral regions above 200 nm. Hence, we focus first on the climatological differences between the solar forcing in CMIP5 and CMIP6. We therefore compare the minimum timeslice simulations from the two CCMs and libradtran in Fig. 6 with respect to the climatological annual mean SW heating rates, as well as the temperatures, and ozone concentrations between the two CCMs resulting from CMIP6-SSI, NRLSSI2, and ~~SATIRE-TS~~SATIRE, respectively, as differences to equivalent simulations forced by NRLSSI1(CMIP5). The profiles represent the tropical (averaged over 25°S-25°N) stratosphere and mesosphere (100–0.01 hPa) for annual mean conditions for the CCMs and libradtran.

Employing CMIP6-SSI results into significantly decreased radiative heating of large parts of the mesosphere and stratosphere (above 10 hPa) compared to NRLSSI1(CMIP5). Whereas the largest differences can be found at the stratopause with approx. -0.35 K/day according to both CCMs, and even more -0.42 K/day for libradtran (without any ozone chemistry feedback), libradtran and EMAC yield slightly increased SW heating rates below ~7 hPa and 10 hPa, respectively. This weaker SW heating in the new CMIP6 SSI datset in the upper stratosphere and the stronger heating in the lower stratosphere are confirmed by the wavelength dependent percentage changes between the CMIP6 and CMIP5 SSI datasets with respect to the radiation and photolysis schemes (Fig.7). Regardless of the number of bands in the radiation code, both models show a smaller percentage difference of -5% below about 300nm and weaker or negligible differences above 300nm (Fig.7).

Significant differences in radiative heating throughout the stratosphere related to the three state-of-the art SSI reconstructions are produced only with radiation codes of high spectral resolution such as in libradtran or – to a lesser degree – in EMAC (for the middle to lower stratosphere). Comparisons between CMIP6-SSI and its constituents NRLSSI2 and ~~SATIRE-TS~~ SATIRE in WACCM and EMAC lead to the conclusion that the choice of the CCM and its specific radiation and photolysis scheme is more important than the choice of the SSI dataset with respect to SW heating rates. In addition the ozone chemistry damps the SW heating response in the CCMs as compared to libradtran which misses the ozone feedback. Less SW radiation below

300nm reduces ozone production (note also the reduced photolysis rates around 240nm in Fig.7) and hence less ozone is available to absorb SW radiation and results in a relative cooling of the upper stratosphere.

Corresponding to the SW heating rate differences, large parts of the stratosphere and mesosphere are significantly cooler (up to -1.6K at the stratopause) in simulations using CMIP6-SSI compared to NRLSSI1(CMIP5) irradiances. Note that libradtran results are shown for the SW heating rate differences only, as temperature and ozone profiles are prescribed for the radiative transfer calculations. No significant differences in temperature are found when employing NRLSSI2 or ~~SATIRE-TS~~ SATIRE instead of CMIP6-SSI in CESM1(WACCM) which has a coarser spectral resolution in the SW heating parameterization than EMAC (Tab.3 and Fig.7). EMAC instead simulates significantly lower (higher) temperatures in the stratosphere when using NRLSSI2 (~~SATIRE-TS~~SATIRE) than CMIP6-SSI forcing and in general a warmer stratosphere (and cooler stratopause and mesosphere) than CESM1(WACCM).

The impact of CMIP6-SSI as compared to NRLSSI1(CMIP5) irradiance changes on ozone are more complicated. In the middle tropical stratosphere, ozone concentrations are significantly lower (peaking at ~7 hPa with approx. -3.2%). In contrast, ozone concentrations around the stratopause are significantly higher for CMIP6-SSI (+0.8% and +1.6% according to EMAC and CESM1(WACCM), respectively) than under NRLSSI1(CMIP5) irradiances. Despite the considerable differences in spectral resolution of the photolysis schemes (Tab.3 and Fig.7)), for larger parts of the stratosphere below about 3hPa, CESM1(WACCM) and EMAC agree fairly well. For both models the ~~SATIRE-TS~~ SATIRE irradiances show larger signals than NRLSSI2 irradiances with the signal for CMIP6 in between. The ozone signals start to differ at and above the stratopause, probably due to the more detailed photolysis code and the higher model top in CESM1(WACCM) as compared to EMAC. The ozone signal is much more uncertain with respect to the different SSI forcings than the SW heating rate and the temperature signals.

In summary, the CMIP6-SSI irradiances lead to lower SW heating rates, lower temperatures as well as smaller ozone signals in the lower stratosphere and larger ozone signals in the upper stratosphere and lower mesosphere than the CMIP5-SSI irradiances. Differences between the three tested SSI datasets occur in the SW heating rates only with a very high spectral resolution of the radiation code (libradtran, EMAC) and more prominent for ozone in a similar way for both CCMs, i.e. stronger effects occur for ~~SATIRE-TS~~ SATIRE than NRLSSI2. These direct radiative effects in the tropical stratosphere lead to a weakening of the meridional temperature gradient and hence to a statistically significant weakening of the stratospheric polar night jet in early winter (not shown).

Impacts of Solar Cycle Variability

The second question tackled by this evaluation is the atmospheric impact of the 11-year solar cycle using different SSI irradiance reconstructions. A special focus lies on the comparison of the new CMIP6 dataset with its predecessor NRLSSI1(CMIP5). Fig. 8 provides annual mean tropical (25°S-25°N) profiles analogue to Fig. 6 but now illustrating differences between perpetual solar maximum and perpetual solar minimum conditions according to simulations forced by the various SSI-datasets.

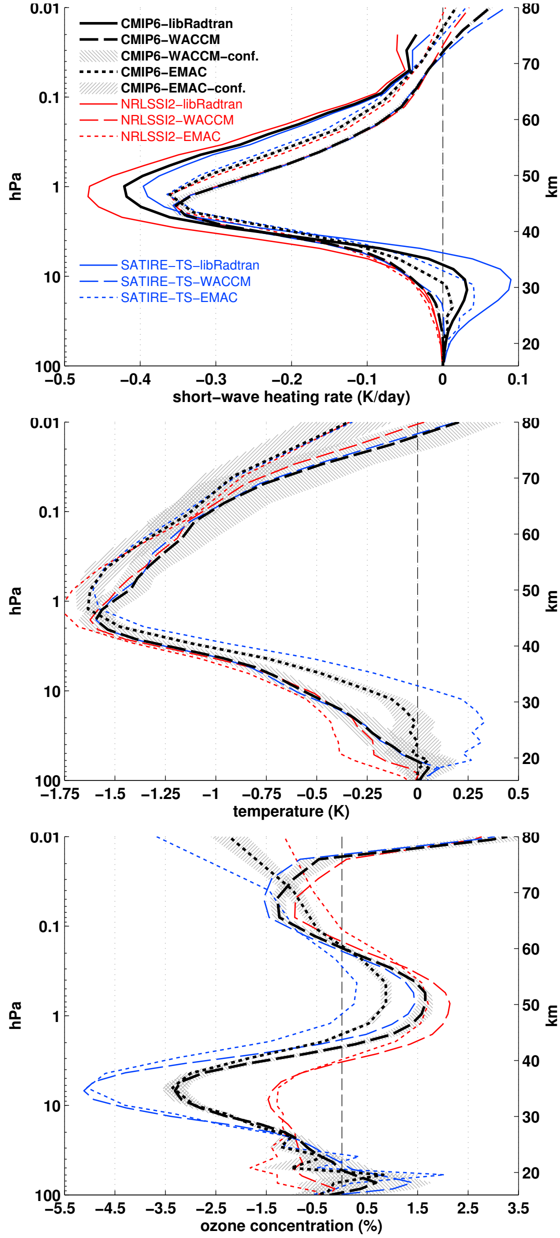

Figure 6. Impact of solar forcing for perpetual solar minimum conditions according to CMIP6 (black) as well as constituent NRLSSI2 (red) and ~~SATIRE-TS~~ SATIRE (blue) datasets on climatological (annual mean) profiles of SW heating rates (top), temperature (center), and ozone concentrations (bottom) averaged over the tropics (25°S–25°N) when compared to NRLSSI1(CMIP5) solar forcing; derived from simulations with CESM1(WACCM) (long-dashed), EMAC (short-dashed), and libradtran radiative transfer calculations (solid, only top panel) only shown for SW heating rates; 95% confidence intervals for CMIP6 simulations (hatched) estimated by bootstrapping.

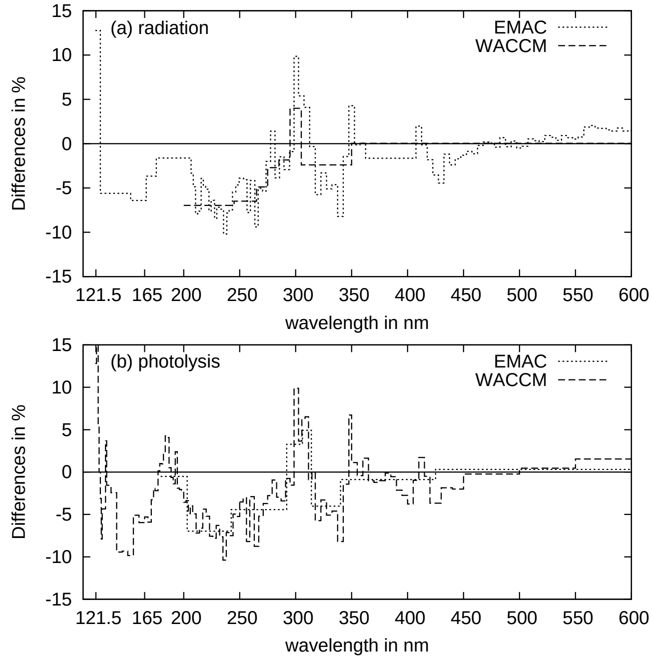

Figure 7. CMIP6 SSI differences of the solar irradiance in % for perpetual solar minimum conditions compared to CMIP5(NRLSSI1). Top: in the spectral resolution of the radiation schemes; bottom: in the spectral resolution of the photolysis schemes of EMAC (short-dashed) and CESM1(WACCM) (long-dashed).

All models and SSI-forcings produce the well-known solar cycle impact of enhanced SW heating at solar maximum throughout the upper stratosphere and mesosphere. Differences to solar minimum forcing peak at the stratopause with approx. +0.19 to +0.23 K/day. Only the libradtran-calculations – that do not include any ozone-feedback – yield considerably weaker responses.

According to libradtran and CESM1(WACCM), CMIP6-SSI produces slightly higher SW heating rates rate differences than NRLSSI1(CMIP5). However, for EMAC this is not the case. For both CCMs and libradtran, the usage of SATIRE-TS SATIRE leads to strongest solar cycle induced SW heating rate signals, while NRLSSI2 is associated with the weakest response (though not significantly different from NRLSSI1(CMIP5) for EMAC and libradtran).

Temperatures in the tropical stratosphere and mesosphere are generally higher during solar maximum than during phases of low solar activity. A local maximum of temperature differences is found at the stratopause with positive differences of 0.8-1.0 K compared to solar minimum. According to both CCMs, CMIP6-SSI forcing yields slightly higher temperatures (up to +0.2 K in the mesosphere in CESM1(WACCM)) for the stratopause region and the (lower) mesosphere than NRLSSI1(CMIP5). However, most of these differences are statistically not significant. Comparing CMIP6-SSI-forced results with its components NRLSSI2 and SATIRE-TS SATIRE yields heterogeneous results. According to EMAC, NRLSSI2 leads to a slightly weaker solar cycle response throughout the stratosphere, while the mesospheric response is stronger than SATIRE-TS SATIRE and CMIP6-SSI. CESM1(WACCM)-results show that the stratospheric (up to approx. 2 hPa) solar cycle response to CMIP6-

SSI-forcing in temperature is slightly weaker than in both, NRLSSI2- and SATIRE-TS-driven SATIRE-driven simulations. As opposed to that, simulations forced by SATIRE-TS SATIRE and CMIP6-SSI yield very similar warming signals in the mesosphere while NRLSSI2 produces a (significantly) weaker response in the mesosphere.

The solar cycle signal in ozone is very consistent for most parts of the stratosphere and mesosphere with respect to the SSI datasets. More important for the solar ozone signals seems to be the choice of the CCM (with its specific photolysis scheme, see also Fig. 9), especially for the lower stratosphere (10 hPa and below). In the lower mesosphere however, the dataset induced differences are larger than the model-induced ones. All analyzed combinations of CCMs and forcing datasets agree very well on the (relative) peak of the ozone response (+2.3-2.5%) to the solar cycle at 3-5 hPa. In the lower mesosphere (0.2-1 hPa) CMIP6-SSI (and SATIRE-TSSATIRE) lead to a significantly weaker solar cycle ozone response (+0.3-0.5% at 0.5 hPa) than NRLSSI1(CMIP5) (and NRLSSI2; +0.6-0.8% at 0.5 hPa). For the lower stratosphere (below 7 hPa) both CCMs agree that SATIRE-TS SATIRE leads to strongest solar cycle ozone signals, though still within the uncertainty associated with CMIP6-SSI-forced simulations. The comparison between CMIP6-SSI and NRLSSI1(CMIP5) yields no unequivocal result: CESM1(WACCM) exhibits a secondary maximum ozone response at approx. 70 hPa that is weaker with CMIP6-SSI than with NRLSSI1(CMIP5) while the opposite is seen in EMAC. Given the large uncertainty in the lower stratospheric solar ozone signal, we can only conclude that the signal is positive.

In summary, the CMIP6-SSI irradiance forcing leads to slightly enhanced solar cycle signals in SW heating rates, temperatures as well as ozone than the CMIP5-SSI irradiance forcing. In general, differences between the different SSI datasets are statistically not significant. Note that statistically significant irradiance differences differences in the irradiance amplitude between CMIP5 and CMIP6-SSI irradiances are particularly observed between 300 and 350nm, a wavelength region important for ozone destruction (below 320nm) consistently in both CCMs (Fig. 9).

The direct radiative effects in the tropical stratosphere from the CMIP6-SSI dataset, i.e. enhanced solar cycle signals in SW heating rates, temperatures, and ozone in the tropical upper stratosphere lead to the expected strengthening of the meridional temperature gradient and hence to a statistically significant stronger stratospheric polar night jet which propagates poleward and downward during winter from December through January (Fig. 10) and significantly affects the troposphere with a positive AO-like signal developing in late winter, i.e. January and February (Fig. 11). This signal is very similar and statistically significant for both CCMs, therefore the ensemble mean of both models is shown. Besides the radiative impact of the solar cycle, also energetic particles have an impact on the atmosphere and will be discussed in the following.

2.2 Particle Forcing

Precipitating energetic particles ionize the neutral atmosphere leading to the formation of NO_x ([N] + [NO] + [NO_2]) and HO_x ([H] + [OH] + [HO_2]) (Porter et al., 1976; Rusch et al., 1981; Solomon et al., 1981) as well as of some more minor species (Verronen et al., 2008; Funke et al., 2008; Winkler et al., 2009; Verronen et al., 2011a; Funke et al., 2011) due to both dissociation and ionization of the most abundant species, as well as due to complex ion chemistry reaction chains. The formation of NO_x and HO_x radicals leads to catalytic ozone loss that further triggers changes of the thermal and dynamical structure of the middle atmosphere. Energetic Particle Precipitation (EPP) introduces thus chemical changes to the middle atmospheric

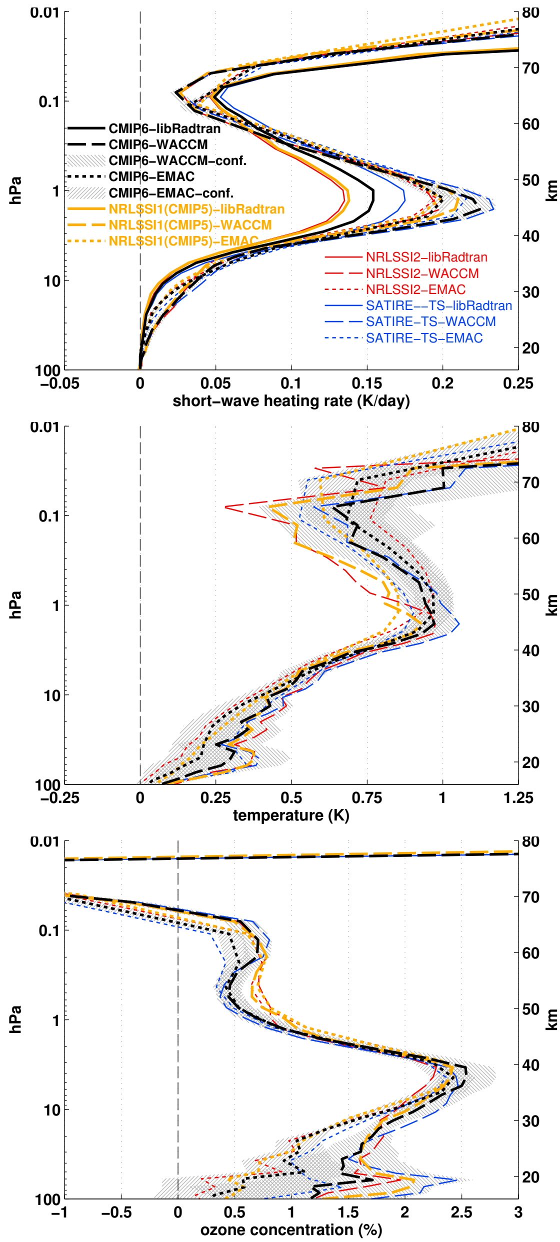

Figure 8. Impact of the 11-year solar cycle (differences between perpetual solar maximum and solar minimum experiments) on climatological (annual mean) profiles of shortwave heating rates (top), temperature (center), and ozone concentrations (bottom) averaged over the tropics (25°S–25°N) according to CMIP6 (black) and CMIP5 (yellow) solar forcing as well as NRLSSI2 (red) and SATIRE (blue) derived from simulations with CESM1(WACCM) (long-dashed), EMAC (short-dashed), and libradtran radiative transfer calculations (solid; only in the top panel); 95% confidence intervals for CMIP6 simulations (hatched) estimated by bootstrapping.

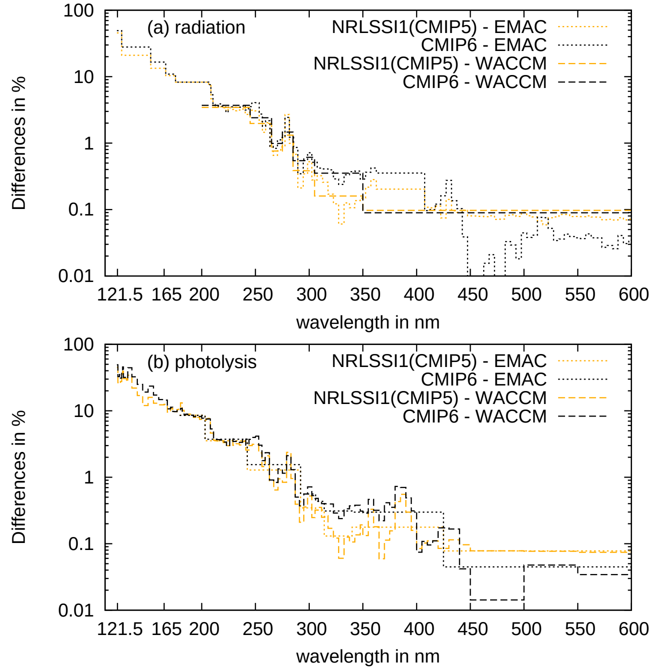

Figure 9. SSI differences in % for the solar amplitude between perpetual solar maximum and perpetual solar minimum conditions. Top: in the spectral resolution of the radiation schemes; bottom: in the spectral resolution of the photolysis schemes of EMAC (short-dashed) and CESM1(WACCM) (long-dashed).

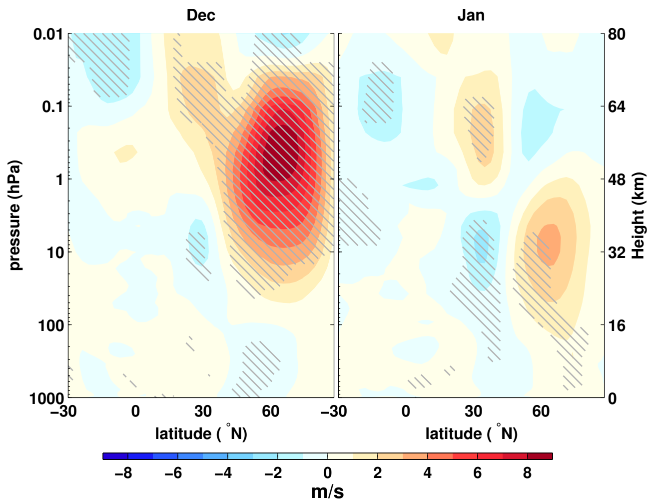

Figure 10. Zonal mean zonal wind response to the 11-year solar cycle according to CMIP6-SSI in December and January as "ensemble mean" of CESM1(WACCM) and EMAC simulations; hatched areas denote statistical significances (p<5%) of shown differences.

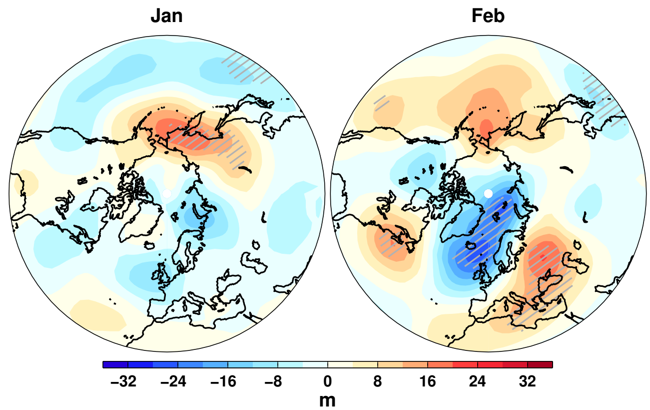

Figure 11. 500 hPa geopotential height response to the 11-year solar cycle according to CMIP6-SSI in January and February as “ensemble mean” of CESM1(WACCM) and EMAC simulations; hatched areas denote statistical significances ($p<5\%$) of shown differences.

composition and can therefore only be considered explicitly in climate simulations that employ interactive chemistry. In the following we provide recommendations for the consideration of EPP effects in CCMs separately for auroral and radiation belt electrons (Sec. 2.2.1), for solar protons (Sec. 2.2.2), and for galactic cosmic rays (Sec. 2.2.3). In most cases, particle forcing can be expressed in terms of ion pair production rates. Recommendations for their implementation into chemistry schemes are provided in Sec. 2.2.4.

2.2.1 Geomagnetic Forcing (Auroral and Radiation Belt Electrons)

Energetic particles are trapped in the space around the Earth dominated by the geomagnetic field (known as the magnetosphere). The loss of electrons into the atmosphere is termed “electron precipitation”. Due to the Earth’s magnetic field configuration electron precipitation occurs mainly in the polar auroral and sub-auroral regions, i.e., at geomagnetic latitudes ~~that~~ typically higher than 50°. Enhanced loss fluxes are associated with geomagnetic storms, which can occur randomly, and also with periodicity’s ranging from the ∼27 day solar rotation to the 11-year solar cycle, and even to multi-decadal timescales. The altitudes at which precipitating electrons deposit their momentum are dependent on their energy spectrum, with lower energy particles impacting the atmosphere at higher altitudes than those with higher energies (e.g. Turunen et al., 2009). Auroral electrons, originating principally from the plasma sheet, have energies <10 keV and affect the lower thermosphere (95–120 km). Processes that occur in the outer radiation belt typically generate mid-energy electron (MEE) precipitation within the energy range ∼10 keV to several MeV, affecting the atmosphere at altitudes of ∼50–100 km (Codrescu et al., 1997).

Odd nitrogen, produced by precipitating electrons, is long-lived during polar winter and can then be transported down from its source region into the stratosphere, to altitudes well below 30 km. This has been postulated already by Solomon et al. (1982) and observed many times (Callis et al., 1996; Randall et al., 1998; Siskind, 2000; Funke et al., 2005; Randall et al., 2007). This so-called EPP “indirect effect” contributes significant amounts of NO_y to the polar middle atmosphere during every winter in both hemispheres, however, with varying magnitude ranging from a few percent up to 40% (Randall et al., 2009; Funke et al., 2014a). Its consideration in climate models with their upper lid in the mesosphere, thus not covering the entire EPP source region, requires the implementation of an upper boundary condition (UBC) that accounts for the transport of NO_x into the model domain, as discussed below.

Stratospheric ozone loss due to electron-induced NO_x production in the upper mesosphere /lower thermosphere and subsequent downward transport has been postulated by model experiments many times (Solomon et al., 1982; Schmidt et al., 2006; Marsh et al., 2007; Baumgaertner et al., 2009; Reddmann et al., 2010; Semeniuk et al., 2011; Rozanov et al., 2012). However, observational evidence for EPP-induced variations of stratospheric ozone linked to geomagnetic activity, characterised by a negative anomaly moving down with time during polar winter, have been given only very recently (Fytterer et al., 2015a; Damiani et al., 2016).

In addition, mesospheric ozone effects have been observed (Andersson et al., 2014a; Fytterer et al., 2015b) which are caused by HO_x increases during MEE precipitation (?)(Verronen et al., 2011b). Although the HO_x-driven response is short-lived, the frequency of MEE events is large enough to cause solar cycle variability in ozone (Andersson et al., 2014a). HO_x response is seen at magnetic latitudes connected to the outer radiation belts, with e.g. the yearly amount of HO_x varying with the observed magnitude of precipitation (Andersson et al., 2014b). The consideration of the effects of MEE on atmospheric species other than NO_x, HO_x, and ozone have not been investigated in detail to date, but they can be expected to be qualitatively similar to those caused by solar proton events (SPEs) (Verronen and Lehmann, 2013).

The impact of magnetospheric particles on the atmosphere is strongly linked to the strength of geomagnetic activity; this has been shown both for the direct production of NO in the thermosphere (Marsh et al., 2004; Hendrickx et al., 2015) and mesosphere (Sinnhuber et al., 2016), for mesospheric OH production Fytterer et al. (2015b)(Fytterer et al., 2015b), and for the EPP indirect effect (Sinnhuber et al., 2011; Funke et al., 2014a). Geomagnetic activity can be constrained over centennial time scales by means of proxy data provided by geomagnetic indices. Since our forcing dataset for magnetospheric particle precipitation relies on these indices, their reconstruction and homogenisation is discussed first.

Reconstruction of Geomagnetic Indices

Geomagnetic indices provide a measure of the level of geomagnetic activity resulting from the response of the magnetosphere-ionosphere system to variability in the solar and near-Earth solar wind forcings. Many geomagnetic indices have been constructed and different indices are sensitive to different aspects of magnetospheric and ionospheric dynamics (Mayaud, 1980). The Kp and Ap geomagnetic indices (Bartels, 1949) are directly related by a quasi-logarithmic conversion; they are proxies for the global level of geomagnetic activity, and are used as inputs to parameterisations of magnetospheric particle precipitation. For the historical solar forcing data, daily values of the Kp and Ap indices from 1850 to 2014 are required. However, these indices, as provided by the International Service of Geomagnetic Indices (http://isgi.unistra.fr/), have only been produced from 1932 onwards. It is not possible to directly and consistently extend the Kp and Ap indices prior to 1932, as they use data from 13 geomagnetic observatories around the globe, and these data are unavailable further back in time. So, before 1932 the Kp and Ap indices must be estimated from other geomagnetic indices. The aa index (Mayaud, 1972) is the most appropriate choice,

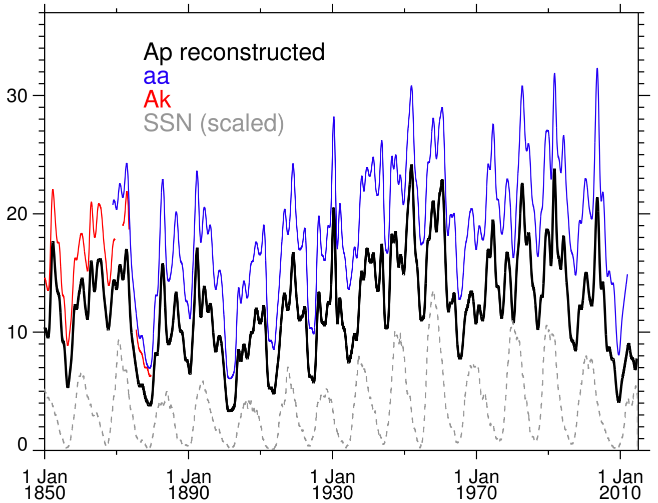

Figure 12. Time series of the reconstructed Ap index (black), together with the aa (blue) and Ak (red) indices used for its reconstruction, with comparison to the sunspot number variability (SSN scaled by a factor of ~~0.67~~0.067, grey dashed). All the data have been smoothed with a 365-day running mean. Note that the reconstructed Ap includes the original Ap data from the International Service of Geomagnetic Indices since 1932.

as it was constructed to be as similar as possible to the Ap index on annual timescales (Lockwood et al., 2013). However, the original aa-index only extends back to 1868 (also available from http://isgi.unistra.fr/), and so an extension (Nevanlinna, 2004) to the aa-index is also employed, extending it back to 1844 by use of the Ak indices from the Helsinki geomagnetic observatory, spanning 1844–1912. In addition, we implement a correction to the aa-index to account for a change in the derivation of the index in 1957, see (Lockwood et al., 2014).

On larger than annual timescales, the response of the aa and Ap indices is similar, and the indices are positively linearly correlated. However, on daily timescales the relationship between aa and Ap is not linear, and also displays a regular annual variation. Therefore, to estimate the daily Ap indices during the period 1868-1931, we used piecewise polynomial fits between the daily Ap and aa values for the period 1932 — present, for each calendar month. These fits were then extrapolated to estimate the Ap values between 1868 and 1931 from the aa values. This process was repeated to estimate the relationship between the Ak indices provided by Nevanlinna (2004), and the Ap values estimated from the aa index. The piecewise polynomial fits for each calendar month were calculated using the overlap period between the Ak and estimated Ap records, 1868–1912. These were then extrapolated to estimate Ap in the period 1850–1867. Figure 12 shows the time series of the reconstructed Ap index and the aa and Ak indices used for extension back to 1850.

The daily Kp index for the period 1868–1931 was estimated by using the monthly piecewise polynomial aa-Ap fits to estimate the 3-hourly ap-index values from the aa index values. These 3-hour ap values were then converted to the corresponding Kp indices, from which the daily mean was calculated. Since only daily Ak data is available, such an approach is not possible for the period 1850–1867, and so here the daily estimates of Ap, derived from Ak, are directly converted into daily Kp. The

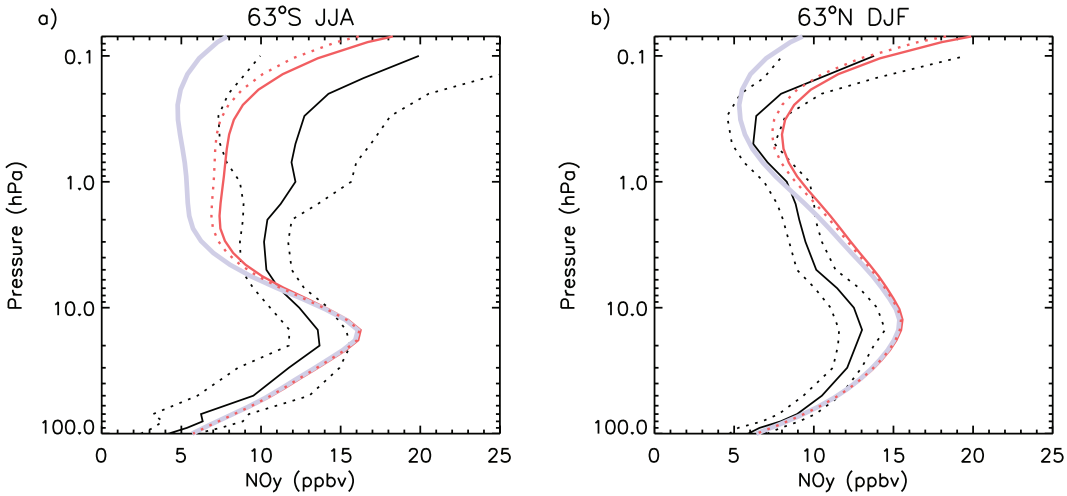

Figure 13. Comparison of 2004–2009 wintertime polar NO_y climatology between ACE-FTS observations and SD-WACCM simulations. Solid black line is ACE, black dots are the average standard deviation of the monthly means. Grey line is WACCM with weak transport of auroral NO_y from the lower thermosphere and no mesospheric production by medium energy electrons (MEE), dot-red line is stronger NO_x transport but no production by MEE, red line is stronger NO_x transport and production by MEE.

quasi-logarithmic nature of the conversion between the hourly Kp and ap indices, means that calculating daily values of Kp in this manner results in lower values than the standard method of averaging the eight 3-hourly values in a day, resulting in a slight bias in the Kp estimates. A statistical correction for this bias was employed by estimating the bias using the difference between the aa-derived Kp and the Ak-derived Kp for the period 1868–1912. The estimated bias was then subtracted from the Ak-derived Kp estimates for the period 1850–1867.

Auroral Electrons

Lower thermospheric nitric oxide production by auroral electron precipitation can only be considered explicitly in CCMs extending up to 120 km or higher. There were only a few Earth system models of this characteristic in CMIP5 and it is expected that the number of such models will not increase significantly within CMIP6. Most of the models falling into this category use parameterizations for the calculation of auroral ionisation rates or NO productions in the polar cusp and polar cap (Schmidt et al., 2006; Marsh et al., 2007). Those parameterisations are typically driven by geomagnetic indices and we hence recommend the use of the extended Ap or Kp time series described above.

Figure 13 demonstrates the improvement in 2004–2009 wintertime polar NO_y modelling when production due to electron precipitation is included. The simulations are from the SD-WACCM model version 4 (Marsh et al., 2013) nudged to the NASA Global Modeling and Assimilation Office Modern-Era Retrospective Analysis for Research and Applications (MERRA) (Rienecker et al., 2011) dynamics, and they are compared to observations from the ACE-FTS instrument (Jones et al., 2011). The auroral electron contribution was calculated with a Kp-based parameterisation and was further controlled through eddy diffusion affecting the NO_x descent from lower thermosphere. MEE ionisation and NO_x production was calculated using electron flux observations from the NOAA SEM-2 medium energy proton and electron detector (MEPED) instrument onboard the POES spacecraft (Evans and Greer, 2000), using methods described in more detail in the following MEE section. Enhancing the transport of auroral NO_x from the lower thermosphere and including the mesospheric NO_x production by MEE clearly improves the wintertime NO_y near the stratopause. Around 0.1 hPa, modelled NO_y increases by 100% in both hemispheres, which leads to better agreement with ACE-FTS. Both auroral electrons and MEE have a clear impact, although the auroral contribution is larger. However, it should be noted that 2004–2009 was a period of weak MEE in general, and during other periods of stronger MEE the contributions become more equal such that the effect on model NO_y is stronger (not shown).

Mid-Energy Electrons (MEE) from the Radiation Belts

Highly energetic particles trapped in the radiation belts mainly consist of electrons and protons, forming inner and outer belts separated by a "slot" region (Van Allen and Frank, 1959). The outer radiation belt (located 3.5–8 Earth radii from the Earth's centre) is highly dynamic, with electron fluxes changing by several orders of magnitude on timescales of hours to days (e.g. Morley et al., 2010). These changes are caused by the acceleration and loss of energetic electrons, through enhancements in radial diffusion and wave-particle interactions, during and after geomagnetic storms (e.g. Reeves et al., 2003). Storm-driven dynamic variations in the underlying cold plasma density influence the effectiveness of such processes in different regions of the inner magnetosphere (e.g. Summers et al., 2007).

In order to characterise the electron precipitation into the atmosphere since 1850 it is necessary to develop a model that uses in-situ satellite observations from the modern era. The most comprehensive, long-duration, and appropriate set of observations are provided by the NOAA SEM-2 MEPED instrument onboard the POES spacecraft (Evans and Greer, 2000; Rodger et al., 2010a). The MEPED instrument covers an energy range from 50 eV to 2700 keV. In this study we are primarily concerned with measurements made with the three medium energy integral electron detectors, i.e., $>$30, $>$100, and $>$300 keV, as the lower "auroral" energy range has been well characterised in previous work. The SEM-2 instrument has been flown on low-Earth orbiting ($\sim$800 km) Sun-synchronous satellites since 1998, with up to 6 instruments operating simultaneously on occasion. Electron precipitation fluxes from the outer radiation belt are measured with the 0 $^\circ$detectors, which are mounted approximately parallel to the Earth-centre-to-satellite vector.

Improved calibration of the SEM-2 detectors has been undertaken by Yando et al. (2011) using modelling techniques contained in the GEANT-4 code to determine the detector geometric conversion factor, or detector efficiency (following the original work described in Evans and Greer, 2000).

Further treatment of the data requires correction for the false counts caused by incident proton fluxes, which we undertake using the technique described in Lam et al. (2010). These calibration and corrections have been tested through comparison with other satellite (e.g. Whittaker et al., 2014b) and ground-based observations (e.g. Rodger et al., 2013; Neal et al., 2015). We convert the satellite position into the geomagnetic latitude parameter L (McIlwain, 1961) using the International Geomagnetic Reference Field IGRF (see Appendix C), and bin the precipitating flux data into zonal means with 0.25 L resolution from L = 2–10 (40–75 $^\circ$geomagnetic latitude).

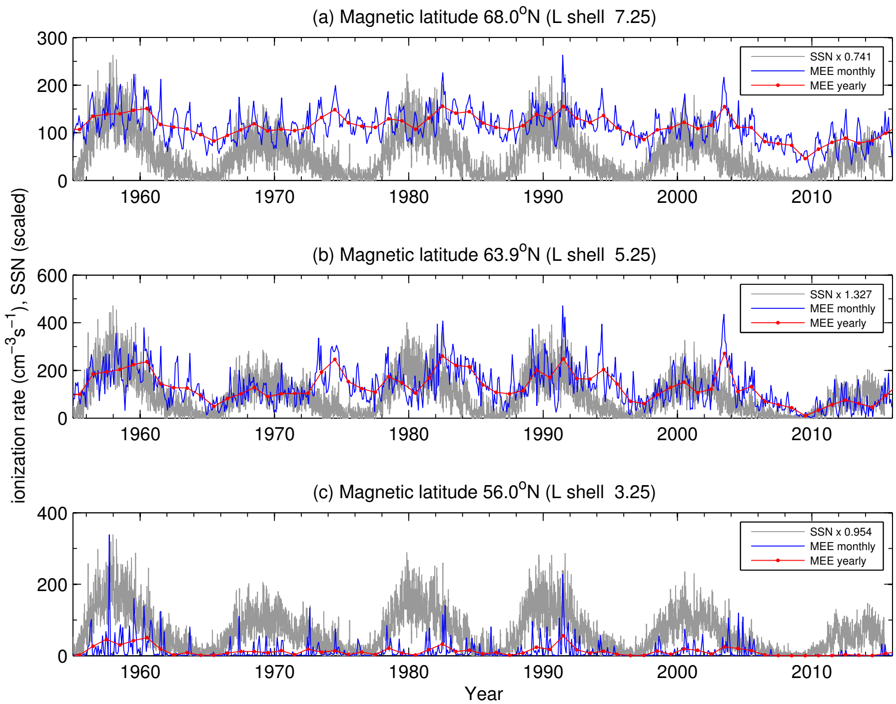

Figure 14. Examples of solar cycle variability of modeled, Ap-driven MEE ionization at ≈80 km altitude, with comparison to the sunspot number variability (SSN, scaled).

Using observed electron flux data in 2002–2012, a precipitation model for radiation belt electrons was created by van de Kamp et al. (2016). The precipitation model was fit to the corrected observations of the MEPED/POES detectors following the approach outlined in Whittaker et al. (2014a). In the CMIP6 application of this model, the Ap index is used as the driving input parameter. Ap defines the level of magnetospheric disturbance and the location of the plasmapause, both of which are needed to calculate precipitating electron fluxes at different magnetic latitudes. Thus, the reconstructed Ap record, as described earlier, can be readily used to create a continuous electron precipitation time series for the whole CMIP6 period. As output, the model provides daily spectral parameters of precipitation: integrated flux at energies above 30 keV and a power-law spectral gradient. A test of high-energy resolved precipitating electron flux measurements made by the DEMETER satellite found that the power-law fit consistently provides the best representation of the flux (Whittaker et al., 2013). The model output has been shown to compare well with the spectral parameters derived from POES satellite data (van de Kamp et al., 2016).

An atmospheric ionisation data set has been calculated based on the Ap-based precipitation model, using a computationally fast ionisation parameterisation (Fang et al., 2010) and atmospheric composition from the NRLMSISE-00 model (Picone et al., 2002). This calculation considered MEE (30–1000 keV) with maximum energy deposition at altitudes between about 60 and 90 km (van de Kamp et al., 2016). Note that the ionization parameterisation does not consider the contribution of Bremsstrahlung which could be significant only at altitudes below 50 km (Frahm et al., 1997).

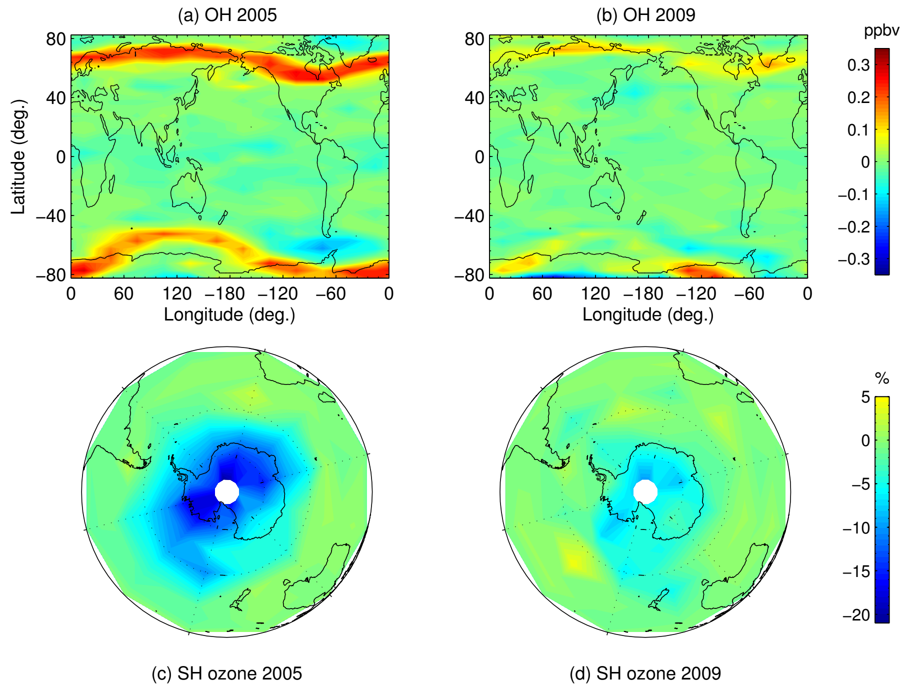

Figure 15. (a) and (b) Difference in yearly median OH mixing ratios at about 70–80 km between SD-WACCM runs with and without MEE ionization. (c) and (d) Relative differences in Southern Hemispheric wintertime mean O_3 at about 70–80 km between SD-WACCM runs with and without MEE ionization.

Figure 14 shows examples of solar cycle variability of the modeled atmospheric MEE ionization rates at ≈80 km altitude. At 68° magnetic latitude (L shell 7.25), MEE precipitation is mostly driven by magnetic substorms and the solar cycle variability is relatively weak, except in around 2009 and the mid 1960s when extended periods of very low geomagnetic activity occurred. At 64° (L shell 5.25), precipitation is driven by high-speed solar wind streams. A more clear solar cycle variability can be seen with maximum ionization lagging the sunspot maximum by 1–2 years. At 56° (L shell 3.25), precipitation is mainly driven by coronal mass ejections which lead to more of an event-type behavior. Relatively infrequent ionization peaks are contrasted with long periods of very low ionization. Similar behavior is seen at other altitudes as well (not shown).

In the following, we demonstrate with examples the MEE impact in WACCM simulations. The purpose is to present a proof of concept, i.e., show that the MEE ionization data set can be used in chemistry-climate modeling, and is producing the expected direct effect in the mesosphere. We simulated the 2002–2012 period, including the Ap-driven MEE ionisation rates, and analysed mesospheric OH and ozone responses at 0.040–0.015 hPa (approx. 70–80 km in altitude). This altitude region was selected because of the clear and direct MEE impact seen in satellite observations (e.g. Andersson et al., 2014a, b; Fytterer et al., 2015b; Sinnhuber et al., 2016). WACCM version 4 (see above) was used with 1.9° ×2.5° horizontal resolution extending from the surface to 5.9×10^{-6} hPa (≈140 km geometric height) in the specified dynamics mode, nudged to MERRA reanalysis at every dynamics time step below about 50 km.

Figures 15a and 15b show global differences in yearly median OH mixing ratios due to MEE. Distinct features on the map are the stripes of enhanced values at magnetic latitudes between 55° and 75° (both hemispheres) which connect through the magnetic field to the outer radiation belt. The impact decreases from 2005 to 2009 due to the decline in geomagnetic activity and MEE precipitation (as shown in Figure 14). These features are of expected quality and magnitude, and similar to those based on Microwave Limb Sounder (MLS) data analysis (Andersson et al., 2014b).

Figures 15c and 15d show relative differences in wintertime (MJJA) mean ozone due to MEE in the Southern Hemisphere. As expected, ozone is affected at high polar latitudes. In 2009, when MEE precipitation was weak, a maximum of 5–10% decrease is seen near the south pole relative to a reference WACCM simulation. In 2005, with much stronger MEE precipitation, the effect reaches up to 10–20% and covers the whole polar cap above about 60° latitude. The magnitude of the 2005 response, tens of percent, is comparable to that seen in MLS observations (Andersson et al., 2014a).

The EPP Indirect Effect: Odd Nitrogen Upper Boundary Condition

Those models with their upper lid in the mesosphere, i.e., which do not represent the entire EPP source region, require an odd nitrogen upper boundary condition (UBC), accounting for EPP productions higher up, in order to allow for simulating the introduced EPP indirect effect in the model domain. Odd nitrogen UBCs have been previously used in CCMs. In some model studies, the UBC was taken directly from NO_x observations (e.g., Reddmann et al., 2010; Salmi et al., 2011), which, however, implies the restriction to the relatively short time period spanned by the observations. In other cases, a simple parameterisation in dependence of the seasonally averaged Ap index (Baumgaertner et al., 2009) was employed (e.g., Baumgaertner et al., 2011; Rozanov et al., 2012), enabling extended simulations over multi-decadal time periods. We recommend the use of the UBC model described in Funke et al. (2016) which is designed for the latter application and represents an improved parameterisation due to its more detailed representation of geomagnetic modulations, latitudinal distribution, and seasonal evolution. This semi-empirical model for computing time-dependent global zonal mean NO_y concentrations (in units of cm^{-3}) or EPP-NO_y molecular fluxes (in units of $cm^{-2}\,s^{-1}$) at pressure levels within 1–0.01 hPa and is available at http://solarisheppa.geomar.de/solarisheppa/cmip6.

The UBC model has been trained with the EPP-NO_y record inferred from Michelson Interferometer for Passive Atmospheric Sounding (MIPAS) observations (Funke et al., 2014a). Inter-annual variations of the EPP indirect effect at a given time of the winter are related to variations of the EPP source strength, the latter being considered to depend linearly on the Ap index. A finite impulse response approach is employed to describe the impact of vertical transport on this modulation. Interannual variations of the EPP-NO_y seasonal dependence, driven by variations of chemical losses and transport patterns, are not considered in the standard mode of the UBC model. Optionally, episodes of accelerated descent associated with Elevated Stratopause (ES) events in Arctic winters can be considered by means of a dedicated parameterisation, taking into account the dependence of the EPP-NO_y amounts and fluxes on the event timing (Holt et al., 2013). Although its application is recommended in principle, we note that it requires the implementation of the UBC model into the climate model system since ES events cannot be predicted in free-running model simulations. Further, the ES detection criterion might need to be tuned for each individual model system.

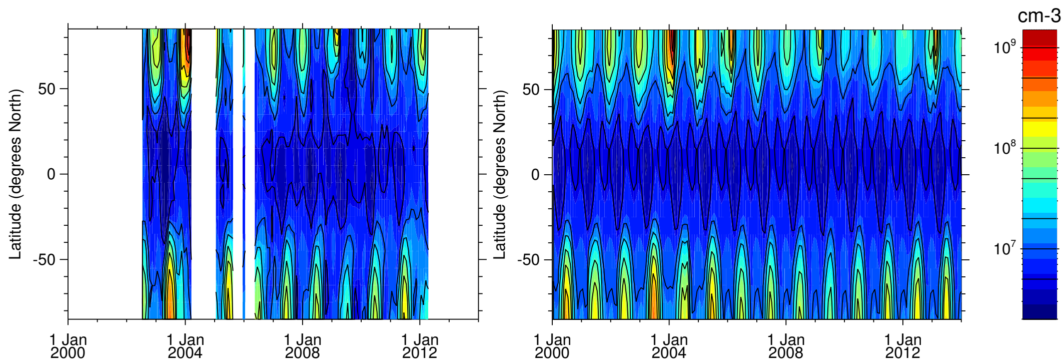

Figure 16. Latitude-time sections of NO_y concentrations observed by MIPAS (left) and from the UBC model (right) at 0.1 hPa.

We recommend to prescribe NO_y concentrations, as this has already been tested successfully in a CCM. As an example, Fig. 16 shows the NO_y concentrations from the UBC model at 0.1 hPa in comparison with the MIPAS observations. Care has to be taken when balancing $[NO_y] = [NO] + [NO_2] + [NO_3] + [HNO_3] + 2[N_2O_5] + [ClONO_2]$ in order to avoid model artifacts at the upper boundary (primarily triggered by the loss reaction of NO_2 with atomic oxygen). The simplest way to achieve this is to set $[NO] = [NO_y]$ while forcing the concentrations of all other NO_y species to be zero. Note that below the vertical domain where NO_y is prescribed, MEE ionization still might occur and its consideration (as described before) is recommended. However, its consideration should be strictly limited to this vertical range since at and above the UBC, MEE is already implicitly accounted for by the prescribed NO_y from the observation-based UBC model.

The UBC was tested in the EMAC CCM version 2.50 (see also Sec. 2.1.2 and Jöckel et al., 2010) with a T42L90 resolution. NO_y concentrations were prescribed as NO in the uppermost four model boxes at pressure levels from 0.09 to 0.01 hPa. NO_y. There, NO_2 was set to zero to suppress artificial NO_2 buildup. The model was run from 1999 to 2010 in the specified dynamics mode, nudged to ERA-Interim reanalysis data (Dee et al., 2011) below 1 hPa. A special treatment of ES events was disabled in the UBC model and SPEs were not considered. A comparison of polar NO_y from EMAC with MIPAS observations is shown in Fig. 17 for 0.1 hPa (just below the prescription altitudes) and 1 hPa. A very good agreement between model predictions and observations is found at 0.1 hPa in both hemispheres, with the exception of periods of large SPEs (October/November 2003) in both hemispheres and ES events (January 2004 and February 2009) in the Northern Hemisphere. At 1 hPa, the agreement is still very good during winter, but EMAC underestimates the summer maximum of NO_y slightly. This is also observed in the base model run without employing the UBC (see Fig. 17).

t

The interannual variation of ozone in the stratosphere and lower mesosphere has been investigated in this model in a similar way as for a three-satellite composite (Fytterer et al., 2015a). The ozone difference between Austral winters with high and low geomagnetic activity during 2005–2010 is shown in Fig. 18 for 27-day running means relative to the mean of all years. This period has been chosen because of its low SSI variability. Cross-correlations between SSI and particle impact are thus

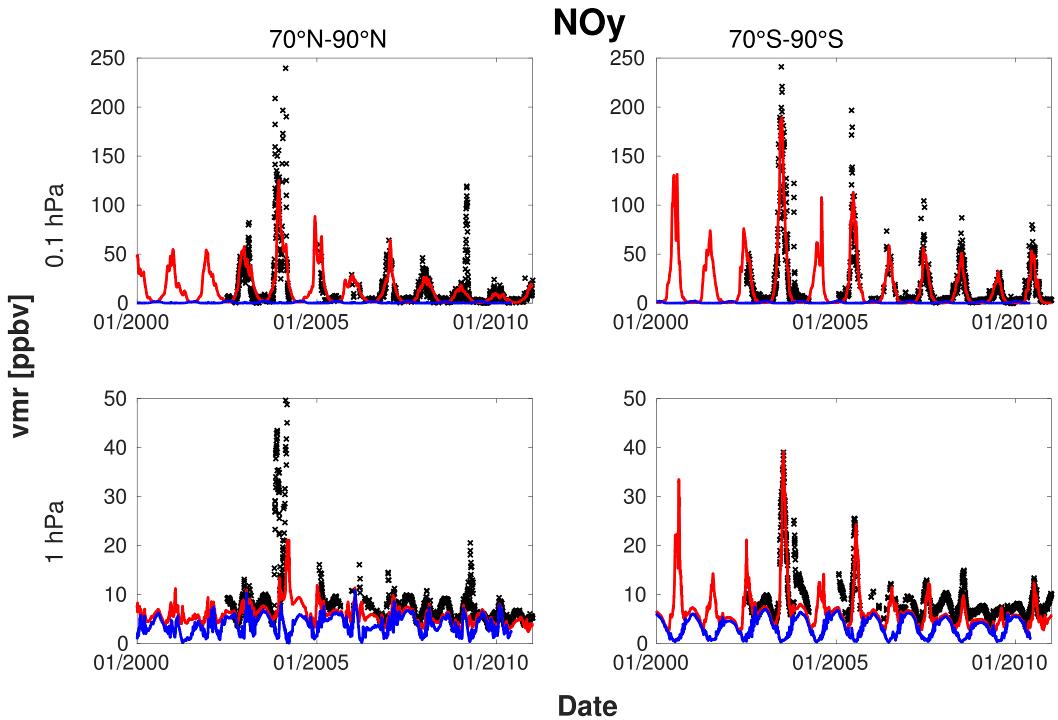

Figure 17. Comparison of NO_y from MIPAS observations and different EMAC model runs at 70–90°~~S~~ N (left) and 70–90°~~N~~ S (right) for ~~0.01~~0.1 hPa (upper panel) and ~~0.1~~1 hPa (lower panel), from 2000–2010. Black crosses: MIPAS observations. Red line: EMAC with the MIPAS-derived UBC for NO_y (see text); blue line: EMAC without UBC for NO_y.

minimized. EMAC results are in excellent agreement with the observations as provided in Fytterer et al. (2015a, Figure 5), showing a clear negative ozone anomaly of 5-10% moving down from the upper stratosphere to below 10 hPa ($\sim$30 km) from July to October. Below, a positive anomaly of smaller amplitude is observed both in EMAC and the three-satellite composite which might be due to a combination of self-healing, dynamical feedbacks, and chemical feedbacks (NO_x-induced chlorine buffering in the processed "ozone hole" area).

~~t~~

2.2.2 Solar Protons

Solar eruptive events sometimes result in large fluxes of high-energy solar protons at the Earth, especially near the maximum and declining periods of activity of a solar cycle. This disturbed time, wherein the solar proton flux is generally elevated for a few days, is known as a solar proton event (SPE). Solar protons are guided by the Earth's magnetic field and impact both the northern and southern polar cap regions (>60° geomagnetic latitude, e.g., see Jackman and McPeters, 2004). These protons can

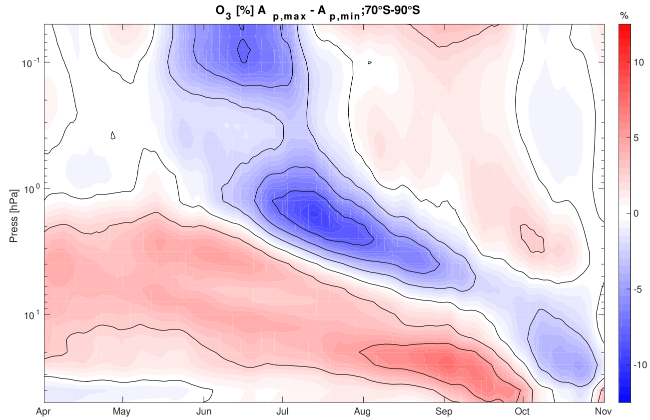

Figure 18. Ozone interannual variation due to geomagnetic forcing in 2005-2011 from EMAC model run using the MIPAS-derived UBC for NO_y. Shown are 27-day running means of the mean of the three years with highest – mean of the three years with lowest geomagnetic activity averaged over 70-90°S. EMAC results are in excellent agreement with O_3 observations using a three-satellite composite for the same period of time (see Figure 5 in Fytterer et al., 2015a).

impact the neutral middle atmosphere (stratosphere and mesosphere) and produce both hydrogen radicals and reactive nitrogen constituents.

The ozone response due to very large SPEs is fairly rapid and substantial and has been observed during and after numerous events to date (e.g., Weeks et al., 1972; Heath et al., 1977; McPeters et al., 1981; Thomas et al., 1983; Solomon et al., 1982; McPeters and Jackman, 1985; Jackman et al., 1990, 1995, 2001, 2005b, 2008, 2011, 2014; López-Puertas et al., 2005a; Rohen et al., 2005; Seppälä et al., 2006; Krivolutsky et al., 2008; Funke et al., 2011; von Clarmann et al., 2013). Ozone within the polar caps (60-90°S or 60-90°N geomagnetic) is generally depleted to some extent in the mesosphere and upper stratosphere (e.g., Jackman et al., 2005b) within hours of the start of the SPE and can last for months beyond the event at lower altitudes in the stratosphere.

Decreases in mesospheric and upper stratospheric ozone are mostly caused by SPE-induced HO_x increases, which were predicted to occur over 42 years ago (e.g., see Swider and Keneshea, 1973). Direct measurements of SPE-caused OH and HO_2 enhancements have confirmed these early predictions (e.g., Verronen et al., 2006; Damiani et al., 2008; Jackman et al., 2011, 2014). Other observations of increased H_2O_2 (Jackman et al., 2011) and of chlorine-containing constituents HOCl (an increase, see von Clarmann et al., 2005; Jackman et al., 2008; Damiani et al., 2008, 2012; Funke et al., 2011) and HCl (a decrease, see Winkler et al., 2009; Damiani et al., 2012) support the SPE-caused HO_x enhancement theory. Since HO_x constituents have relatively short lifetimes (hours), these SPE-enhanced species have only a short-term impact on ozone.

The SPE-induced NO_y enhancements, on the other hand, cause a much lengthier reduction in ozone, given their much longer atmospheric lifetime (∼months) in the stratosphere. SPE-caused NO_x increases have been shown in several studies (e.g., McPeters, 1986; Zadorozhny et al., 1992, 1994; Randall et al., 2001; López-Puertas et al., 2005a; Jackman et al., 1995, 2005b, 2008, 2011, 2014; Funke et al., 2011; von Clarmann et al., 2013; Friederich et al., 2013). Other NO_y constituents like HNO_3, HNO_4, N_2O_5, and $ClONO_2$ (e.g., López-Puertas et al., 2005b; Jackman et al., 2008; Funke et al., 2011; Damiani et al., 2012; von Clarmann et al., 2013) as well as the total NO_y family (e.g., Funke et al., 2011, 2014a, b) have also been shown to increase as a result of large SPEs. Additionally, N_2O has been measured to increase as a result of large SPEs (Funke et al., 2008; von Clarmann et al., 2013).

Solar proton fluxes have been measured by a number of satellites in interplanetary space or in orbit around the Earth. The National Aeronautics and Space Administration (NASA) Interplanetary Monitoring Platform (IMP) series of satellites provided measurements of proton fluxes from 1963–1993. IMPs 1-7 were used for the fluxes from 1963-1973 (Jackman et al., 1990) and IMP 8 was used for the fluxes from 1974–1993 (Vitt and Jackman, 1996). The National Oceanic and Atmospheric Administration (NOAA) Geostationary Operational Environmental Satellites (GOES) were used for proton fluxes from 1994–2014 (e.g., Jackman et al., 2005a, 2014).

Other precipitating particles are associated with SPEs, besides protons. These include alpha particles, which comprise, on average (but this value may vary from event to event) about 10% of the positively charged solar particles, other ions, which account for less than 1% of the remainder, and electrons (e.g., Mewaldt et al., 2005). Only solar protons are included in energy deposition computations given in this paper. Please note that other charged particles could add modestly to this energy deposition in the middle atmosphere during SPEs.

The proton fluxes of energies 1-300 MeV were used to compute daily average ion pair production profiles using an energy deposition scheme first discussed in Jackman et al. (1980). The scheme includes the deposition of energy by the protons and assumes 35 eV are required to produce one ion pair (Porter et al., 1976). Note that this approach misses development of the atmospheric cascade (Sec. 2.2.3). This process, crucial for GCRs, is minor for SPEs in the upper atmosphere but may contribute modestly to the energy deposition in the lower stratosphere.

The dataset for daily average ion pair production rates at 60–90° geomagnetic latitudes from SPEs was computed over a 52 year time period (1963–2014), when proton flux measurements from satellites were available. A longer-term dataset for these SPE-caused ion pair production rates was created for the 1850–1962 time period using activity levels of the measured sunspots over the solar cycles. SPEs are much more frequent during years of maximum solar activity and vice versa. This longer-term dataset was reconstructed for years 1850–1962 in a random way using solar activity levels combined with the 52-year calculated SPE-caused ion pair production. Thus, an historical record of atmospheric forcing by SPEs in the form of a daily average ion pair production rate is available over the entire period 1850–2014 for use in global models.

2.2.3 Galactic Cosmic Rays

The Earth's atmosphere is continuously irradiated by Galactic cosmic rays (GCR), which consist mostly of protons and α-particles with a small amount of heavier fully ionized species up to iron and beyond. These cosmic rays originate from galactic (mostly supernova shocks) and exotic extra-galactic sources and may have an energy up to 10^{20} eV but the bulk energy is in the range of several GeV/nucleon. While the GCR flux can be assumed (at time scales shorter than thousands of year) constant and isotropic in the interstellar space, it is subject to strong modulations within the heliosphere (the region of about 200 AU across hydromagnetically controlled by the solar wind and the heliospheric magnetic field). This modulation is driven by solar magnetic activity – the stronger the solar activity, the lower is the GCR flux near the Earth. This flux is often described by the so-called force-field model (Caballero-Lopez and Moraal, 2004) parameterized via the time-variable modulation potential ϕ and the fixed shape of the local interstellar spectrum (see, e.g., Usoskin et al., 2005, for more details). Typically, the value of the modulation potential is defined by fitting data from the world-wide network of ground-based neutron monitors calibrated to fragmentary space-borne measurements of GCR energy spectra. These data are available since 1951 or, with caveats of using the ground-based ionization chambers, since 1936 (Usoskin et al., 2011).

Before impinging on the Earth's atmosphere, GCR are additionally deflected by the geomagnetic fieldso that there is no shielding in the polar regions, but particles must have rigidity (the ratio of a particles momentum and charge) exceeding 15–18 GV to be able to penetrate in equatorial regions. Since fast transient solar energetic particle events often occur at the background of enhanced geomagnetic disturbances, straight-forward computation of the particle trajectories in a realistic geomagnetic field is needed (e.g., Smart et al., 2000). However, for slowly changing GCR variability, this shielding is often .

This shielding is usually parameterized in the form of the effective geomagnetic rigidity cutoff, so that only particles with rigidity/energy exceeding the cutoff can penetrate to the atmosphere at a given location while less energetic particles are fully rejected (Cooke et al., 1991).

When energetic cosmic rays enter the atmosphere, they initiate a nucleonic-muon-electromagnetic cascade in the atmosphere, ionizing ambient air. As a sub-product of this cascade cosmogenic isotopes such as ^{14}C, ^{10}Be and others can be produced. These cosmogenic isotopes are long-lived and can be used for the reconstruction of solar activity over several thousand years (see Sec. 3).

Between the surface and 25—30 km cosmic rays are the main source of atmospheric ionization (Mironova et al., 2015) causing the production of NO_x and HO_x. The influence of GCRs on atmospheric chemistry has been investigated in several model studies (Krivolutsky et al., 2002; Calisto et al., 2011; Rozanov et al., 2012; Mironova et al., 2015; Jackman et al., 2015). GCR-induced ozone reductions of more than 10% in the tropopause region and up to a few percent in the polar lower stratosphere have been reported. The potential impact on surface climate has been studied by Calisto et al. (2011) and Rozanov et al. (2012).

The process of development of the atmospheric cascade, initiated by energetic cosmic rays, is complicated and needs to be modelled using direct Monte-Carlo simulations of all the processes involved in the development of the cascade, including all types of interactions, scattering and decay of various species. We note that older models based on empirical parameterisations or on solution of Boltzmann-type equations may introduce significant biases in the results, especially in the lower atmosphere. Accordingly, we use a full Monte-Carlo model CRAC:CRII (Usoskin and Kovaltsov, 2006; Usoskin et al., 2010) based on the CORSIKA Monte-Carlo package. A similar result can be obtained with the PLANETOCOSMIC (Desorgher et al., 2005) based on the GEANT package. The agreement between the two models has been verified (Usoskin et al., 2009) to be within 10%.

GCR ion pair production rates are provided as a function of the barometric pressure and geomagnetic latitude and were calculated from the modulation potential values ϕ of the 9400-year long record by Steinhilber et al. (2012). Since this dataset

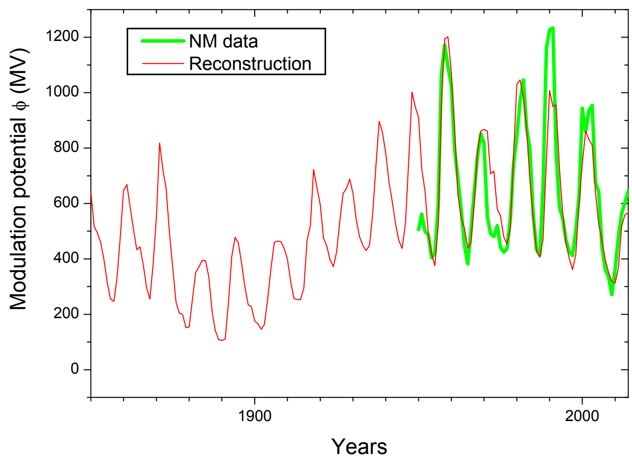

Figure 19. Time series of the reconstructed heliospheric modulation potential ϕ including solar cycle variations. The thick green line is the modulation potential reconstructed for the period 1951–2014 using data from the worldwide neutron monitor (NM) network (Usoskin et al., 2011).

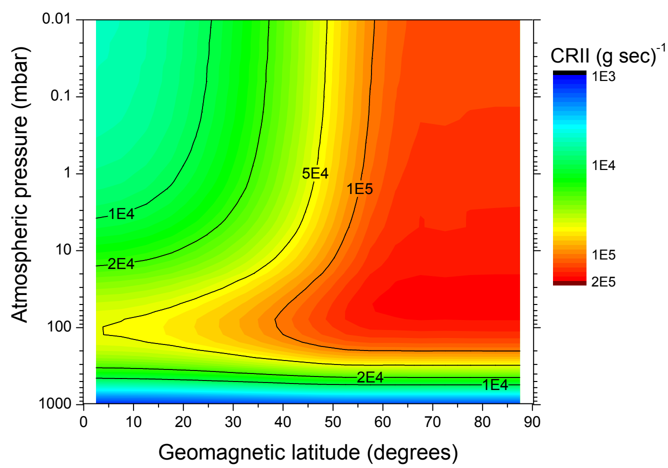

Figure 20. Calculated annual mean ion pair production rate for the year 2014 as a function of barometric pressure and geomagnetic latitude. Computations were done using the CRAC:CRII model.

has a 22-year time resolution, it has been interpolated to interannual time scales to resolve individual solar cycles, based on the sunspot numbers (see Fig. 19). One can see that this agrees well with the values of ϕ reconstructed using data from the worldwide network of neutron monitors (NM) (Usoskin et al., 2011). An example of the calculated ionisation rate is shown in Fig. 20. The ionisation maximizes in polar regions at heights of 15–20 km, while in the equatorial region the maximum of ionisation occurs at about 12 km (note that in case of using ionization per cm^3, the ionisation maximizes at about 10 km in the equatorial region and 12 km over the poles).

2.2.4 Implementation of Chemical Changes Induced by Particle-Induced Ionisation

MEE, SPE, and GCR-induced atmospheric ionisation is expressed in the CMIP6 forcing dataset in terms of ion pair production rates (IPR). Note that IPR data are provided in units of ion pairs per gram per second as a function of the barometric pressure. These units are natural for the ionisation processes and are mostly independent of the atmospheric conditions. Conversion into units of $cm^{-3}\,s^{-1}$ (by multiplying with mass density) should be done on the model grid ideally at each time step, but at least once per day. Recommendations for the projection of ion pair production rates onto geographic coordinates can be found in Appendix C.

Particle-induced ionisation causes, along with the generation of the ion pairs, the production of NO_x and HO_x. As a basic approach, we recommend to consider these NO_x and HO_x productions in CCMs with interactive chemistry by using the parameterisations provided by Porter et al. (1976) and Solomon et al. (1981), respectively. More detailed information about these approaches is provided in Appendix D and E. Recommendations for the implementation of EPP effects on minor species are given in Appendix F.

3 Future Scenarios (2015-2300)

One of the key questions in the CMIP6 project is our ability to assess future climate changes given climate variability, predictability and uncertainties in scenarios. In CMIP5, climate projections were based on a stationary Sun scenario, obtained by simply repeating solar cycle 23, which ran from April 1996 till June 2008 (Lean and Rind, 2009). ~~In CMIP6, we~~ Clearly, such a stationary scenario is not representative of true solar activity, which exhibits cycle-to-cycle variations, and trends. Therefore, in CMIP6 we decided to include a more realistic solar forcing, and provide two different scenarios:

- a reference (REF) scenario with the most likely level of solar activity;
- an extreme (EXT) scenario with an exceptionally low level of solar activity, corresponding to the lower 5th percentile of all forecasts. This extreme scenario is meant to be used for sensitivity studies.

~~We ignore scenarios with high levels of solar activity because~~ There are several reasons why our extreme scenario is a low one. First, the Sun just ~~left such an episode (~~exited a high amplitude one, called grand solar maximum~~)~~, and several empirical studies suggest that it is very unlikely to return to one in the next 300 years (Abreu et al., 2008; Barnard et al., 2011; Steinhilber et al., 2012). Secondly, dynamo models of the solar cycle indicate that grand maxima are more likely to be followed by a grand minimum than by another grand maximum. And thirdly, when we generated an ensemble of 1000 scenarios with two of the empirical models to be described below (the different runs were based on different training intervals and model parameters) none of the forecasts gave rise to a grand maximum within the next century.

The main challenge consists in forecasting solar activity up to 2300. Ever since the solar cycle was first observed, people have been trying to predict what future cycles may look like. Prediction methods were empirical, and at best could give some clue of what the amplitude of the next cycle could be (Petrovay, 2010). This situation prevailed until the early 21st century, when physical models of the magnetic dynamo that drives solar activity started unveiling a more realistic picture (Charbonneau, 2010). Many were confident that in a near future one would be able to predict the solar cycle several decades ahead. The unusually long solar cycle number 23 that ended in 2009, and the weak one (nr. 24) that followed came as a surprise, and manifested our evident lack of understanding of the solar cycle. As of today, even predicting the cycle amplitude one cycle ahead remains a major challenge (Pesnell, 2012).

In this context, predicting solar activity several tens of cycles ahead may seem like a hopeless task. However, erratic as the solar cycle may be, solar activity on multi-decadal time scales (i.e. averaged over solar cycles) does ~~show~~ exhibit some regularity, which may be used to predict it, see for example (Hanslmeier and Brajša, 2010) and references therein. The solar cycle is driven by the solar dynamo, by which the dynamical interactions of flows and magnetic fields in the solar convection zone lead to periodic reversals of polarity of the solar magnetic field (Charbonneau, 2010). One of its consequences is the emergence of regions with enhanced magnetic field, namely sunspots, whose number are the most widely known proxy for solar activity. During that emergence process, the predominantly toroïdal magnetic field generates a dipole moment, which in turns generates a new toroïdal magnetic component through rotational shearing. Because these inductive processes are operating in the turbulent environment of the solar convection zone, memoryless stochastic forcing of the dynamo is certainly ~~presentat~~ present at some level. Nonetheless, memory effects associated with these periodic reversals play a major role in determining solar variability on multi-decadal time scales, and to some degree are decoupled from the short-term variability. This is our prime motivation for considering predictions on multi-decadal time scales. Entry into grand minima typically involves extended excursions at the edge of the attractor defining normal cyclic behavior, with associated higher-than-average cycle amplitudes, until collapse to the trivial solution (or transition to another low-amplitude attractor) is triggered; this behavior is known as intermittency, and in this context a grand maximum is usually more likely to be followed by a grand minimum than by another grand maximum (e.g. Passos et al., 2012).

There are two approaches for constraining such predictions. One is to learn from solar dynamo models, and the other is to infer from past variations of solar activity. Recent years have witnessed significant advances in solar dynamo modeling, and the development of several physical models (Charbonneau, 2014). Most models exhibit some persistence in the solar cycle-averaged level of activity, with a memory of up to a few cycles. However, among models that do succeed in producing deep activity minima similar to the Maunder minimum, most show onsets ~~occuring~~ occurring surprisingly fast, typically within one or two cycles.

The best gauge of past solar variability is the production rate of the ^{14}C and ^{10}Be cosmogenic isotopes, as already described in Sec. 2.2.3. The level of activity is usually expressed in terms of the modulation potential Φ (Usoskin, 2008; Beer et al., 2012), which is intimately related to the open solar magnetic flux. There exist today different records of cosmogenic isotopes, which are gradually improving as new observations are being added, and underlying assumptions, such as the strength of the geomagnetic dipole, are better constrained. Here, we consider the 9400-year long record by Steinhilber et al. (2012), which is a composite of ^{14}C and ^{10}Be data, and is available from http://www.ncdc.noaa.gov/paleo/forcing.html. The record is sampled every 22 years, and runs from 7439 BC till 1977 AD. For making better predictions, we want our historic observations to end as close as possible to the present. Therefore we extended the record from 1977 to 1999, using the geomagnetic reconstruction of the open solar flux ~~Lockwood et al. (2014)~~(Lockwood et al., 2014). The geomagnetic reconstruction provides annual values of the open solar flux back to 1845, and we extrapolate the linear regression between the 22-year boxcar smoothed geomagnetic reconstruction and the cosmogenic reconstruction to provide an estimate of the cosmogenic Φ in 1999.

Figure 21 displays the complete modulation potential record, which exhibits occasional periods of low solar activity (i.e. grand solar minima) separated by periods during which the fluctuations seem more erratic. It is noteworthy that the Sun was more active during the recent decades (the ~~Modern~~ modern grand maximum) than during most of the other periods.

In the following, we ~~shall~~ consider three different (and ~~to some degree,~~ mostly complementary) approaches for predicting Φ up to 300 years ahead, and use their weighted average as the most likely value. To convert these 22-year averages of Φ into quantities that are relevant for climate forcing, we first convert the 22-year averaged modulation potential into an average sunspot number. Historic solar cycles that have the same average sunspot number are subsequently stitched together to obtain a record with daily-resolved sunspot numbers. Using the latter, we estimate the SSI, and particle forcing, as described in Sec. 3.5.

According to solar dynamo models, the solar-cycle averaged modulation potential (and the sunspot number) cannot be meaningfully predicted more than ~~a few decades~~ one solar cycle ahead. The autocorrelation function of the observed modulation potential ~~has an autocorrelation function that~~ indeed decays exponentially with a characteristic time of 48 ± 5 years. This quantity can be interpreted as the time beyond which ~~memory is lost~~successive values become uncorrelated. As we shall see below, two of our three prediction methods ~~too~~ exhibit prediction horizons of approximately 60 years. ~~However, one of them (the~~ The deterministic harmonic model ~~)~~ maintains substantial predictive capacity on much longer time scales because by construction it assumes the potential to vary periodically. To the best of our knowledge, no ~~existing method~~method, except for harmonic ones, has been able to ~~meaningfully predict solar activity more than 60 years ahead~~provide meaningful forecasts that go beyond this 60-year horizon. For that reason, we shall from now on speak in terms of *forecast* rather than *prediction*, and concentrate on *scenarios* of solar activity.

3.1 Forecast Methods

Here we construct the reference (REF) and extreme (EXT) solar activity scenarios by applying three prediction methods to the heliospheric modulation potential time series produced by Steinhilber et al. (2012). ~~Other prediction techniques exist which could have also been used, but we choose to use only~~ The reason for choosing three techniques only out of many is motivated by our desire to build an ensemble of reasonable forecasts that involve different assumptions. We consider these three techniques ~~as we consider them~~ to reflect a fair range of possibilities for the future evolution of the heliospheric modulation potential, and it would be impractical to include an exhaustive set of techniques. The ones we consider have been widely advocated for making predictions with climate data (Mudelsee, 2010) but do so in completely different ways. The first one (analogue forecast) is non parametric and does not make any assumptions on linearity; the second one (autoregressive model) is parametric and linear; and the third one (harmonic model) is parametric too, but can handle nonlinear systems. Below we describe each of ~~the prediction methods~~them, before detailing how the two scenarios were constructed.

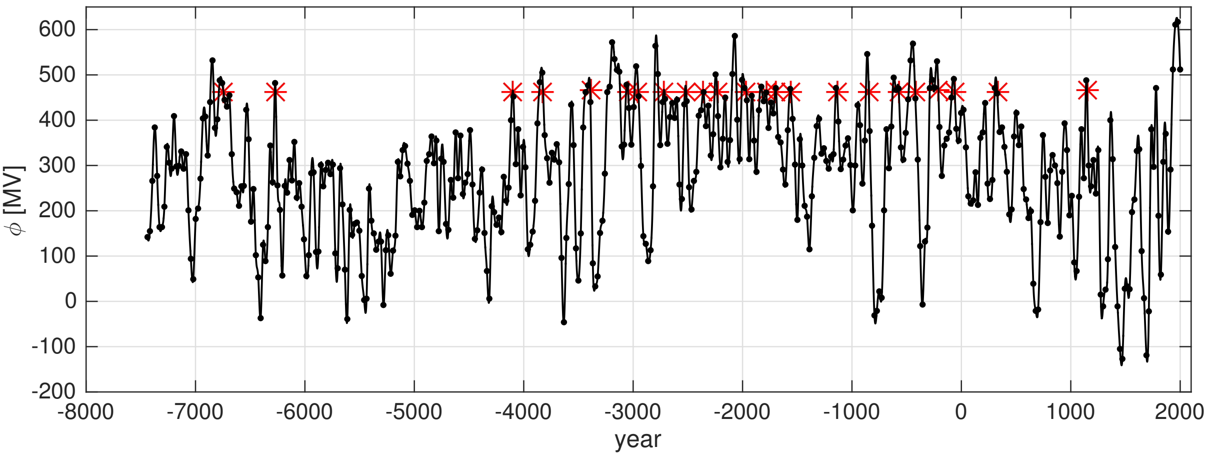

Figure 21. Modulation potential record Φ [MV] used for forecasting solar activity. What matters is the relative variation in Φ, which reflects that in the TSI: large values of Φ correspond to grand solar maxima, whereas low values correspond to grand solar minima. Red stars refer to the events used in the analogue forecast, see Sec. 3.1.1. Negative values of the modulation potential are unphysical, but occur in the original record because of our poor knowledge of the cosmic ray spectrum during deep solar minima.

3.1.1 Analogue Forecast

The analogue forecast (AF) is calculated with a simple non-parametric technique, known across disciplines by various names including compositing, superposed-epoch analysis, conditional sampling and Chree analysis. In a data sequence that exhibits a low amplitude response to a specific trigger event, the response may be obscured by sources of random variability. The AF technique aims to reveal the response to a specific trigger event by averaging the responses to many occurrences of the trigger event, such that over many events random variability will be suppressed and the response will emerge (Laken and Čalogović, 2013). Barnard et al. (2011) used this technique with the Steinhilber et al. (2012) Φ record to estimate the possible future Φ evolution given the expected decline from the grand solar maximum that persisted through the late 20th century. Here we perform an updated version of the procedure employed by Barnard et al. (2011).

Defining grand solar maxima in the Φ record as any period above the 90^{th} percentile of the Φ distribution (462 MV), identifies 23 grand solar maxima in the Φ record prior to the most recent one. Here the declines from the grand solar maxima are used as the event triggers from which the AF is calculated, and these times are marked on the Φ time series shown in Figure 21 by red stars. Figure 21 also shows that the most recent values in the Φ record have not yet fallen below grand solar maxima threshold. Therefore, as the end date of the most recent grand solar maxima is not known, it must be estimated, to provide a date from which the AF applies. The grand solar maximum end date was estimated to be 2004, by extrapolating the regression of the 22-yr smoothed Lockwood et al. (2014) annual geomagnetic reconstruction of the open solar flux onto the Steinhilber et al. (2012) Φ record. So the forecast was applied from 2004 onwards and interpolated onto the dates required to continue 22-year sample sequence defined by the Φ record.

3.1.2 Autoregressive Model

Autoregressive (AR) models are widely used in time series forecasting (Box et al., 2015). These linear parametric models assume that variations can be described by means of a linear stochastic difference equation, so that future values are expressed as a linear combination of present and past values. In our context, we have

$$\hat{\Phi}_{k+h} = a_1 \Phi_{k-1} + a_2 \Phi_{k-2} + \ldots + a_p \Phi_{k-p} \,, \tag{1}$$

where Φ_k is the heliospheric modulation potential (after subtracting its time average) at the k'th time step, and $\hat{\Phi}_{k+h}$ is its value predicted $h \geq 0$ time steps ahead. Since Φ_k is measured with a cadence of 22 years, each value of k corresponds to a 22-year time step. AR models are capable of describing a variety of dynamical behavior, including oscillations, red noise, etc. The main free parameter is the model order p, for which there exist several selection criteria (Ljung, 1997). In our case, we obtain $p = 20$. According to this value, our forecasts are based on observations that go back at most 440 years into the past.

Because AR models are linear, they cannot properly describe nonlinear dynamical effects such as the occasional occurrence of grand solar minima, which appear as a different mode of solar activity (Usoskin et al., 2014). To partly overcome this limitation, we train the model by considering time intervals whose conditions are similar to those prevailing at the end of the 20th century. More specifically, we train the model by using only observations that belong to either of the 23 time intervals $[t_{GSM} - 1100\text{years}, t_{GSM} + 1100\text{years}]$ that are centered on the same occurrences t_{GSM} of the 23 grand solar maxima as in the analogue forecast (see Sec, 3.1.1, and Fig. 21). We exclude observations that follow t_{GSM} by up to 300 years in order to give us a means for testing the prediction on a time interval that is (mostly) independent of the one the model has been trained on. The only exception in this list is the last grand solar maximum of the late 20th century, for which we do not have future observations available. The 2200-year duration of the time interval is the shortest one below which the performance of the AR model starts degrading.

Using AR models, we now forecast the heliospheric potential 22, 44, ..., 308 years ahead by training a different model for each value of the forecast horizon h in Eq. 1. The forecast error, which is the usual metric for describing forecast performance, is classically defined as

$$s(h) = \sqrt{\langle \left(\hat{\Phi}_{k+h} - \Phi_{k+h} \right)^2 \rangle} \sqrt{\langle \left(\hat{\Phi}_{k+h} - \Phi_{k+h} \right)^2 \rangle} \,, \tag{2}$$

where the ensemble average $\langle \ldots \rangle$ runs over all 23 grand solar maxima. Clearly, the AR model can be improved in several ways. One of them consists in modelling the full record of the heliospheric potential, and use threshold AR models to account for mode changes. These issues will be addressed in a forthcoming publication.

3.1.3 Harmonic Model

Several studies have reported the existence of periodicities in cosmogenic solar proxies, with outstanding periods of approximately 87 years (known as the Gleissberg cycle), 208 years (de Vries cycle), 350 years, and more (McCracken et al., 2013). The origin of these elusive periodicities has been hotly debated, and is beyond the scope of our study. Steinhilber and Beer

(2013) successfully used them to model solar activity on multi-decadal time scales, and produced a 500 year forecast of the heliospheric potential. We consider the same approach, and thus assume that the dynamical evolution of the heliospheric potential obeys a deterministic model.

$$\hat{\Phi}_k = b_0 + \sum_{i=1}^{N} (b_i \sin(2\pi t_k / T_i) + c_i \cos(2\pi t_k / T_i)) \ . \tag{3}$$

We parameterize and train this harmonic model in a way that is similar to the preceding AR model. First, we select 2600-year intervals that are centered on the timings t_{GSM} of each of the 23 grand solar maxima, and exclude the 300 years that follow each t_{GSM}. In contrast to the AR model, however, we estimate the model coefficients separately for each interval in order to account for possible phase drifts. To select the periods T, and reduce their number, we start from an initial set of $N = 19$ periods of less than 2200 years, taken either from ~~McCracken et al. (2013)~~McCracken et al. (2013), or obtained from spectral analysis. We then estimate the forecast error after discarding one period at a time, only keeping those that do not lead to a significant increase of the forecast error. Finally, we end up with a set of 12 periods of $\{88, 105, 130, 150, 197, 208, 233, 285, 353, 509, 718, 974\}$ years. Likewise, the forecast error is used to fix the 2600-year duration of the intervals. Longer intervals give a better statistic, but result in a poorer fit because of possible phase drifts in short-period oscillations.

3.2 Summary of Forecasts

Figure 22A shows the results of the AF, AR and HM forecasts, as well as the observed Φ record from 1845-1999. All three methods forecast a decrease in solar activity out to approximately 2100. In the HM model, oscillations with largest amplitudes occur, on average, at 88, 208, and 285 years, and so periodicities are clearly present in the HM forecast. In contrast, forecasts obtained from the AF and AR models tend to converge toward a climatological mean.

3.3 Prediction Errors

The error of each prediction method was assessed with a bootstrap approach. Defining grand solar maxima as any period in the Φ record larger than the 90^{th} percentile of the Φ distribution, there are 23 other grand solar maxima in the Φ record prior to the one that persisted through the late 20th century. For each prediction method, hindcasts were made for the 308 years following the decline from each prior grand solar maximum. For each method and each grand solar maximum, the models were trained analogously to the descriptions above, such that no Φ data from within the prediction window is used to generate each hindcast. The typical error in each prediction method as a function of prediction horizon was then calculated as the root mean square of the error of the 23 hindcasts at each prediction horizon.

Although not used in the scenario construction, a simple persistence forecast and the corresponding error was also calculated, to serve as a benchmark to compare the AF, AR and HM methods against. The typical prediction error as a function of prediction horizon for the AF, AR, HM and persistence (PS) methods is shown in Figure 22C. The AF, AR and HM methods have similar error levels and each quickly outperforms the simple persistence model. For most of the prediction window, the AR method shows the lowest error, although the error in the HM decreases near a prediction horizon of 220 years, arguably due to the strength of the de Vries cycle, a 208 year periodicity observed in the power spectrum of the Φ record, and an important component of the HM model.

3.4 Scenario Construction

The REF scenario was calculated as the weighted average of the AF, AR and HM predictions for the current grand solar maximum, where the prediction errors shown in Figure 22C were used as the weightings. Here again, the maximum likelihood estimate of the average scenario is obtained simply by making a weighted average of the AF, AR and HM predictions. A different approach was used to calculate the EXT scenario. Here, : the AF, AR and HM methods were used to generate hindcasts of the 23 prior grand solar maxima, also for a 308 year prediction window. The extreme scenario was then calculated as the 5th percentile of the 3×23 hindcasts at each prediction horizon. The REF and EXT scenarios are shown in Figure 22B. Let us stress again that EXT scenario is meant to be used primarily for sensitivity studies, in contrast to the REF scenario, which is the reference one.

Figure 22B shows that both scenarios start with a phase of low solar activity, which extends from approximately 2050 to 2110. In the reference scenario, the deepest level is comparable to the Gleisberg minimum that occcurred in the late 19th century, whereas in the extreme scenario, it is considerably deeper, and reaches a Maunder-type minimum. The extreme scenario lingers in that state, whereas the reference one recovers to a climatological mean that is comparable to levels observed during the 1st half of the 20th century. Let us stress that none of the forecasts exhibits a grand solar maximum similar to the one that just ended.

3.5 Future Solar Cycle Definition and Scaling Procedure

Future cycles are constructed from historical cycles by projecting them into the future. The average solar activity level of the projected historical cycles was thereby scaled in accordance to the predicted activity level of the scenarios. Solar activity variations on time scales shorter than a solar cycle are hence preserved. This strategy ensures consistency between the different types of radiative and particle forcing on all time scales also in the future. The historical cycles used for projection into the future are listed in Table 6 of Appendix G.

We assume a linear dependence of the 22-year average sunspot number $<\mathrm{SSN}>_{22}$ on Φ for the scaling of future solar cycles:

$$< \mathrm{SSN} >_{22} = 0.084\,\Phi + 20.6. \qquad (4)$$

The coefficients of Eq. 4 have been obtained from a regression fit, based on SSN and Φ in the time period 1768–2010 (see Fig. 23). We use international sunspot number version 1.0, because most SSI models rely on that version (see Sec. 2.1.1).

t

The resulting SSN time series of both future scenarios have then be been used to calculate the SSI with the SATIRE-TS SATIRE and NRLSSI2 models with annual time resolution. As for the historical CMIP6 dataset, we took for each scenario the arithmetic mean of the two model results. SSI variations on shorter time scales are taken from the corresponding past solar

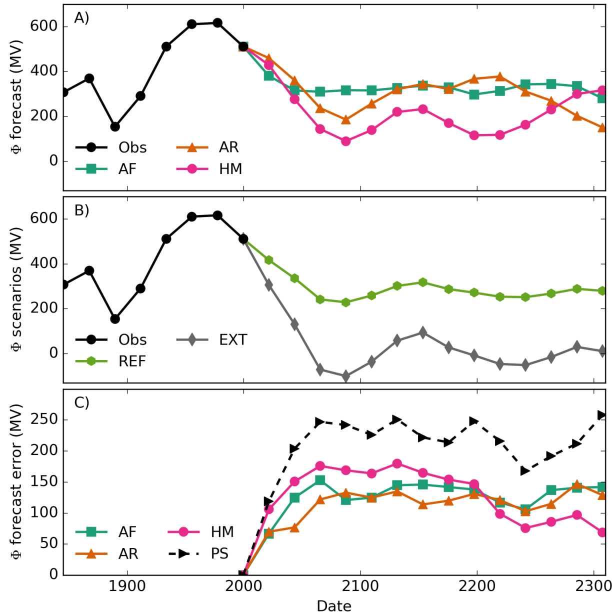

Figure 22. A) Observations of Φ (Obs) from 1850 until 1999, and the three forecasts from 1999 until 2300, from the analogue forecast (AF), auto-regressive model (AR) and harmonic analysis (HM) methods. B) The CMIP6 reference scenario (REF) and extreme scenario (EXT). C) The forecast error for the AF, AR, HM and PS methods, estimated by employing a bootstrap hindcast approach, calculating the root-mean-square of the hindcast errors for 23 prior grand solar maxima in the ϕ record. The occurrence of unphysical negative values comes from the original modulation potential data, and not necessarily from the prediction methods, see Fig. 21.

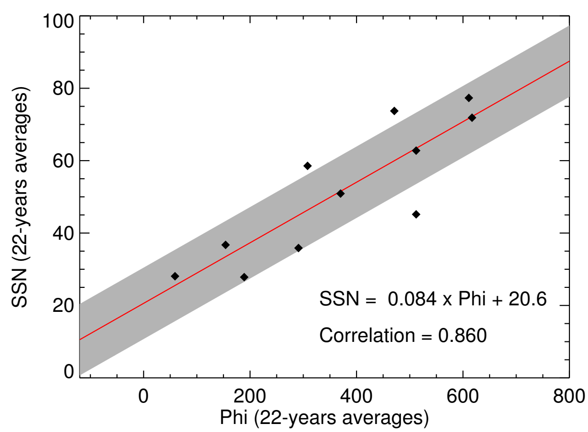

Figure 23. Regression of 22-year averaged SSN to the modulation potential Φ. The grey-shaded area represents the 1σ uncertainty range of the fit. Regression coefficients and the correlation coefficient are also indicated.

cycles, and are scaled to a comparable cycle-average level of activity by means of a dedicated scaling procedure, as described in Appendix H. F10.7 radio flux data has been constructed from the resulting future SSI record as described in Sec. 2.1.2.

A similar approach has also been chosen for the future particle forcing. Magnetospheric particle forcing (Sec. 2.2.1) relies on the geomagnetic indices Ap and Kp, being closely related to sunspot number on decadal time scales (e.g., Cliver et al., 1998). The scaling of these indices in past solar cycles into the future on basis of <SSN> is described in Appendix I. The 2015–2300 Ap time series we obtained have then been used to calculate MEE ionization rates for the REF and EXT scenarios. Similarly, odd nitrogen upper boundary conditions for the consideration of the EPP indirect effect in climate models with their upper lid in the mesosphere can be computed on basis of the future Ap index with the recommended UBC model (Funke et al., 2016). Future GCR-induced ionization (see Sec. 2.2.3) is calculated from the Φ of the respective scenarios and interpolated to interannual timescales by using the future SSN time series. The proton forcing of past solar cycles (Sec. 2.2.2) has also been projected into the future, however, no scaling of the proton ionization in dependence of the future cycles' activity level has been made. This is primarily motivated by the lack of knowledge on long-term variations of proton fluxes, related to the short availability of observational records (since 1962).

3.6 Solar Forcing in Future Scenarios

~~ht~~

~~ht~~

As mentioned before, we provide two scenarios of future solar activity: the reference one is based on the most likely evolution of solar activity from 2015 to 2300, while the extreme one corresponds to the lower 5th percentile of all forecasts. We first forecast the modulation potential Φ with the three approaches described in Sec. 3.1.1 to 3.1.3, and define then the reference scenario as their average, weighted by their inverse forecast error (Eq. 2). Note that the analogue forecast, and to a lesser degree, the AR forecast tend to converge toward a climatological mean, whereas the harmonic forecast keeps on oscillating. Because of that, our forecasts are likely to exhibit somewhat less variability than the observed Φ.

Figures 24 and 25 present an overview of the entire daily CMIP6 solar forcing file from 1850 through 2300, respectively for the reference and extreme scenarios. Both show the the TSI, the F10.7cm solar radio flux, which is a good proxy for Lyman-α line, and three different SSI wavelength ranges in the UV, VIS, and NIR. Also shown are the Ap index as a proxy for auroral electron precipitation, and the ionization rates due to solar protons and galactic cosmic rays. In Fig.25, MEE instead of proton ionization rates are shown, as the latter are identical in both scenarios.

~~Both scenarios start with a phase of low solar activity, which extends from approximately 2050 to 2110: in the reference scenario, the deepest level is comparable to the Gleissberg minimum that occurred in the late 19th century, whereas in the extreme scenario, it is considerably deeper, and reaches a Maunder-type minimum. The extreme scenario lingers in that state, whereas the reference one recovers to a climatological mean that is comparable to levels observed during the 1st half of the 20th century. Let us stress that none of the forecasts exhibits a grand solar maximum similar to the one that just ended.~~

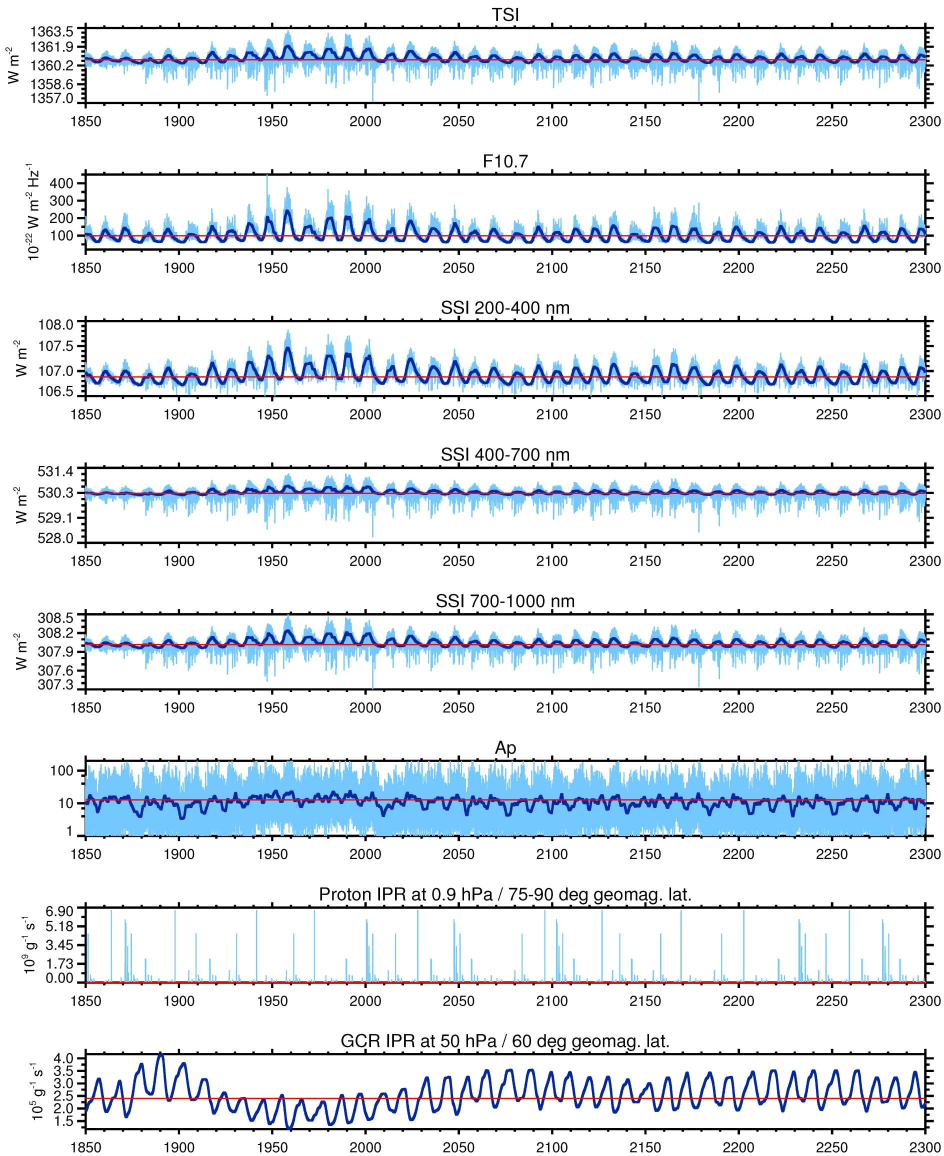

Figure 24. CMIP6 Reference (REF) scenario forcing shown for (from top to bottom) TSI, F10.7, SSI at 200–400 nm, SSI at 400–700 nm, SSI at 700-1000 nm, Ap, proton IPR at 1 hPa and 70° geomagnetic latitude, and GCR IPR 50 hPa and 60° geomagnetic latitude. Annually smoothed values are shown by dark blue lines. Constant values of the PI control forcing (see Sec. 4) are shown with red lines as reference.

As explained in Appendix G, our scenarios are built out of past solar cycles; therefore, both the solar cycles and their daily variations are consistent with the average level of heliospheric potential. In this sense, the future scenarios for CMIP6 are much more realistic than the stationary Sun scenario that went into CMIP5.

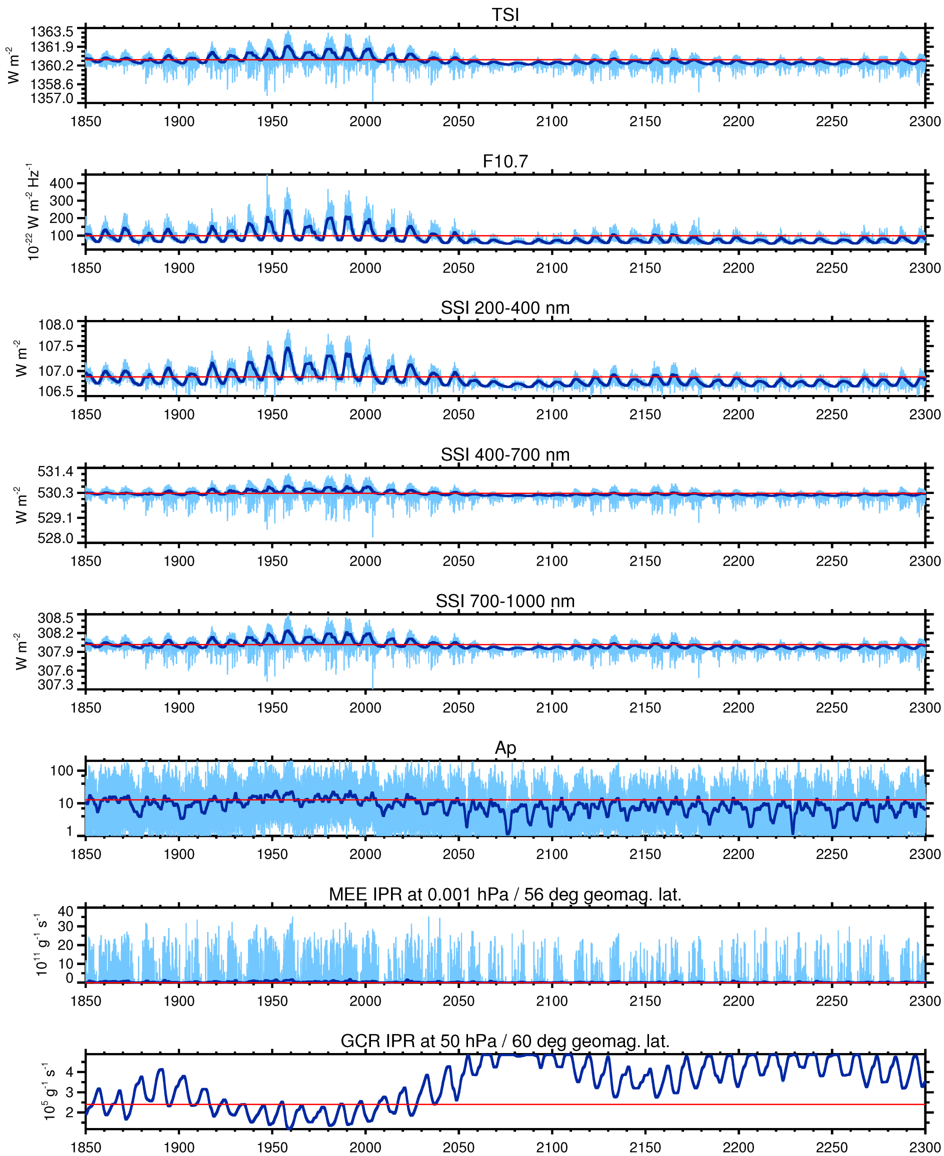

Figure 25. CMIP6 Deep minimum (EXT) scenario forcing shown for (from top to bottom) TSI, F10.7, SSI at 200–400 nm, SSI at 400–700 nm, SSI at 700-1000 nm, Ap, MEE IPR at 0.001 hPa and 56° geomagnetic latitude, and GCR IPR 50 hPa and 60° geomagnetic latitude. Annually smoothed values are shown by dark blue lines. Constant values of the PI control forcing (see Sec. 4) are shown with red lines as reference.

4 Pre-industrial (PI) Control Forcing

~~ht~~

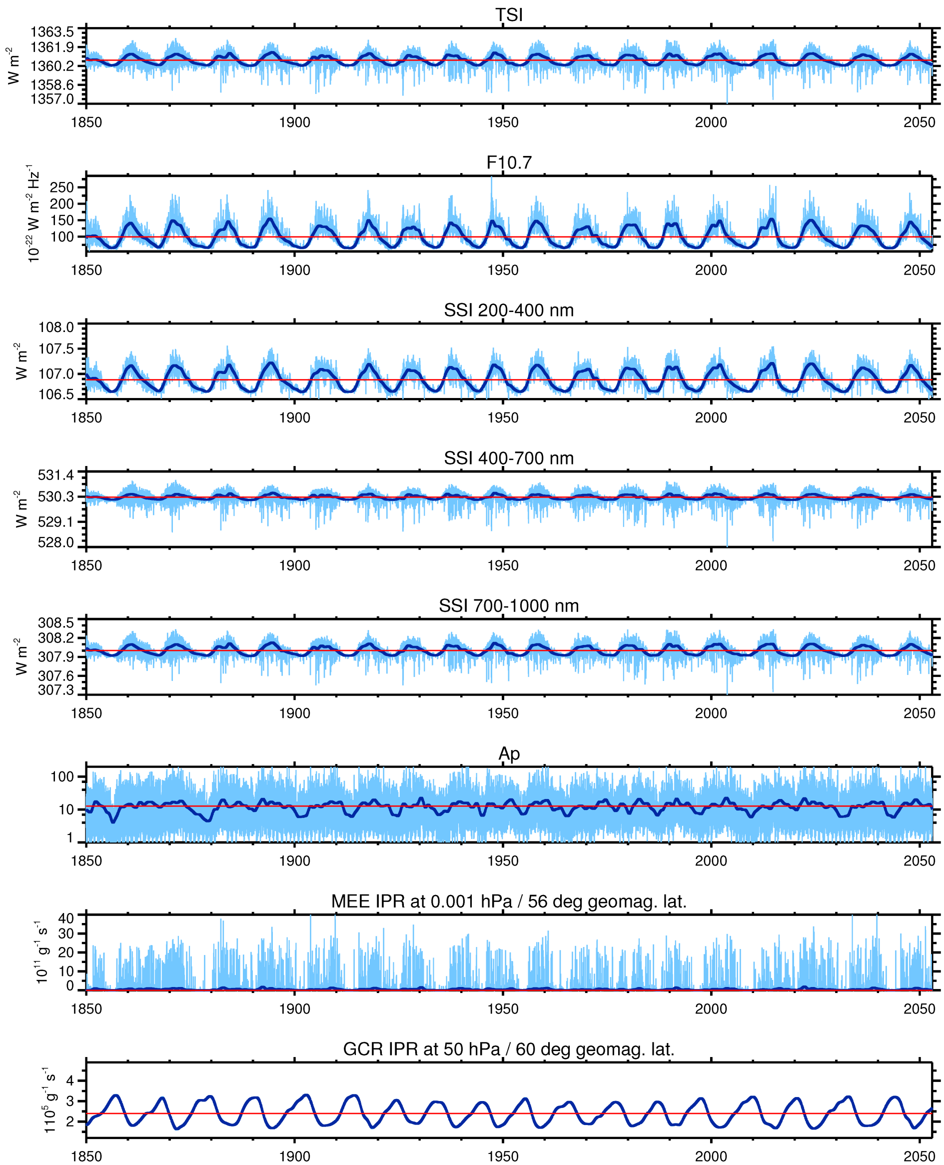

Figure 26. CMIP6 Variable (light blue) and constant PI-control (red) forcing shown for (from top to bottom) TSI, F10.7, SSI at 200–400 nm, SSI at 400–700 nm, SSI at 700-1000 nm, Ap, MEE IPR at 0.001 hPa and 56° geomagnetic latitude, and GCR IPR 50 hPa and 60° geomagnetic latitude. Annually smoothed values are shown by dark blue lines. Note the different scale for F10.7 in comparison with Figures 24 and 25.

For the PI control experiment, we recommend to use one constant (solar cycle averaged) value for the TSI and SSI spectrum representative for 1850 conditions (Fig.26). The average in TSI, SSI, Ap, Kp, F10.7, as well as the ion-pair production rate by GCRs covers the time period from 1.1.1850 to 28.1.1873, which is two full solar cycles. For the ion-pair production rates by SPEs and MEEs median values representative for the background are provided in order to avoid the occurrence of large sporadic events in the PI control experiment.

As usual the PI control run is supposed to provide an estimate of the unforced climate system to understand internal model variability. It is also used for detection and attribution studies to disentangle contributions from different natural and anthropogenic forcings (some of which include a long-term trend, such as GHGs, aerosols, solar forcing).

For those groups that are interested, we also provide a 1000-year solar forcing time series with 11-year solar cycle variability included but without long-term trend (Fig.26). This time series still has slightly different solar cycle amplitudes and also preserves the variable phase of the solar cycle, however, the solar cycle mean activity level is held constant as compared to the reference scenario in Fig. 24. By running a second PI control experiment with solar cycle variability, this provides one additional periodic forcing on top of the seasonal cycle. Since the PI control is also used to determine model variability at decadal ~~time scales~~timescales, including a solar cycle would certainly change the mean climate and the variance of the control experiment as compared to the “standard” control experiment with constant 1850 solar forcing. However, not including the solar cycle variability may underestimate the variance of the climate system and may lead to climate system biases. Ideally the groups would do two PI control experiments: one with and one without solar cycle variability.

~~The~~ Note that the variable PI control dataset is meant solely for sensitivity experiments in order to understand physical mechanisms for internal natural climate variability such as a potential synchronization of North Atlantic climate variability by the 11-year solar cycle (Thieblemont et al., 2015) in the atmosphere-ocean system. It avoids on purpose any long-term trend in solar activity, and should therefore not be used for historical model simulations andor solar forcing reconstructions. More realistic solar forcing timeseries for the past 1000 years are provided within the PMIP (Paleoclimate Modeling Intercomparison Project) exercise (Kageyama et al., 2016) and the solar forcing is described in more detail in (Jungclaus and et al., 2016).

The radiative part of the variable PI control forcing has been generated by scaling the annual and sub-annual components of the REF forcing dataset to a constant solar cycle mean activity level~~representative for the time period from 1.1.1850 to 28.1.1873~~. The scaling procedure for SSI and F10.7 is described in Appendix H. Constant background components have been added. These have been adjusted such that the mean values of the resulting SSI and F10.7 time series are consistent with the constant PI control forcing. In order to enhance the contrast for this sensitivity experiment, we scale the annual and sub-annual components of SSI at wavelengths greater than 115 nm to the mean activity level of solar cycles 18–22 (grand solar maximum) rather than to 1850–1873 conditions. For the EUV channels (10–115 nm) and for F10.7, such an enhanced mean activity level would result in unreasonably low background values (due to the adjustment to the constant PI control forcing). Therefore, the annual and sub-annual components of these quantities were scaled to 1850–1873 conditions.

Similarly, the particle part of the variable PI control forcing has been generated by scaling the annual and sub-annual components of the REF forcing dataset to the 1850—1873 mean activity level. The scaling of ~~geomagentic~~ geomagnetic Ap and Kp indices is described in Appendix I. MEE-induced ion-pair production rates for the variable PI control forcing have then been calculated from the scaled Ap data. GCR-induced ion-pair production rates have been calculated using a constant value of Φ representative for the ~~1850–1873~~ 1850–1873 period. Solar cycle variations have been added~~by using the future SSN time series~~, however, scaled to the ~~1850–1873~~ 1850–1873 mean activity level. The variable PI control proton forcing is identical to the REF forcing since it does not include any long-term trend. Note that the temporal averages of SSI, TSI, F10.7, Ap, Kp, as well as GCR-induced ion-pair production rates are fully consistent ~~wit~~ with the values provided in the constant PI control forcing dataset. This, however, is not the case for the proton and MEE forcings, which, in the latter case, do not account for large, sporadic events.

The variable PI control dataset (see Fig. 26) covers the time period from 1.1.1850 until 9.9.2053 (end of solar cycle 27). The dataset can be extended to cover 1000 years by multiple repetition of the solar cycle sequence 12–27. The first 450 years of the resulting forcing time series are consistent in solar cycle phase and short-term fluctuations with the REF and EXT datasets. Solar forcing only experiments based on variable PI control, REF, and EXT forcing data would therefore be ideally suited to address the impact of long-term solar activity variations on the climate system.

5 Solar Signal in Stratospheric Ozone

The climate response to solar variability depends not only on the ‘direct’ impact of changes in TSI and SSI on atmospheric and surface heating rates, but also on the ‘indirect’ effects on stratospheric and mesospheric ozone abundances (e.g. Haigh, 1994). The associated solar-ozone response can contribute more than 50% of the total stratospheric heating response to solar variability in some regions (Shibata and Kodera, 2005; Gray et al., 2009). It is therefore important to include the solar-ozone response in global model simulations to realistically capture the impacts of solar variability on climate.

In reality, the ‘direct’ and ‘indirect’ parts of the heating are highly coupled, since they reflect the same fundamental process (i.e. absorption of ~~incoming~~ solar photons by molecules). In (~~chemistry~~chemistry-)climate models, the effects of these processes on atmospheric heating rates and temperatures ~~is captured~~ are incorporated through the radiation scheme as a result of variations in the ozone field and the specified values of TSI and SSI (see Tab. 3). The ozone field in a model can be produced by an interactive photochemical scheme, as presented above for CESM1(WACCM) and EMAC, or it can be externally prescribed in models that do not have a chemistry scheme. Models with a chemistry scheme must adequately represent SSI variability in their photolysis schemes (e.g. in the UV part of the spectrum) to simulate a realistic solar-ozone response. As described above, variations in EPP also affect stratospheric and mesospheric ozone abundances. These effects will be implicitly captured in CCMs with the capability of prescribing EPP and/or their effects on chemical processes (e.g. NOx).

Several CMIP5 models included stratospheric chemical schemes (Hood et al., 2015), and it seems likely that more models will have this capability in CMIP6. However, there ~~are still likely to~~ will be CMIP6 models that do not include chemistry ~~,~~ but which resolve the stratosphere and specify SSI, ~~so~~ and thus have some of the major ingredients for simulating a top-down pathway for solar-climate coupling (Mitchell et al., 2015b). For these models, the simulated climate response to solar variability will partly depend on ~~how the~~ the representation of the solar-ozone response ~~is represented~~ in their prescribed ozone field.

CMIP5 models without chemistry were recommended to use the SPARC/AC&C Ozone Database (Cionni et al., 2011). The historical part of this dataset for the stratosphere provided monthly and zonal mean ozone concentrations based on a multiple regression analysis of ~~data~~ measurements from the Stratospheric Aerosol and Gas Experiment (SAGE) satellite instruments. The regression coefficients for various key drivers (e.g. ODS, GHG, solar forcing) were used to reconstruct ozone values back to 1850 as a function of latitude and pressure. The historical part of the CMIP5 ozone dataset therefore implicitly included a solar-ozone response derived from satellite observations. However, the SAGE data only cover uncertainties in the amplitude of the solar-ozone response in SAGE II measurements, which cover only around two solar cyclesand there are significant uncertainties associated with the solar-ozone response in these data that , have been recently documented (Maycock et al., 2016a)by Maycock et al. (2016a). It is therefore desirable to update the representation of the solar-ozone response in the upcoming WCRP/SPARC Chemistry Climate Model Initiative (CCMI) Ozone Database being developed for CMIP6 (Hegglin, 2016).

To determine a "best approach" for including the At the time of writing, this database is still under development and readers are referred to Hegglin (2016) for final details. However, for illustrative purposes, Figure 27 shows the monthly mean fractional solar-ozone response in the CCMI Ozone Database, Maycock et al. (2016a, b) conducted a detailed analysis of current satellite ozone datasets and CCM simulations. The emphasis of these studies was on utilising the available data sources to define and solar-ozone response that meets the necessary minimum criteria for the CCMI Ozone Database (Hegglin, 2016). The main properties of the database are that it provides monthly mean ozone mixing ratios on pressure levels covering 1000-0.01 hPa and as a function of latitude for the period 1850-2100.

Maycock et al. (2016a) found that the solar-ozone response in SAGE II mixing ratio data, which has been used extensively for stratospheric ozone studies, shows a strong dependency on the independent temperature record used to convert retrievals from their native number density on altitude coordinates to mixing ratios on pressure levels. Given the current large uncertainties in the historical evolution of stratospheric temperatures in reanalysis datasets (Mitchell et al., 2015a), Maycock et al. (2016a) concluded that the SAGE II number density data likely provide the most reliable estimate of the solar-ozone response from SAGE data at the current time. However, the relatively sparse spatial and temporal sampling of SAGE means that these data can only provide an annual mean solar-ozone response for the tropics and midlatitudes.

The Solar Backscatter Ultraviolet (SBUV) dataset is another long-term ozone record that has been used extensively for stratospheric ozone studies (e.g Tummon et al., 2015). As a nadir-viewing instrument, the SBUV data provide relatively good spatial coverage, which allows for an assessment of the solar-ozone response on seasonal timescales; however, it possesses much poorer vertical resolution below ∼15 hPa compared to SAGE II. Maycock et al. (2016a) identified some differences between the solar-ozone response in two versions of the recent SBUV VN8.6 data, which must be related to data selection, calibration and merging procedures. However, the differences in the upper stratospheric solar-ozone response were smaller than between the different versions of SAGE II mixing ratio data. An analysis of the solar-ozone response on monthly timescales in SBUV data suggested substantial sub-annual variations in the magnitude of the solar-ozone response, particularly in the extratropics in the winter hemisphere. These shorter timescale variations in the solar-ozone response may be important for the climate response to solar variability (Hood et al., 2015), but were absent in the CMIP5 Ozone Database; it is therefore desirable to incorporate them into the CCMI CMIP6 Ozone Database.

Since the core of the CCMI CMIP6 Ozone Database is based on CCMI simulations evaluated against observations (Hegglin, 2016), a similar approach has been adopted for defining the solar-ozone response in this database. Maycock et al. (2016b) examined the solar-ozone response in seven CCMI models. These models provided simulations of the recent past (1960-2009) that include all known external forcing agents (SSI, ODS, GHGs, volcanic aerosols, observed SSTs and sea ice). The annual mean solar-ozone responses in the CCMs were compared to a subset of observational datasets that were determined by Maycock et al. (2016a) to currently provide the most reliable estimate of the solar-ozone response. Three of the seven CCMs were assessed to show key areas where their responses disagreed with the observations after the uncertainties in the modelled and observed solar-ozone responses were accounted for. The remaining four models were combined to create a CCMI multi-model mean (MMM) monthly and zonal mean fractional solar-ozone response that includes global coverage from 1000-0.01 hPa. Tropospheric points were masked out using a monthly mean tropopause climatology. Data between the uppermost CCMI data output level (0.1 hPa) at the uppermost level of the CCMI Ozone Database (0.01 hPa) were filled at each latitude using an exponentially decaying extrapolation with decreasing pressure of the ozonecoefficients at 0.1 hPa.

As described above, variations in EPP also affect stratospheric and mesospheric ozone abundances. These effects will be implicitly captured in CCMs with the capability of prescribing EPP and/or their effects on chemical processes (e.g.NOx). The approach of Maycock et al. (2016b) uses a multiple regression onto the per 130 units of the F10.7cm solar flux to extract the cm solar flux that has been diagnosed using a multiple linear regression model (see Maycock et al. (2016a)) for the period 1960-99 from the CMIP6 historical ozone files (file: vmro3_input4MIPs_ozone_CMIP_UReading-CCMI-1-0_gr_195001-199912.nc) recently made available through input4MIPs (https://pcmdi.llnl.gov/projects/input4mips/). There is currently no information available about how the solar-ozone response from CCMs. Two of the four CCMI models included in their composite EPP effects (CESM1-WACCM and SOCOL). Thus, although the analysis conducted by Maycock et al. (2016b) did not explicitly account for a solar-ozone response associated with EPP effects, it may implicitly include some component of this if the various indices for EPP (e. g. Ap) are correlated with the F10.7cm flux. will be represented in the ozone files for the future period and readers are referred to Hegglin (2016) for details.

The monthly mean fractional solar-ozone response per 130 units of the F10.7cm solar flux defined by Maycock et al. (2016b) is shown in Figure 27 . These show Figure 27 shows a solar-ozone response of up to ∼2% in the tropical mid-stratosphere which peaks at ∼5 hPa. The greatest fractional Since the peak amplitude of the solar-ozone response occurs in the high latitudes, particularly in the winter hemispheres, and in the lowermost stratosphere. Since the solar-ozone response has been defined as a function of the F10.7cm flux alone, a sequence of spatially and temporally evolving ozone anomalies can readily be constructed for all relevant CMIP6 simulations (historical, future, PI-control) using the time series of CMIP6 recommended F10.7cm solar fluxes described above. These anomalies are being incorporated into the in Figure 27 is considerably smaller, and exhibits a different vertical structure, compared to the SAGE data used in the SPARC/AC&C CMIP5 Ozone Database (Maycock et al., 2016a), we anticipate that the magnitude of the solar cycle temperature response in models using the CCMI CMIP6 Ozone Database (Hegglin, 2016). A stratosphere-resolving climate model without chemistry that adopts both the may also be smaller.

We recommend that CMIP6 models without interactive chemistry use the recommended SSI forcing described above and the CCMI Ozone Database will therefore include a consistent (i.e. in phase) CMIP6 Ozone Database described by Hegglin (2016) to ensure consistency in the representation of the impact of solar variability on atmospheric heating rates. If a climate model uses the recommended solar cycle forcing across models. If CMIP6 solar forcing dataset, but prescribes models use an alternative ozone dataset ~~that includes a substantially different~~ with a different representation of the solar-ozone response ~~,~~ it would be ~~expected to show a different solar-climate response compared to other models (Hood et al., 2015). If such cases arise, a minimum requirement is that the temporal evolution of the solar-ozone response should match that of the CMIP6 solar forcing dataset. If this is not the case, then the simulated solar-climate response in a model will not be realistic. It is therefore important to know the methods adopted for implementing stratospheric ozone and the solar-ozone response in CMIP6 models without chemistry.~~ very valuable for this to be documented so that differences in modelled responses to the solar cycle might be understood (Mitchell et al., 2015b).

~~The ozone anomalies in Figure 27 have been implemented and tested in the Hadley Centre Global Environmental Model 3 (HadGEM3) climate model (Maycock et al., 2016b) using timeslice experiments for solar maximum and minimum conditions similar to those for (CESM1)WACCM and EMAC described above, but using the CMIP5 recommended SSI dataset (Lean, 2000). Equivalent experiments using the solar-ozone response from the CMIP5 ozone database have been conducted for comparison. The net (irradiance + ozone) tropical mean temperature response between 11 year solar maximum and minimum is 0.8 K at 1 hPa using the CMIP6 solar-ozone response from Figure 27. This can be compared to a peak tropical mean solar cycle temperature response of ~1.2 K for the same model using the CMIP5 SPARC/AC&C Ozone Database. The new recommended solar-ozone response for CMIP6 therefore results in a smaller amplitude solar cycle signal in upper stratospheric temperature by around 30%.~~

6 Conclusions

This paper provides a comprehensive description of the solar forcing for CMIP6. The dataset consists of time series from 1850 through 2300 of radiative (TSI, SSI, F10.7cm) and particle (Ap, Kp, ionization rates due to SPEs, MEEs, and GCRs) forcings. This is the first time that solar-driven particle forcing has been included as part of the CMIP recommendation and represents a new capability for CMIP6. TSI and SSI time series are defined as averages of two ~~(semi-) empirical~~ solar irradiance models, ~~namely the~~ the empirical NRLTSI2/NRLSSI2 ~~and SATIRE-TS~~model and the semi-empirical SATIRE model. Since this represents a change from the CMIP5 recommended NRLTSI1 and NRLSSI1 dataset, the paper puts special emphasis on the comparison between the radiative properties of the CMIP5 and CMIP6 solar forcing recommendation. Solar forcing is provided in daily as well as monthly resolution separately for the reference period of the historical simulation, i.e. 1850–2014, for the future, i.e. 2015–2300, including an additional extreme Maunder Minimum-like sensitivity scenario, as well as for a constant and a time-varying PI-Control forcing. The particle forcing is only included in the daily resolution files. The dataset as well as a metadata description and a number of tools to convert and implement the solar forcing data can be found here: http://solarisheppa.geomar.de/cmip6. In the following we highlight the most important points of the CMIP6 solar forcing dataset in comparison to CMIP5 that provide the reader with an overview without reading the paper in detail.

Radiative Forcing

- A new and lower TSI value is recommended: the contemporary solar cycle-average is now 1361.0 ± 0.5 W/m^2 ~~(Mamajek et al., 2015)~~

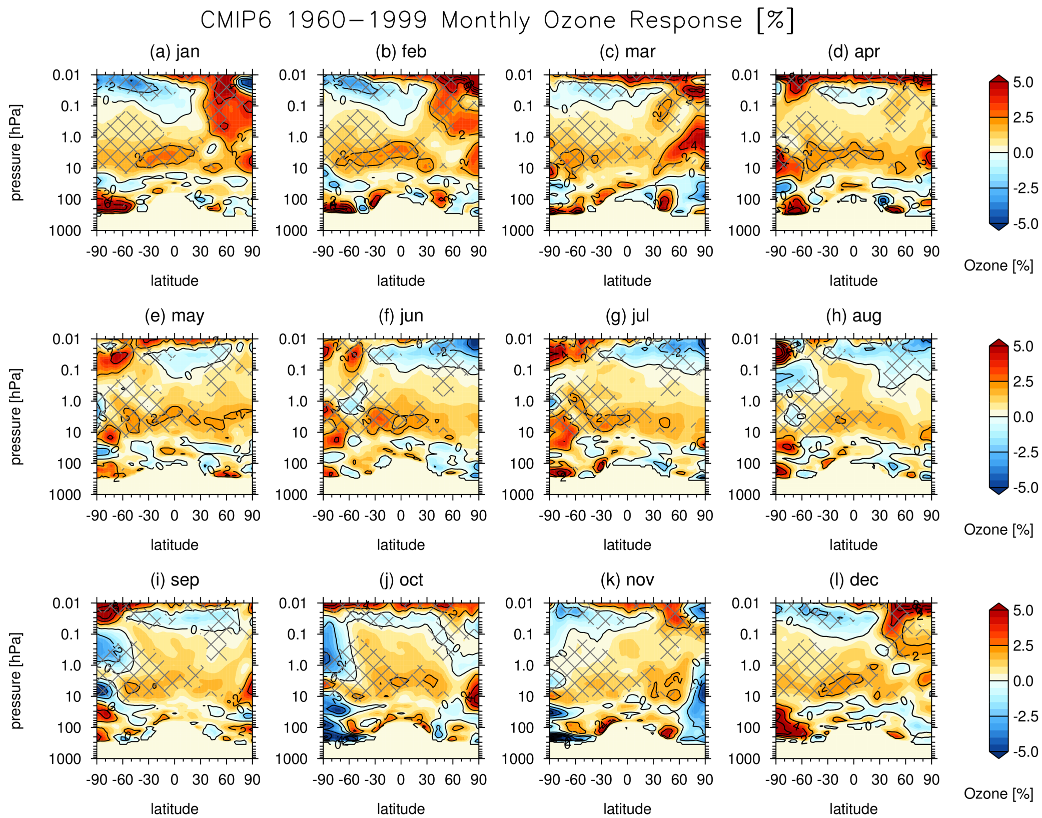

Figure 27. ~~The CMIP6 recommended monthly percent~~ A preliminary estimate of the fractional (%) monthly solar-ozone ~~coefficients based on 4~~ response per 130 units of the F10.7cm flux in the CCMI ~~models~~ Ozone Database for CMIP6 extracted using multiple linear regression for the period 1960-99 using the ozone mixing ratio files (~~CESM1-WACCM, LMDZrepro, MRI-ESM1, SOCOL3~~vmro3_input4MIPs_ozone_CMIP_UReading-CCMI-1-0_gr_195001-199912.nc) downloaded from inputs4MIPs. ~~Figure reproduced~~ The hatching denotes regions where the extracted solar-ozone response is estimated to be significantly different from ~~Maycock et al. (2016b)~~zero at the 95% confidence level. Please note that the details of the CMIP6 Ozone Database are still being finalised at the time of writing and we refer readers to Hegglin (2016) for further details.

- During the last three solar cycles in the satellite era there is a slight negative TSI trend in CMIP6 which is statistically indistinguishable from available observations (Dudok de Wit et al., 2016a). This trend leads to a radiative forcing on a global scale of -0.04 W/m^2 which is small in comparison with other forcings.
- The new CMIP6 SSI dataset is the arithmetic mean of the empirical NRLSSI2 and the semi-emipirical SATIRE-TS SATIRE irradiance models and covers wavelengths from 10–10,000 nm.
- The CMIP6 SSI dataset agrees very well with available satellite measurements (i.e. those which are used for building the SOLID observational composite) in the contribution of solar cycle variability to TSI in the 120–200 nm wavelength range. In the 200–400 nm range, which is also important for ozone photochemistry, CMIP6 shows a larger solar cycle variability contribution to TSI than CMIP5 (50% as compared to 35%). However, there is a lack of accurate satellite measurements to validate variations in this spectral region. In the VIS part of the spectrum, CMIP6 shows smaller solar cycle variability than CMIP5 (25% as compared to 40%). In the NIR, CMIP6 shows slightly larger variability than CMIP5. The implications of the differences in the spectral characteristics of SSI between CMIP5 and CMIP6 on climatological and solar cycle variability in atmospheric heating rates and ozone photochemistry have been tested using two state-of-the art CCMs, EMAC and CESM1(WACCM), and a line-by-line radiative transfer model, libradtran.
- When comparing the annual mean climatological differences under perpetual solar minimum conditions, the CMIP6-SSI irradiances lead to lower SW heating rates (-0.35 K/day at the stratopause), cooler stratospheric temperatures (-1.5 K in the upper stratosphere), lower ozone abundances in the lower stratosphere (-3%), and higher ozone abundances (+1.5%) in the upper stratosphere and lower mesosphere, as compared to the CMIP5-SSI irradiances. These radiative effects lead to a weakening of the meridional temperature gradient between the tropics and high latitudes and hence to a statistically significant weakening of the stratospheric polar night jet in early winter.
- The changes in solar irradiances between solar cycle maximum and minimum in the CMIP6-SSI dataset result in increases in SW heating rates (+0.2 K/day at the stratopause), temperatures ($\sim$1 K at the stratopause), and ozone (+2.5% in the upper stratosphere) in the tropical upper stratosphere. These direct radiative effects lead to a strengthening of the meridional temperature gradient between the tropics and high latitudes and a statistically significant strengthening of the stratospheric polar night jet in early winter, which propagates poleward and downward during mid-winter and affects tropospheric weather, with a positive Arctic Oscillation signal in late winter. This regional surface climate response is similar and statistically significant in both CCMs. The CMIP6-SSI irradiances lead to slightly enhanced solar cycle signals in SW heating rates, temperatures and ozone, as compared to the CMIP5-SSI. However, the differences between the solar cycle signals for the two SSI datasets are generally not statistically significant and the solar signal is smaller than the before mentioned climatological differences between CMIP6 and CMIP5.

Particle Forcing

- The reconstruction of geomagnetic Ap and Kp indices backwards in time (starting in 1850) allowed to generate a consistent historical dataset of geomagnetic particle forcing for the consideration of the atmospheric impact of precipitating auroral and radiation belt electrons. Regarding the latter, we employed a novel precipitation model for mid-energy electrons (MEE), based on the Ap index. Computed MEE ionisation rates have been successfully tested in the WACCM model. For the consideration of polar winter descent of EPP-generated NO_x in climate models with their upper lid in the mesosphere (i.e., below the EPP source region), recommendations for the implementation of an odd nitrogen upper boundary condition (UBC) are provided. The UBC has been successfully tested with the EMAC model by comparison to observations. Inclusion of the recommended CMIP magnetospheric particle forcing in climate model simulations improves significantly the agreement with observed NO_x, HO_x, and ozone distributions in the polar stratosphere and mesosphere.

- Solar proton and Galactic Cosmic Ray forcings have been built from well-established datasets which have been used in many atmospheric model studies. Observed proton fluxes, however, are only available since 1963. Before, the proton forcing included in our dataset is fictitious, although resembling the expected overall strength and distribution along the solar cycles.

- In most cases, particle forcing can be expressed in terms of ion pair production rates. We have provided detailed recommendations for their implementation into chemistry schemes.

- CMIP6 model simulations utilizing the recommended particle forcing for the historic (1850–2014) period will allow to address the potential long-term effect of particles as planned to be assessed in upcoming coordinated WCRP/SPARC SOLARIS-HEPPA studies.

Future Forcing

In CMIP5, future solar irradiances assumed no long-term changes in the Sun and were obtained by simply repeating solar cycle 23 into the future. In CMIP6, we include a more realistic evolution for future solar forcing based on the weighted average of three statistical forecast models; this shows a moderate decrease to a Gleissberg-type level of solar activity until 2100 for the reference (REF) scenario. We ignore scenarios with high levels of solar activity because the Sun just left such an episode (called grand solar maximum), and several studies suggest that it is very unlikely to return to it in the next 300 years. In addition, we provide an extreme (EXT) scenario to be used for sensitivity studies, which includes an evolution to an exceptionally low level of solar activity similar to that estimated for the Maunder Minimum.

PI-Control Forcing

For the PI control experiment, we recommend to use one constant (solar cycle averaged) value for the TSI and SSI spectrum representative for 1850 conditions. The average values in TSI, SSI, Ap, Kp, F10.7, as well as the ion-pair production rate by GCRs are derived from the time period 1.1.1850 to 28.1.1873, which is two full solar cycles. For the ion-pair production rates by SPEs and MEEs, median values representative of background conditions are provided in order to avoid the occurrence of large sporadic events in the PI control experiment.

We also provide a second PI control forcing time series with a time-varying solar cycle component, but without long-term trend. This time series contains some variation in solar cycle amplitude, and also preserves the variable phase of the solar cycle, however, the mean level of solar activity is held constant~~at the same values as for the reference PI control experiment~~. The PI control experiment with solar cycle variability included may reproduce decadal scale climate variability better. Ideally the groups will run two PI control experiments: one with and one without solar cycle variability.

Solar Ozone Forcing

~~For climate~~ Climate models that do not calculate ozone interactively ~~, monthly solar cycle induced ozone anomalies have been calculated from an ensemble of CCMI models and will be used in conjunction with the CMIP6 recommended F10.7cm solar flux to construct a sequence of spatially and temporally varying ozone anomalies that will be incorporated into~~ are recommended to use the CCMI Ozone Database for CMIP6 (Hegglin, 2016)~~.~~ , which includes a representation of the solar-ozone response derived from CCM simulations. Readers are referred to Hegglin (2016) for further details. Please note that particle-induced ozone anomalies are not yet explicitly considered in this ozone database. CMIP6 models that include both CMIP6-SSI and solar induced-ozone variations are expected to show a better representation of solar climate variability compared to models that exclude the solar-ozone response.

7 Data Availability

The CMIP6 solar forcing dataset described in this paper as well as the metadata description will be published at http://solarisheppa.geomar.de/cmip6 and linked to the Earth System Grid Federation (ESGF) with version control and digital objective identifiers (DOIs) assigned. An overview of the CMIP6 Special Issue can be found in Eyring et al. (2015).

Appendix A: Reconstruction of the SSI in the EUV

The EUV spectrum is a complex mix of spectral lines and continua that are associated with different elements, and have each their specific variability in time. In spite of this, there is strong observational evidence for the spectral variability in the EUV to have remarkably few degrees of freedom (Amblard et al., 2008). We make use of this property to reconstruct the EUV at wavelengths shortward of 105 nm (in a range that is not covered by NRLSSI2 and SATIRE) as a function of the SSI provided by these same models between 115.5 and 123.5 nm (i.e. including the intense Lyman-α line).

Let $\Phi(\lambda, t)$ denote the logarithm of the SSI in the EUV, and $\bar{\Phi}(t)$ its value averaged between 115.5 and 123.5 nm. The logarithm is used mainly to guarantee that the SSI, whose amplitude spans several orders of magnitude, never goes negative. The ratio between solar-cycle amplitude and short-term variability is strongly wavelength-dependent. For that reason, the SSI is frequently decomposed into short- and long-timescale terms, with a cutoff around 81 days (e.g. Woods et al., 2005). Let the 81-day average Φ be $\langle\Phi\rangle_{81}$. Our empirical model then reduces to

$$\Phi(\lambda, t) = A(\lambda)\langle\bar{\Phi}(t)\rangle_{81} + B(\lambda)\left(\bar{\Phi}(t) - \langle\bar{\Phi}(t)\rangle_{81}\right) + C(\lambda) \quad \text{(A1)}$$

The model coefficients $A(\lambda)$, $B(\lambda)$ and $C(\lambda)$ are estimated from 9 years of EUV observations by the TIMED/SEE instrument (Woods et al., 2005), spanning the period from February 2002 to February 2011.

This simple model matches the SOLID observational composite well within its uncertainty range. Note, however, that TIMED/SEE data below 28 nm, and between 115–129 nm are partly modeled, and thus the variability of the EUV spectrum prior to the space age should be considered with great care.

Appendix B: Recommendations for Model Implementation of SSI

The SSI dataset recommended for CMIP6 covers the solar spectrum from 10 to 100,000 nm. It is provided as irradiance averages for 3890 spectral bins (in W/(m^2 nm)). Sampling and equivalently bin width range from 1 nm (UV and VIS) to 50 nm (NIR). Tab. 4 contains more details regarding the resolution changing with wavelength.

Table 4. Sampling and bin width of CMIP6-SSI

spectral range	sampling/bin width
10-750 nm	1 nm
750-5,000 nm	5 nm
5,000-10,000 nm	10 nm
10,000-100,000 nm	50 nm

Most climate models prescribe either TSI or SSI in their respective radiation schemes. If the model's radiation code is able to handle spectrally resolved solar irradiance changes, SSI needs be integrated over the specific wavelength bands to generate Top of the Atmosphere (TOA) fluxes. Using CMIP6-SSI this is done for a given spectral band by simply summing up the irradiances of all (partially) contained bins, each multiplied by the bin width (subtracting potential bin parts that reach beyond the boundaries of the target band). A sample routine for the integration can be found here: http://solarisheppa.geomar.de/cmip6. Climate models that calculate ozone interactively also have to integrate SSI to the respective wavelength bands in their photolysis code. An example of the numbers of bands in the radiation and photolysis schemes of two state-of-the-art CCMs, WACCM and EMAC, is shown in Section 2.1.3.

Appendix C: Recommendations for Geographic Projection of IPR Data

In order to characterize the electron precipitation into the atmosphere since 1850 we must take into account the offset between geographic and magnetic field coordinates, and how the relationship between them changes with time. We recommend the following approach. For years 1850–1900, the gufm1 model may be used (Jackson et al., 2000). Note that this model would allow calculations earlier in time (1590). From 1900–2015 magnetic field conversions should use the current International Geomagnetic Reference Field (IGRF), which at the time of writing is IGRF-12 (Thébault, 2015). It is highly likely that the magnetic field will continue to evolve in the future, and as such we do not recommend fixing the field in any set configuration based on a specific year. Physics-based simulations are now providing representations of future geomagnetic field changes. For the years 2015–2115, Gauss coefficients based on the predicted evolution of the geodynamo can be used from the modelling of Aubert (2015). For years after 2115, secular variation values from 2115 (also from the Aubert (2015) model) are used to extrapolate forward in time, though obviously with increasing uncertainty. Matlab modelling code implementing the above recommendations is available on the SOLARIS-HEPPA CMIP6 website, which allows users to calculate the geomagnetic latitude for any given date, geographic location and altitude for the period 1590 onwards.

Appendix D: NOx Production by Particle-Induced Ionization

Following Porter et al. (1976) it is assumed that 1.25 N atoms are produced per ion pair. This study also further divided the proton impact of N atom production between the ground state $\mathrm{N}(^4\mathrm{S})$ (45% or 0.55 per ion pair) and the excited state $\mathrm{N}(^2\mathrm{D})$ (55% or 0.7 per ion pair). Ground state [$\mathrm{N}(^4\mathrm{S})$] nitrogen atoms can create other $\mathrm{NO_y}$ constituents, such as NO, through

$$N(^4S) + O_2 \rightarrow NO + O, \tag{DR1}$$

$$N(^4S) + O_2 \rightarrow NO + O_2 \tag{DR2}$$

or can lead to $\mathrm{NO_y}$ destruction through

$$N(^4S) + NO \rightarrow N_2 + O. \tag{DR3}$$

Generally, excited states of atomic nitrogen, such as $\mathrm{N}(^2\mathrm{D})$, result in the production of NO through

$$N(^2D) + O_2 \rightarrow NO + O \tag{DR4}$$

(e.g., Rusch et al., 1981; Rees, 1989) and do not cause significant destruction of $\mathrm{NO_y}$. If a model does not include the excited state of atomic nitrogen in their computations, the $\mathrm{NO_y}$ production from EPP can still be included by assuming that its production is instantaneously converted into NO, resulting in a $\mathrm{N}(^4\mathrm{S})$ production of 0.55 per ion pair and a NO production of 0.7 per ion pair.

Appendix E: HOx Production by Particle-Induced Ionization

The production of $\mathrm{HO_x}$ relies on complicated ion chemistry that takes place after the initial formation of ion pairs (Swider and Keneshea, 1973; Frederick, 1976; Solomon et al., 1981; Sinnhuber et al., 2012). Solomon et al. (1981) computed $\mathrm{HO_x}$ production rates as a function of altitude and ion pair production rate. Each ion pair typically results in the production of around two $\mathrm{HO_x}$ constituents in the stratosphere and lower mesosphere. Sinnhuber et al. (2012) have shown that $\mathrm{HO_x}$ is formed as H and OH in nearly equal amounts, with small differences of less than 10% due to different ion reaction chains. In the middle and upper mesosphere, one ion pair is computed to produce less than two HO_x constituents per ion pair because water vapor decreases sharply with altitude there, and is no longer available as a source of HO_x. For models which do not include D-region ion chemistry, we recommend to use the parameterisation of Solomon et al. (1981), which is summarized following Jackman et al. (2005b) in Table 5. If the partitioning between HO_x species is considered in the model, H and OH should be formed in equal amounts. Below 40 km altitude and for ionization rates less than $10^2 cm^{-3} s^{-1}$ below 70 km altitude, two HO_x can be formed per ion pair. Above 90 km altitude, HO_x-production can be set to zero; between 70 and 90 km, values need to be extrapolated for ion pair production rates smaller than $10^2 cm^{-3} s^{-1}$ and larger than $10^4 cm^{-3} s^{-1}$, taking care not to exceed zero and two.

Table 5. HO_x production per ion pair as a function of altitude and ion pair production rate (IPR). Table adapted from ~~Jackman et al. (2005b)~~Jackman et al. (2005b).

Altitude [km]	HO_x	production per ion pair	(no units)
		IPR $[cm^{-3} s^{-1}]$	
	10^2	10^3	10^4
40	2.00	2.00	1.99
45	2.00	1.99	1.99
50	1.99	1.99	1.98
55	1.99	1.98	1.97
60	1.98	1.97	1.94
65	1.98	1.94	1.87
70	1.94	1.87	1.77
75	1.84	1.73	1.60
80	1.40	1.20	0.95
85	0.15	0.10	0.00
90	0.00	0.00	0.00

Appendix F: Minor Constituent Changes due to Particle-Induced Ionization

If available, the use of more comprehensive parameterizations for productions of individual HO_x (OH and H) and NO_y ($N(^4S)$, $N(^2D)$, NO, NO_2, NO_3, N_2O_5, HNO_2, and HNO_3) compounds (e.g., Verronen and Lehmann, 2013; Nieder et al., 2014) is encouraged. Similarly, if atmospheric models include detailed cluster ion chemistry of the lower ionosphere (D region), then the ionization rates should be used to drive the production rates of the primary ions (N_2^+, N^+, O_2^+, O^+) and neutrals (N, O) produced in particle impact ionization/dissociation (Sinnhuber et al., 2012). Since such a comprehensive treatment of EPP effects on minor species may introduce more sensitive composition changes via chemical feedbacks, it would be important to document the adopted approaches.

Appendix G: Projection of Historical Solar Cycles in Future Scenarios

Table 6. Historical solar cycles used for construction of future cycles (starting on 2015-01-01).

Current cycle nb.	Historic cycle nb.	Start current cycle yyyy-mm-dd	Start hist. cycle yyyy-mm-dd
24	12	2015-01-01	1883-02-01
25	13	2020-02-02	1890-01-28
26	14	2031-12-18	1901-12-14
27	15	2043-06-19	1913-06-15
28	12	2053-09-10	1878-12-13
29	13	2064-10-26	1890-01-28
30	14	2076-09-10	1901-12-14
31	15	2088-03-12	1913-06-15
32	16	2098-06-04	1923-09-07
33	17	2108-07-05	1933-10-07
34	18	2118-11-21	1944-02-23
35	19	2129-01-16	1954-04-20
36	20	2139-07-02	1964-10-03
37	21	2150-12-04	1976-03-07
38	22	2161-04-21	1986-07-24
39	23	2171-05-21	1996-08-22
40	24	2183-08-19	2008-11-20
	12	2189-11-07	1883-02-01
41	13	2194-10-31	1890-01-28
42	14	2206-09-16	1901-12-14
43	15	2218-03-18	1913-06-15
44	12	2228-06-09	1878-12-13
45	13	2239-07-26	1890-01-28
46	14	2251-06-10	1901-12-14
47	15	2262-12-10	1913-06-15
48	16	2273-03-03	1923-09-07
49	17	2283-04-03	1933-10-07
50	18	2293-08-19	1944-02-23

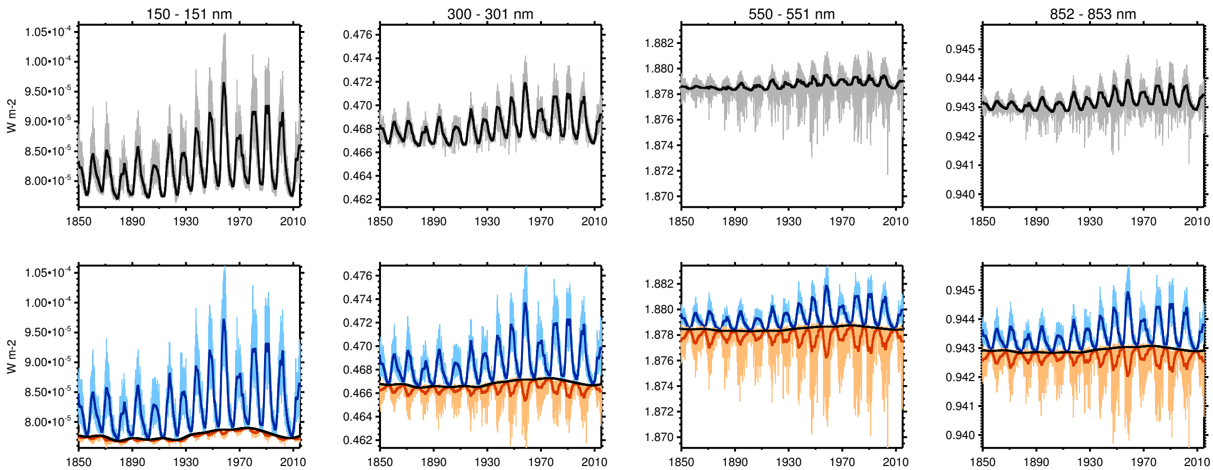

Figure 28. Decomposition of SSI in the scaling procedure (shown for wavelength bins centered at 150.5, 300.5, 550.5, and 852.5 nm, from left to right). Upper panels: daily (grey) and annually (black) resolved SSI. Lower panels: Individual components after decomposition: background SSI^{bg} (black solid); facular brightening related SSI^{+} annual, A^{+}, (dark-blue) and sub-annual, D^{+}, (light-blue); sunspot darkening related SSI^{-} annual, A^{-}, (dark-red) and sub-annual, D^{-}, (light-red).

Appendix H: Scaling of SSI in Future Scenarios and Variable PI-Control Forcing

SSI variability is closely linked to solar magnetic activity variations, and hence sunspot number. However, the form of this relationship may differ significantly at different wavelengths, and time scales (i.e., decadal, annual, sub-annual). Indeed, the contribution to the SSI from different solar features such as faculae, sunspots, the network and ephemeral regions, show different temporal responses (e.g. Vieira and Solanki, 2010). As a consequence, a simple, wavelength-independent scaling of historic SSI sequences for projection into the future or for the generation of the variable PI control forcing would lead to unrealistic results

t

Instead, we first decompose the SSI time series at individual wavelength bins λ into components corresponding to the background variability $SSI^{bg}(\lambda)$ (i.e., long-term variations of the SSI at solar minima), to facular brightening-related variability $SSI^{+}(\lambda)$, and to sunspot darkening related variability $SSI^{-}(\lambda)$. The latter two components are further decomposed into annual (A^{+} and A^{-}) and sub-annual (D^{+} and D^{-}) contributions (see Fig. 28).

t

For the projection of past solar cycles into the future only the D^{+} and D^{-}components need to be scaled since the annually resolved SSI is already provided by the SSI models. These components are shown in Fig. 29 for selected wavelength bins. The distributions of D^{+} values within a given solar cycle are rather symmetric around zero and show a close to normal distribution. Variability differences between solar cycles are therefore well represented by the corresponding standard deviations $SD(D^{+})_{SC}$ of individual cycles. This quantity also shows good correlation with <SSN> and we therefore use it to construct

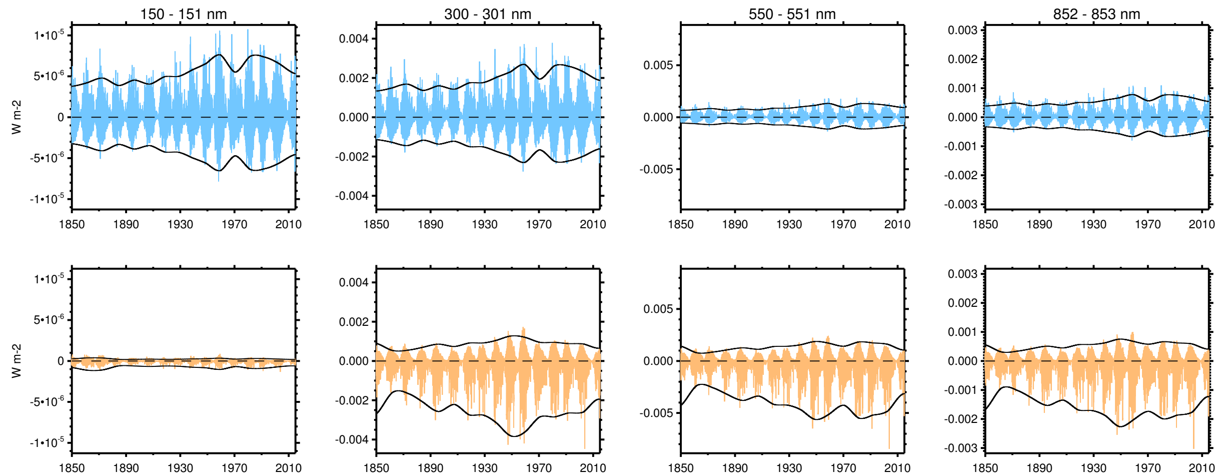

Figure 29. D^+ (top, light blue) and D^- (bottom, light red) components of SSI at wavelength bins centered at 150.5, 300.5, 550.5, and 852.5 nm (from left to right). The corresponding scaling functions SD(D^+) (top) and MAD(D^-) (bottom), multiplied by 3.5 and -3 in the case of SD(D^+) (5 and -15 in the case of MAD(D^-)) are shown by black solid lines.

time-resolved scaling functions. The distributions of D^- values are largely skewed towards negative values and do not exhibit the characteristics of a normal distribution. This behavior is expected because of the more intermittent response of SSI to sunspot darkening, as compared to facular brightening. Variability differences between solar cycles are therefore best represented by the corresponding median absolute deviations MAD$(D^-)_{SC}$, which are therefore used to construct the time-resolved scaling functions for the D^- components.

~~t~~

The coefficients for the scaling of SSI variability with <SSN> have been obtained from linear regression fits of SD$(D^+)_{SC}$ and MAD$(D^-)_{SC}$ to <SSN> for each individual wavelength bin (see Fig. 30). In all fits, a nonzero offset is obtained, with particularly large values in the case of MAD$(D^-)_{SC}$. Sub-annual SSI variations are expected to be very low in the absence of sunspots, with variations mainly coming from the solar network (Bolduc et al., 2014). For that reason, we apply a non-linear correction in the scaling for low <SSN> values in order to obtain realistic results for solar cycles with very low activity in the EXT scenario. This has been achieved by multiplying a <SSN>-dependent exponential correction f to the obtained offsets:

$$f = \frac{1-\exp(-0.1<SSN>)}{1+\exp(-0.1<SSN>)} \tag{H1}$$

For the construction of the variable PI control forcing, ~~all~~ annual and sub-annual SSI components are scaled individually to ~~1850–1873 average conditions~~ a constant solar cycle mean activity level at each wavelength bin. The scaling has been performed for the D^+ and D^- components based on SD(D^+) and MAD(D^-), respectively, as in the ~~the~~ future scenario construction. For A^+ and A^-, we use the corresponding solar cycle averages to construct time-resolved scaling functions. The

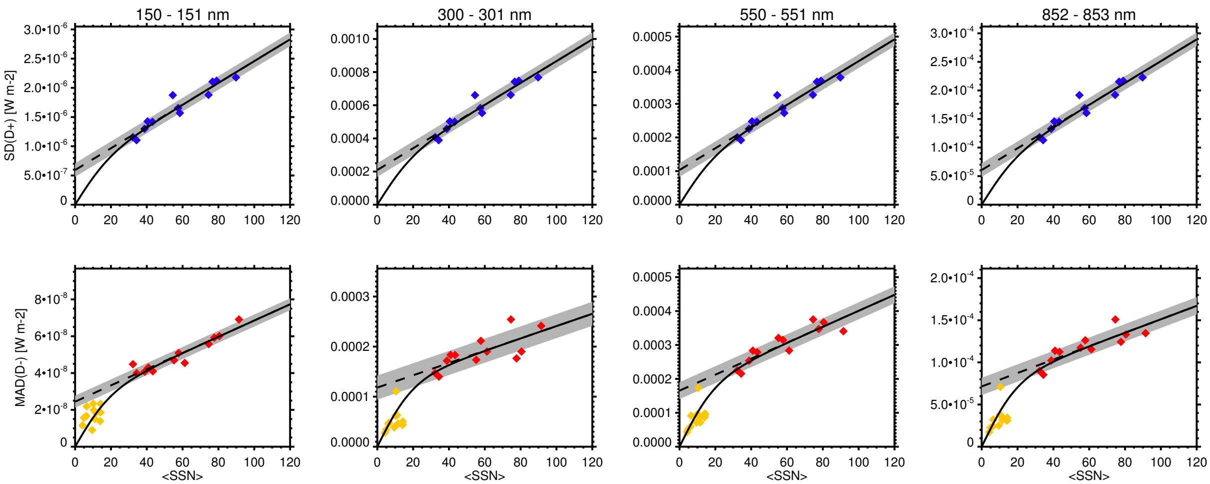

Figure 30. Regression of SD(D$^+$)$_{SC}$ (top, blue symbols) and MAD(D$^-$)$_{SC}$ (bottom, red symbols) to <SSN> at wavelength bins centered at 150.5, 300.5, 550.5, and 852.5 nm (from left to right). The resulting linear fit is shown by dashed black lines, the grey shaded areas reflect the RMS errors. The solid black lines show the functional dependence used in the scaling after application of a non-linear correction for low <SSN> values. MAD(D$^-$) values calculated from the low activity part of the solar cycles provide an estimate for very weak solar cycles and are shown with orange symbols (only lower panels).

background contributions SSI^{bg} were set to constant values~~corresponding to the 1850–1873 averages~~. The same procedure was also applied to the F10.7 radio flux.

Appendix I: Scaling of Geomagnetic Indices in Future Scenarios and Variable PI-Control Forcing

~~t~~

The geomagnetic activity level is strongly linked to solar activity by the solar wind – magnetosphere interaction. The relationship of geomagnetic activity (and hence geomagnetic indices) and SSN depends strongly on the considered time scales. Therefore, we decompose the Ap index in components corresponding to different time scales in order to scale them individually for projection of historic Ap sequences into the future or for the generation of the variable PI control forcing (see Fig. 31). The magnitude of sub-annual Ap variations is large and ruled by the mid-term geomagnetic activity level. Since there is strong evidence for Ap to be described by a multiplicative process (Watkins et al., 2005), we decompose Ap as follows:

$$\mathrm{Ap}(t) = \left(\mathrm{Ap}^{bg}(t) + \mathrm{Ap}^{a}(t)\right) D(t), \tag{I1}$$

where Ap^{bg} is the background component obtained from the Ap solar cycle averages, Ap^a the annually averaged component, and D a multiplicative daily component, the latter characterized by a nearly constant magnitude of variability on decadal to secular time scales. The Ap^a variability shows only a weak dependence on the long-term geomagnetic activity level. We use its standard deviation from individual solar cycles for construction of a time-dependent scaling function SD(Ap^a).

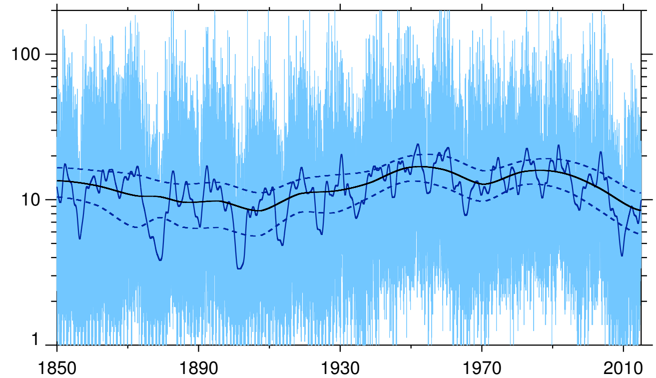

Figure 31. Decomposition of the reconstructed Ap index in the scaling procedure. Light blue: daily resolved Ap; black: background component Ap^{bg}; solid dark blue: annual component Ap^{a}; dashed dark blue: scaling function SD(Ap^{a}), multiplied by 1 and -1, used to scale the annual component.

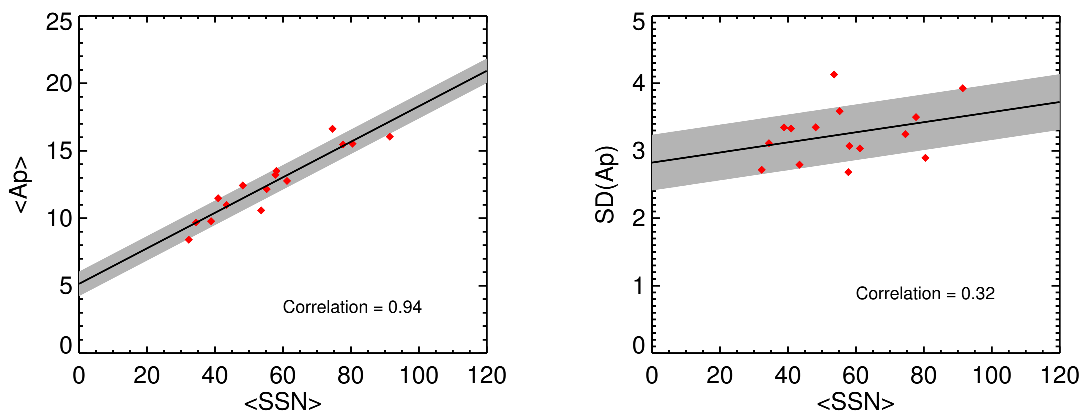

Figure 32. Regression of Ap^{bg} (red symbols, left) and SD$(Ap^{a})_{SC}$ (red symbols, right) to <SSI>. The resulting linear fit is shown by black lines, the grey shaded areas reflect the RMS errors.

ŧ

For the projection of past solar cycles into the future, the components Ap^{bg} and Ap^{a} need to be scaled in relation to <SSN>. Linear regression fits of Ap^{bg} and SD(Ap^{a}) to <SSN> are shown in Fig. 32. The correlation of Ap^{bg} and <SSN> is very tight with a correlation coefficient of 0.94. As expected, this is not the case for SD(Ap^{a}). The pronounced offsets of the regression fits at <SSN>=0 suggest residual geomagnetic activity for very low solar activity (i.e., Maunder Minimum) conditions in agreement with previous studies (e.g., Cliver et al., 1998).

For the construction of the variable PI control forcing, the Ap index is scaled to 1850–1873 average conditions. The scaling has been performed for the Ap^a component on basis of SD(Ap^a). The background contributions Ap^{bg} was set to a constant value corresponding to the 1850–1873 average.

In both future scenario and variable PI control forcing constructions, Ap has been converted into Kp using a statistical correction to account for biases related to the conversion from hourly to daily indices as described in Sec. 2.2.1.

Author contributions. This paper was initiated, coordinated, and edited by K. Matthes and B. Funke. M. E. Andersson made WACCM simulations for Sec. 2.2 and made Figure 15. L. Barnard contributed text to Sections 2.2 and 3.1, and made Fig.22. M. A. Clilverd and C. J. Rodgers led the processing and analysis of the SEM-2 MEPED precipitating electron flux data and wrote part of the text in Sec. 2.2. T. Dudok deWit wrote parts of Sections 1, 2.1.1, 3, and made Figures 1 and 21. B. Funke developed and conducted the extrapolation and scaling of geomagnetic indices, F10.7, and SSI data, made Figures 12, 16, 23–26, 28-32, and wrote parts of Sections 1-4, 6, C-H. M. Haberreiter contributed to writing and interpretations in Sec. 2.1.1. A. Hendry developed the code for geographic-to-geomagnetic conversions with support from C. J. Rodger and M. E. Andersson. C. H. Jackman provided the solar proton IPR dataset and wrote Sec. 2.2.2. M. Kretzschmar contributed to writing and interpretations in Sec. 2.1.1 and made Figures 2-4. T. Kruschke set up and conducted the CESM1(WACCM) simulations for Sec. 2.1.3, made Figs. 6, 8, 10-11, and contributed to the text in Sections 2.1.3 and B. M. Kunze performed the EMAC model runs for Sec. 2.1.3, made Figures 7 and 9, and contributed to the text in Sec. 2.1.3. U. Langematz contributed to the design, analysis and interpretation of the CCM simulations in Sec. 2.1.3 and assisted in editing the manuscript. D. R. Marsh made WACCM simulations for Sec. 2.2 and provided Fig. 13. K. Matthes wrote the abstract and parts of Sections 1-6, A, and coordinated the design, analysis and interpretation of the CCM and libradtran simulations in Sec. 2.1.3. A. Maycock made Fig. 27 and wrote Sec. 5. S. Misios performed the libradtran simulations and contributed to the text in Sec. 2.1.3. M. Shangguan performed the radiative forcing calculations with libradtran in Sec. 2.1.2. M. Sinnhuber contributed to the analysis of the EMAC tests of the NOy UBC and wrote parts of the text in Sections 1 and 2.2. K. Tourpali contributed to the design and analysis of the libradtran simulations and to the text in Sec. 2.1.3. I. Usoskin provided the GCR ionisation data, wrote Sec. 2.2.3, and made Figures 19 and 20. M. van de Kamp developed the MEE precipitation model and calculated the spectral parameters with support and coordination from A. Seppälä, P. T. Verronen, M. A. Clilverd and C. J. Rodger. P. T. Verronen calculated the MEE ionisation rates, provided Fig. 14, and wrote the MEE text in Sec. 2.2. S. Versick made Figures 17 and 18, did the EMAC model setup, performed the model runs, and contributed to the analysis of the EMAC tests with the NOy UBC. L. Barnard, J. Beer, P. Charbonneau, T. Dudok de Wit, B. Funke, K. Matthes, A. Maycock, I. Usoskin, and A. Scaife designed the future solar activity scenarios and assisted in editing the manuscript. The final solar forcing dataset for CMIP6 available at http://solarisheppa.geomar.de/cmip6 was generated by B. Funke and T. Kruschke.

Acknowledgements. We are very grateful to the SATIRE and NRL teams for providing their respective solar irradiance reconstructions. Without ~~theses input~~ these datasets the CMIP6 solar forcing recommendation as well as this paper wouldn't have been possible. We also thank the researchers and engineers of NOAA's Space Environment Center for the provision of the data and the operation of the SEM-2 instrument carried onboard the POES spacecraft. This work has been conducted in the frame of the WCRP/SPARC SOLARIS-HEPPA activity, and an early part inside the EU COST Action ES1005 (TOSCA) which some authors were involved in. This work contributes to the ROSMIC activity within the SCOSTEP VarSITI programme. Part of the work described in this article emanates from two teams at the International

Space Science Institute (ISSI) in Bern, i.e. *Quantifying Hemispheric Differences in Particle Forcing Effects on Stratospheric Ozone* (Leader: D. R. Marsh) and *Scenarios of Future Solar Activity for Climate Modelling* (Leader: T. Dudok de Wit), which we gratefully acknowledge for hospitality. MK, TD, MH, KT and SM acknowledge that the research leading to the results has received funding from the European Community's Seventh Framework Programme (FP7 2012) under grant agreement no 313188 (SOLID, http://projects.pmodwrc.ch/solid). PTV, MEA, AS, and MvdK were supported by the Academy of Finland projects #276926 (SECTIC: Sun-Earth Connection Through Ion Chemistry) and #258165/#265005 (CLASP: Climate and Solar Particle Forcing). KM, TK, MK, UL, SV and MS gratefully acknowledge funding by the German Ministry of Research (BMBF) within the nationally funded project ROMIC-SOLIC (grant number 01LG1219). KM also acknowledges support from the Helmholtz-University Young Investigators Group NATHAN funded by the Helmholtz-Association through the President's Initiative and Networking Fund and the GEOMAR Helmholtz Centre for Ocean Research Kiel. MS gratefully acknowledges funding by the Helmholtz Association of German Research Centres (HGF), grant 608 VH-NG-624. BF was supported by the Spanish MCINN under grant ESP2014-54362-P and EC FEDER funds. LB thanks the Science and Technology Facilities Council (STFC) for support under grant ST/M000885/1. AS was supported by the joint DECC/Defra Met Office Hadley Centre Climate Programme (GA01101) and the EU SPECS project (GA308378). UL and MK thank the North-German Supercomputing Alliance (HLRN) for support and computer time. KM and TK thank the computing centre at Kiel University for support and computer time.

References

Abreu, J. A., Beer, J., Steinhilber, F., Tobias, S. M., and Weiss, N. O.: For how long will the current grand maximum of solar activity persist?, Geophysical Research Letters, 35, 20 109, doi:10.1029/2008GL035442, 2008.

Alley, R. B., Berntsen, T., and Bindoff, N. L.: Climate Change 2007 - The Physical Science Basis. Working Group I Contribution to the Fourth Assessment Report of the IPCC, Cambridge University Press, Cambridge, 2007.

Amblard, P., Moussaoui, S., Dudok de Wit, T., Aboudarham, J., Kretzschmar, M., Lilensten, J., and Auchère, F.: The EUV Sun as the superposition of elementary Suns, Astronomy and Astrophysics, 487, L13–L16, doi:10.1051/0004-6361:200809588, 2008.

Andersson, M. E., Verronen, P. T., Rodger, C. J., Clilverd, M. A., and Seppälä, A.: Missing driver in the Sun–Earth connection from energetic electron precipitation impacts mesospheric ozone, Nature Commun., 5, doi:10.1038/ncomms6197, 2014a.

Andersson, M. E., Verronen, P. T., Rodger, C. J., Clilverd, M. A., and Wang, S.: Longitudinal hotspots in the mesospheric OH variations due to energetic electron precipitation, Atmos. Chem. Phys., 14, 1095–1105, doi:10.5194/acp-14-1095-2014, 2014b.

Anet, J. G., Rozanov, E. V., Muthers, S., Peter, T., Brönnimann, S., Arfeuille, F., Beer, J., Shapiro, A. I., Raible, C. C., Steinhilber, F., and Schmutz, W. K.: Impact of a potential 21st century "grand solar minimum" on surface temperatures and stratospheric ozone, Geophysical Research Letters, 40, 4420–4425, doi:10.1002/grl.50806, 2013.

Aubert, J.: Geomagnetic forecasts driven by thermal wind dynamics in the Earth's core, Geophysical Journal International, 203, 1738–1751, doi:10.1093/gji/ggv394, 2015.

Austin, J., Tourpali, K., Rozanov, E., Akiyoshi, H., Bekki, S., Bodeker, G., Brühl, C., Butchart, N., Chipperfield, M., Deushi, M., Fomichev, V. I., Giorgetta, M. A., Gray, L., Kodera, K., Lott, F., Manzini, E., Marsh, D., Matthes, K., Nagashima, T., Shibata, K., Stolarski, R. S., Struthers, H., and Tian, W.: Coupled chemistry climate model simulations of the solar cycle in ozone and temperature, J. Geophys. Res., 113, D11 306, 2008.

Ball, W. T., Unruh, Y. C., Krivova, N. A., Solanki, S., Wenzler, T., Mortlock, D. J., and Jaffe, A. H.: Reconstruction of total solar irradiance 1974-2009, Astronomy & Astrophysics, 541, A27, doi:10.1051/0004-6361/201118702, 2012.

Ball, W. T., Haigh, J. D., Rozanov, E. V., Kuchar, A., Sukhodolov, T., Tummon, F., Shapiro, A. V., and Schmutz, W.: High solar cycle spectral variations inconsistent with stratospheric ozone observations, Nature Geoscience, 9, 206–209, doi:10.1038/ngeo2640, 2016.

Barnard, L., Lockwood, M., Hapgood, M. A., Owens, M. J., Davis, C. J., and Steinhilber, F.: Predicting space climate change, Geophys. Res. Lett., 38, doi:10.1029/2011GL048489, 2011.

Bartels, J.: The standardized index, Ks, and the planetary index, Kp, IATME Bulletin, 12b, 97, 1949.

Baumgaertner, A., Seppälä, A., Jöckel, P., and Clilverd, M.: Geomagnetic activity related NOx enhancements and polar surface air temperature variability in a chemistry climate model: modulation of the NAM index, Atmospheric Chemistry and Physics, 11, 4521–4531, doi:10.5194/acp-11-4521-2011, 2011.

Baumgaertner, A. J. G., Jöckel, P., and Brühl, C.: Energetic particle precipitation in ECHAM5/MESSy – Part 1: Downward transport of upper atmospheric NO_x produced by low energy electrons, Atmos. Chem. Phys., 9, 2729–2740, doi:10.5194/acp-9-2729-2009, 2009.

Beer, J., McCracken, K., and von Steiger, R.: Cosmogenic Radionuclides, Springer Verlag, Berlin, 2012.

Bolduc, C., Charbonneau, P., Barnabé, R., and Bourqui, M. S.: A Reconstruction of Ultraviolet Spectral Irradiance During the Maunder Minimum, Solar Physics, 289, 2891–2906, doi:10.1007/s11207-014-0503-0, 2014.

Box, G. E. P., Jenkins, G. M., Reinsel, G. C., and Ljung, G. M.: Time Series Analysis: Forecasting and Control, Wiley Series in Probability and Statistics, Wiley, 5th edn., 2015.

Caballero-Lopez, R. A. and Moraal, H.: Limitations of the force field equation to describe cosmic ray modulation, J. Geophys. Res., 109, doi:10.1029/2003JA010098, a01101, 2004.

Calisto, M., Usoskin, I., Rozanov, E., and Peter, T.: Influence of Galactic Cosmic Rays on atmospheric composition and dynamics, Atmos. Chem. Phys., 11, 4547–4556, doi:10.5194/acp-11-4547-2011, 2011.

Callis, L. B., Boughner, R. E., Baker, D. N., Mewaldt, R. A., Bernard Blake, J., Selesnick, R. S., Cummings, J. R., Natarajan, M., Mason, G. M., and Mazur, J. E.: Precipitating electrons: Evidence for effects on mesospheric odd nitrogen, Geophys. Res. Lett., 23, 1901–1904, doi:10.1029/96GL01787, 1996.

Charbonneau, P.: Dynamo Models of the Solar Cycle, Living Reviews in Solar Physics, 7, 3, doi:10.12942/lrsp-2010-3, 2010.

Charbonneau, P.: Solar Dynamo Theory, Annual Review of Astronomy and Astrophysics, 52, 251–290, doi:10.1146/annurev-astro-081913-040012, 2014.

Chiodo, G., Calvo, N., Marsh, D. R., and Garcia-Herrera, R.: The 11 year solar cycle signal in transient simulations from the Whole Atmosphere Community Climate Model, J. Geophys. Res., 117, doi:10.1029/2011JD016393, 2012.

Chiodo, G., Garcia-Herrera, R., Calvo, N., Vaquero, J. M., A?el, J. A., Barriopedro, D., and Matthes, K.: The impact of a future solar minimum on climate change projections in the Northern Hemisphere, Environmental Research Letters, 11, 034 015, doi:10.1088/1748-9326/11/3/034015, 2016.

Cionni, I., Eyring, V., Lamarque, J.-F., Randel, W. J., Stevenson, D. S., Wu, F., Bodeker, G. E., Shepherd, T. G., Shindell, D. T., and Waugh, D. W.: Ozone database in support of CMIP5 simulations: Results and corresponding radiative forcing, Atmos. Chem. Phys., 11, 11,267–11,292, 2011.

Clette, F., Svalgaard, L., Vaquero, J. M., and Cliver, E. W.: Revisiting the Sunspot Number, Space Science Reviews, 186, 35–103, doi:10.1007/s11214-014-0074-2, 2014.

Cliver, E. W., Boriakoff, V., and Bounar, K. H.: Geomagnetic activity and the solar wind during the Maunder Minimum, Geophysical Research Letters, 25, 897–900, doi:10.1029/98GL00500, 1998.

Coddington, O., Lean, J. L., Pilewskie, P., Snow, M., and Lindholm, D.: A Solar Irradiance Climate Data Record, Bulletin of the American Meteorological Society, 97, 1265, doi:BAMS-D-14-00265.1, 2016.

Codrescu, M. V., Fuller-Rowell, T. J., Roble, R. G., and Evans, D. S.: Medium energy particle precipitation influences on the mesosphere and lower thermosphere, J. Geophys. Res., 102, 19 977–19 987, doi:10.1029/97JA01728, 1997.

Collins, W. D.: A global signature of enhanced shortwave absorption by clouds, J. Geophys. Res., 103, 31 669–31 679, 1998.

Cooke, D. J., Humble, J. E., Shea, M. A., Smart, D. F., Lund, N., Rasmussen, I. L., Byrnak, B., Goret, P., and Petrou, N.: On cosmic-ray cut-off terminology, Il Nuovo Cimento C, 14, 213–234, doi:10.1007/BF02509357, 1991.

Damiani, A., Storini, M., Laurenza, M., and Rafanelli, C.: Solar particle effects on minor components of the Polar atmosphere, Annales Geophysicae, 26, 361–370, doi:10.5194/angeo-26-361-2008, 2008.

Damiani, A., Funke, B., Marsh, D. R., López-Puertas, M., Santee, M. L., Froidevaux, L., Wang, S., Jackman, C. H., von Clarmann, T., Gardini, A., Cordero, R. R., and Storini, M.: Impact of January 2005 Solar Proton Events on chlorine species, Atmos. Chem. Phys., 12, 4159–4179, doi:10.5194/acp-12-4259-2012, 2012.

Damiani, A., Funke, B., López-Puertas, M., Santee, M. L., Cordero, R. R., Laurenza, M., and Watanabe, S.: Energetic particle precipitation: a major driver of the ozone budget in the Antarctic upper stratosphere, Geophys. Res. Lett., doi:10.1002/2016GL068279, 2016GL068279, 2016.

Dasi-Espuig, M., Jiang, J., Krivova, N. A., and Solanki, S. K.: Modelling total solar irradiance since 1878 from simulated magnetograms, Astronomy & Astrophysics, 570, A23, doi:10.1051/0004-6361/201424290, 2014.

Dee, D. P., Uppala, S. M., Simmons, A. J., Berrisford, P., Poli, P., Kobayashi, S., Andrae, U., Balmaseda, M. A., Balsamo, G., Bauer, P., Bechtold, P., Beljaars, A. C. M., van de Berg, L., Bidlot, J., Bormann, N., Delsol, C., Dragani, R., Fuentes, M., Geer, A. J., Haimberger, L., Healy, S. B., Hersbach, H., Hólm, E. V., Isaksen, L., Kållberg, P., Köhler, M., Matricardi, M., McNally, A. P., Monge-Sanz, B. M., Morcrette, J.-J., Park, B.-K., Peubey, C., de Rosnay, P., Tavolato, C., Thépaut, J.-N., and Vitart, F.: The ERA-Interim reanalysis: configuration and performance of the data assimilation system, Quarterly Journal of the Royal Meteorological Society, 137, 553–597, doi:10.1002/qj.828, 2011.

Desorgher, L., Flückiger, E. O., Gurtner, M., Moser, M. R., and Bütikofer, R.: Atmocosmics: a Geant 4 Code for Computing the Interaction of Cosmic Rays with the Earth's Atmosphere, Internat. J. Modern Physics A, 20, 6802–6804, doi:10.1142/S0217751X05030132, 2005.

Dietmüller, S., Jöckel, P., Tost, H., Kunze, M., Gellhorn, C., Brinkop, S., Frömming, C., Ponater, M., Steil, B., Lauer, A., and Hendricks, J.: A new radiation infrastructure for the Modular Earth Submodel System (MESSy, based on version 2.51), Geosci. Model Dev. Discuss., 2016, 1–21, doi:10.5194/gmd-2015-277, 2016.

Dudok de Wit, T.: A method for filling gaps in solar irradiance and solar proxy data, Astronomy and Astrophysics, 533, A29, doi:10.1051/0004-6361/201117024, 2011.

Dudok de Wit, T., Kopp, G., Fröhlich, C., and Schöll, M.: Methodology to create a new Total Solar Irradiance record: Making a composite out of multiple data records, Geophys. Res. Lett., submitted, 2016a.

Dudok de Wit, T., Lefèvre, L., and Clette, F.: Uncertainties in the sunspot numbers: estimation and implications, Solar Physics, in press, doi:10.1007/s11207-016-0970-6, 2016b.

Ermolli, I., Matthes, K., Dudok de Wit, T., Krivova, N. A., Tourpali, K., Weber, M., Unruh, Y. C., Gray, L., Langematz, U., Pilewskie, P., Rozanov, E., Schmutz, W., Shapiro, A., Solanki, S. K., and Woods, T. N.: Recent variability of the solar spectral irradiance and its impact on climate modelling, Atmospheric Chemistry and Physics, 13, 3945–3977, doi:10.5194/acp-13-3945-2013, 2013.

Evans, D. and Greer, M.: Polar Orbiting Environmental Satellite Space Environment Monitor - 2: Instrument Descriptions and Archive Data Documentation, NOAA Technical Memorandum OAR version 1.4 SEC-93, Oceanic and Atmospheric Research Laboratories, Space Environment Center, Boulder, Colorado, 2000.

Eyring, V., Bony, S., Meehl, G. A., Senior, C., Stevens, B., Stouffer, R. J., and Taylor, K. E.: Overview of the Coupled Model Intercomparison Project Phase 6 (CMIP6) experimental design and organisation, Geoscientific Model Development Discussions, 2015, 10 539–10 583, doi:10.5194/gmd-2015-265, 2015.

Fang, X., Randall, C., Lummerzheim, D., Solomon, S., Mills, M., Marsh, D., Jackman, C., Wang, W., and Lu, G.: Electron impact ionization: A new parameterization for 100 eV to 1 MeV electrons, Journal of Geophysical Research, 113, doi:10.1029/2008JA013384, 2008.

Fang, X., Randall, C. E., Lummerzheim, D., Wang, W., Lu, G., Solomon, S. C., and Frahm, R. A.: Parameterization of monoenergetic electron impact ionization, Geophys. Res. Lett., 37, n/a–n/a, doi:10.1029/2010GL045406, l22106, 2010.

Feulner, G. and Rahmstorf, S.: On the effect of a new grand minimum of solar activity on the future climate on Earth, Geophysical Research Letters, 37, L05707, doi:10.1029/2010GL042710, 2010.

Fligge, M., Solanki, S. K., and Unruh, Y. C.: Modelling irradiance variations from the surface distribution of the solar magnetic field, Astronomy & Astrophysics, 353, 380–388, 2000.

Forster, P. M., Fomichev, V. I., Rozanov, E., Cagnazzo, C., Jonsson, A. I., Langematz, U., Fomin, B., Iacono, M. J., Mayer, B., Mlawer, E., Myhre, G., Portmann, R. W., Akiyoshi, H., Falaleeva, V., Gillett, N., Karpechko, A., Li, J., Lemennais, P., Morgenstern, O., Oberländer, S., Sigmond, M., and Shibata, K.: Evaluation of radiation scheme performance within chemistry climate models, J. Geophys. Res., 116, 2156–2202, 2011.

Fouquart, Y. and Bonnel, B.: Computations of solar heating of the Earth's atmosphere: A new parameterization, Beitr. Phys. Atmos., 53, 35–62, 1980.

Frahm, R. A., Winningham, J. D., Sharber, J. R., Link, R., Crowley, G., Gaines, E. E., Chenette, D. L., Anderson, B. J., and Potemra, T. A.: The diffuse aurora: A significant source of ionization in the middle atmosphere, J. Geophys. Res., 102, 28 203–28 214, doi:10.1029/97JD02430, 1997.

Frederick, J. E.: Solar corpuscular emission and neutral chemistry in the Earth's middle atmosphere, J. Geophys. Res., 81, 3179–3186, doi:10.1029/JA081i019p03179, 1976.

Friederich, F., von Clarmann, T., Funke, B., Nieder, H., Orphal, J., Sinnhuber, M., Stiller, G. P., and Wissing, J. M.: Lifetime and production rate of NO_x in the upper stratosphere and lower mesosphere in the Southern Hemisphere after the solar proton event in October-November 200, Atmos. Chem. Phys., 13, 2531–2539, doi:10.5194/acp-13-2531-2013, 2013.

Funke, B., López-Puertas, M., Gil-López, S., von Clarmann, T., Stiller, G. P., Fischer, H., and Kellmann, S.: Downward transport of upper atmospheric NO_x into the polar stratosphere and lower mesosphere during the Antarctic 2003 and Arctic 2002/2003 winters, J. Geophys. Res., 110, D24308, doi:10.1029/2005JD006463, 2005.

Funke, B., López-Puertas, M., García-Comas, M., Stiller, G. P., von Clarmann, T., and Glatthor, N.: Mesospheric N_2O enhancements as observed by MIPAS on Envisat during the polar winters in 2002-2004, Atmos. Chem. Phys., 8, 5787–5800, doi:10.5194/acp-8-5787-2008, 2008.

Funke, B., Baumgaertner, A., Calisto, M., Egorova, T., Jackman, C. H., Kieser, J., Krivolutsky, A., López-Puertas, M., Marsh, D. R., Reddmann, T., Rozanov, E., Salmi, S.-M., Sinnhuber, M., Stiller, G. P., Verronen, P. T., Versick, S., von Clarmann, T., Vyushkova, T. Y., Wieters, N., and Wissing, J. M.: Composition changes after the "Halloween" solar proton event: the High-Energy Particle Precipitation in the Atmosphere (HEPPA) model versus MIPAS data intercomparison study, Atmos. Chem. Phys., 11, 9089–9139, doi:10.5194/acp-11-9089-2011, 2011.

Funke, B., López-Puertas, M., Stiller, G. P., and von Clarmann, T.: Mesospheric and stratospheric NOy produced by energetic particle precipitation during 2002–2012, J. Geophys. Res., 119, doi:10.1002/2013JD021404, 2014a.

Funke, B., Puertas, M. L., Holt, L., Randall, C. E., Stiller, G. P., and von Clarmann, T.: Hemispheric distributions and interannual variability of NO_y produced by energetic particle precipitation in¡ 2002–2012, J. Geophys. Res., 119, 13 565–13 582, doi:10.1002/2014JD022423, 2014b.

Funke, B., López-Puertas, M., Stiller, G. P., Versick, S., and von Clarmann, T.: A semi-empirical model for mesospheric and stratospheric NOy produced by energetic particle precipitation, Atmos. Chem. Phys. Discuss., 2016, 1–44, doi:10.5194/acp-2016-198, 2016.

Fytterer, T., Mlynczak, M., Nieder, H., Perot, K., Sinnhuber, M., Stiller, G., and Urban, J.: Energetic particle induced intra-seasonal variability of ozone inside the Antarctic polar vortex observed in satellite data, Atmospheric Chemistry and Physics, 15, doi:10.5194/acp-15-3327-2015, 2015a.

Fytterer, T., Santee, M. L., Sinnhuber, M., and Wang, S.: The 27day solar rotational effect on mesospheric nighttime OH and O3 observations induced by geomagnetic activity, Journal of Geophysical Research, 120, doi:10.1002/2015JA021183, 2015b.

Giorgetta, M. A. and Bengtsson, L.: Potential role of the quasi-biennial oscillation in the stratosphere-troposphere exchange as found in water vapor in general circulation model experiments, J. Geophys. Res.: Atmos., 104, 6003–6019, doi:10.1029/1998JD200112, 1999.

Gray, L., Scaife, A., Mitchell, D., Osprey, S., Ineson, S., Hardiman, S., Butchart, N., Knight, J., Sutton, R., and Kodera, K.: A Lagged Response to the 11-year Solar Cycle in Observed Winter Atlantic/European Weather Patterns, J. Geophys. Res., 118, 1–16, 2013.

Gray, L. J., Rumbold, S., and Shine, K. P.: Stratospheric temperatures and radiative forcing response to 11-year solar cycle changes in irradiance and ozone, J. Atmos. Sci., 66, 2402–2417, 2009.

Gray, L. J., Beer, J., Geller, M., Haigh, J. D., Lockwood, M., Matthes, K., Cubasch, U., Fleitmann, D., Harrison, G., Hood, L., Luterbacher, J., Meehl, G. A., Shindell, D., van Geel, B., and White, W.: Solar influences on climate, Rev. Geophys., 48, 1–53, doi:10.1029/2009RG000282, 2010.

Haberreiter, M., Schöll, M., Dudok de Wit, T., Kretzschmar, M., Misios, S., Tourpali, K., and Schmutz, W.: A new observational solar irradiance composite, Journal of Geophysical Research (Space Physics), submitted, 2017.

Haigh, J.: The impact of solar variability on climate, SCIENCE, 272, 981–984, doi:10.1126/science.272.5264.981, http://dx.doi.org/10.1126/science.272.5264.981, 1996.

Haigh, J. D.: The Role of Stratospheric Ozone in Modulating the Solar Radiative Forcing of Climate, Nature, 370, 544–546, doi:10.1038/370544a0, 1994.

Hanslmeier, A. and Brajša, R.: The chaotic solar cycle. I. Analysis of cosmogenic ^{14}C-data, Astronomy & Astrophysics, 509, A6, doi:10.1051/0004-6361/200913095, 2010.

Harder, J. W., Lawrence, G., Fontenla, J., Rottman, G., and Woods, T.: The Spectral Irradiance Monitor: Scientific Requirements, Instrument Design, and Operation Modes, Solar Physics, 230, 141–167, doi:10.1007/s11207-005-5007-5, 2005.

Harder, J. W., Fontenla, J. M., Pilewskie, P., Richard, E. C., and Woods, T. N.: Trends in solar spectral irradiance variability in the visible and infrared, Geophysical Research Letters, 36, doi:10.1029/2008GL036797, 2009.

Heath, D. F., Krueger, A. J., and Crutzen, P. J.: Solar proton event: influence on stratospheric ozone, Science, 197, 886–889, 1977.

Hegglin, M. I. e. a.: A CCMI Ozone Database for CMIP6, Glob. Mod. Devel. Disc., in preparation, 2016.

Hendrickx, K., Megner, L., Gumbel, J., Siskind, D. E., Orsolini, Y. J., Tyssøy, H. N., and Hervig, M.: Observation of 27day solar cycles in the production and mesospheric descent of EPP-produced NO, J. Geophys. Res., 120, 8978–8988, doi:10.1002/2015JA021441, 2015.

Holt, L. A., Randall, C. E., Peck, E. D., Marsh, D. R., Smith, A. K., and Lynn Harvey, V.: The influence of major sudden stratospheric warming and elevated stratopause events on the effects of energetic particle precipitation in WACCM, J. Geophys. Res., doi:10.1002/2013JD020294, 2013.

Hood, L. L., Misios, S., Mitchell, D. M., Rozanov, E., Gray, L. J., Tourpali, K., Matthes, K., Schmidt, H., Chiodo, G., Thiéblemont, R., Shindell, D., and Krivolutsky, A.: Solar signals in CMIP-5 simulations: The ozone response, Q. J. Roy. Meteorol. Soc., 141, 2670–2689, doi:10.1002/qj.2553, 2015.

Horne, R., Lam, M., and Green, J.: Energetic electron precipitation from the outer radiation belt during geomagnetic storms, Geophysical Research Letters, 36, doi:10.1029/2009GL040236, 2009.

Hurrell, J. W., Holland, M. M., Gent, P. R., Ghan, S., Kay, J. E., Kushner, P. J., Lamarque, J. F., Large, W. G., Lawrence, D., Lindsay, K., Lipscomb, W. H., Long, M. C., Mahowald, N., Marsh, D. R., Neale, R. B., Rasch, P., Vavrus, S., Vertenstein, M., Bader, D., Collins, W. D., Hack, J. J., Kiehl, J., and Marshall, S.: The Community Earth System Model: A Framework for Collaborative Research, Bull. Amer. Meteor. Soc., 94, 1339–1360, doi:10.1175/bams-d-12-00121.1, 2013.

Ineson, S., Scaife, A. A., Knight, J. R., Manners, J. C., Dunstone, N. J., Gray, L. J., and Haigh, J. D.: Solar forcing of winter climate variability in the Northern Hemisphere, Nature Geoscience, 4, 753–757, doi:10.1038/ngeo1282, 2011.

Ineson, S., Maycock, A. C., Gray, L. J., Scaife, A. A., Dunstone, N. J., Harder, J. W., Knight, J. R., Lockwood, M., Manners, J. C., and Wood, R. A.: Regional climate impacts of a possible future grand solar minimum, Nature Communications, 6, doi:10.1038/ncomms8535, 2015.

Jackman, C. H. and McPeters, R. D.: The Effect of solar proton events on ozone and other constituents, Solar Variability and its Effects on Climate, Geophys. Mon., 141, 305–319, 2004.

Jackman, C. H., Frederick, J. E., and Stolarski, R. S.: Production of odd nitrogen in the stratosphere and mesosphere: An intercomparison of source strengths, J. Geophys. Res., 85, 7495–7505, doi:10.1029/JC085iC12p07495, 1980.

Jackman, C. H., Douglass, A. R., Rood, R. B., McPeters, R. D., and Meade, P. E.: Effect of solar proton events on the middle atmosphere during the past two solar cycles as computed using a two-dimensional model, J. Geophys. Res., 95, 7417–7428, doi:10.1029/JD095iD06p07417, 1990.

Jackman, C. H., Cerniglia, M. C., Nielsen, J. E., Allen, D. J., Zawodny, J. M., McPeters, R. D., Douglass, A. R., Rosenfield, J. E., and Rood, R. B.: Two-dimensional and three-dimensional model simulations, measurements, and interpretation of the influence of the October 1989 solar proton events on the middle atmosphere, Journal of Geophysical Research: Atmospheres, 100, 11 641–11 660, doi:10.1029/95JD00369, 1995.

Jackman, C. H., McPeters, R. D., Labow, G. J., Fleming, E. L., Praderas, C. J., and Russell, J. M.: Northern Hemisphere atmospheric effects due to the July 2000 solar proton event, Geophys. Res. Lett., 28, 2883–2886, 2001.

Jackman, C. H., DeLand, M. T., Labow, G. J., Fleming, E. L., Weisenstein, D. K., Ko, M. K. W., Sinnhuber, M., Anderson, J., and Russell, J. M.: The Influence of the Several Very Large Solar Proton Events in Years 2000-2003 on the Neutral Middle Atmosphere, Adv. Space Res., 35, 445–450, 2005a.

Jackman, C. H., DeLand, M. T., Labow, G. J., Fleming, E. L., Weisenstein, D. K., Ko, M. K. W., Sinnhuber, M., and Russell, J. M.: Neutral atmospheric influences of the solar proton events in October–November 2003, J. Geophys. Res., 110, A09S27, doi:10.1029/2004JA010888, 2005b.

Jackman, C. H., Marsh, D. R., Vitt, F. M., Garcia, R. R., Fleming, E. L., Labow, G. J., Randall, C. E., López-Puertas, M., Funke, B., von Clarmann, T., and Stiller, G. P.: Short- and medium-term atmospheric effects of very large solar proton events, Atmos. Chem. Phys., 8, 765–785, doi:10.5194/acp-8-765-2008, 2008.

Jackman, C. H., Marsh, D. R., Vitt, F. M., Roble, R. G., Randall, C. E., Bernath, P. F., Funke, B., López-Puertas, M., Versick, S., Stiller, G. P., Tylka, A. J., and Fleming, E. L.: Northern Hemisphere atmospheric influence of the solar proton events and ground level enhancement in January 2005, Atmos. Chem. Phys., 11, 6153–6166, doi:10.5194/acp-11-6153-2011, 2011.

Jackman, C. H., Randall, C. E., Harvey, V. L., Wang, S., Fleming, E. L., López-Puertas, M., Funke, B., and Bernath, P. F.: Middle atmospheric changes caused by the January and March 2012 solar proton events, Atmos. Chem. Phys., 14, 1025–1038, doi:10.5194/acp-14-1025-2014, 2014.

Jackman, C. H., Marsh, D. R., Kinnison, D. E., Mertens, C. J., and Fleming, E. L.: Atmospheric changes caused by galactic cosmic rays over the period 1960–2010, Atmos. Chem. Phys. Discuss., 15, 33 931–33 966, doi:10.5194/acpd-15-33931-2015, 2015.

Jackson, A., Jonkers, A. R. T., and Walker, M. R.: Four centuries of geomagnetic secular variation from historical records, Phil. Trans. R. Soc. Lond. A, 358, 957–990, doi:10.1098/rsta.2000.0569, 2000.

Jöckel, P., Kerkweg, A., Pozzer, A., Sander, R., Tost, H., Riede, H., Baumgaertner, A., Gromov, S., and Kern, B.: Development cycle 2 of the Modular Earth Submodel System (MESSy2), Geosci. Model Dev., 3, 717–752, doi:10.5194/gmd-3-717-2010, 2010.

Jöckel, P., Tost, H., Pozzer, A., Kunze, M., Kirner, O., Brenninkmeijer, C. A. M., Brinkop, S., Cai, D. S., Dyroff, C., Eckstein, J., Frank, F., Garny, H., Gottschaldt, K.-D., Graf, P., Grewe, V., Kerkweg, A., Kern, B., Matthes, S., Mertens, M., Meul, S., Neumaier, M., Nützel, M., Oberländer-Hayn, S., Ruhnke, R., Runde, T., Sander, R., Scharffe, D., and Zahn, A.: Earth System Chemistry integrated Modelling (ESCiMo) with the Modular Earth Submodel System (MESSy) version2.51, Geosci. Model Dev., 9, 1153–1200, doi:10.5194/gmd-9-1153-2016, 2016.

Jones, A., Qin, G., Strong, K., Walker, K. A., McLinden, C. A., Toohey, M., Kerzenmacher, T., Bernath, P. F., and Boone, C. D.: A global inventory of stratospheric NOy from ACE-FTS, J. Geophys. Res., 116, n/a–n/a, doi:10.1029/2010JD015465, d17304, 2011.

Jungclaus, J. and et al.: The PMIP4-CMIP6 simulations of the last millennium, Climate Past, Special Issue on "Paleoclimate Modelling Intercomparison Project phase 4 (PMIP4), n/a–n/a, doi:to be submitted, 2016.

Kageyama, M., Braconnot, P., Harrison, S. P., Haywood, A. M., Jungclaus, J., Otto-Bliesner, B. L., Peterschmitt, J.-Y., Abe-Ouchi, A., Albani, S., Bartlein, P. J., Brierley, C., Crucifix, M., Dolan, A., Fernandez-Donado, L., Fischer, H., Hopcroft, P. O., Ivanovic, R. F., Lambert, F., Lunt, D. J., Mahowald, N. M., Peltier, W. R., Phipps, S. J., Roche, D. M., Schmidt, G. A., Tarasov, L., Valdes, P. J., Zhang, Q., and Zhou, T.: PMIP4-CMIP6: the contribution of the Paleoclimate Modelling Intercomparison Project to CMIP6, Geosci. Model Dev. Discuss., pp. n/a–n/a, doi:doi:10.5194/gmd-2016-106, 2016.

Kinnison, D. E., Brasseur, G. P., Walters, S., Garcia, R. R., Marsh, D. R., Sassi, F., Harvey, V. L., Randall, C. E., Emmons, L., Lamarque, J. F., Hess, P., Orlando, J. J., Tie, X. X., Randel, W., Pan, L. L., Gettelman, A., Granier, C., Diehl, T., Niemeier, U., and Simmons, A. J.: Sensitivity of chemical tracers to meteorological parameters in the MOZART-3 chemical transport model, J. Geophys. Res., 112, D20302, doi:10.1029/2006JD007879, 2007.

Kodera, K.: Solar cycle modulation of the North Atlantic Oscillation: Implication in the spatial structure of the NAO, Geophys. Res. Lett., 29, doi:10.1029/2001GL014557, 2002.

Kopp, G. and Lean, J. L.: A new, lower value of total solar irradiance: Evidence and climate significance, Geophysical Research Letters, 38, L01 706, doi:10.1029/2010GL045777, 2011.

Kopp, G., Lawrence, G., and Rottman, G.: The Total Irradiance Monitor (TIM): Science Results, Solar Physics, 230, 129–139, doi:10.1007/s11207-005-7433-9, 2005.

Kopp, G., Krivova, N., Lean, J., and Wu, C. J.: The Impact of the Revised Sunspot Record on Solar Irradiance Reconstructions, Solar Physics, in press, doi:10.1007/s11207-016-0853, 2016.

Krivolutsky, A., Bazilevskaya, G., Vyushkova, T., and Knyazeva, G.: Influence of cosmic rays on chemical composition of the atmosphere: data analysis and photochemical modelling, Physics and Chemistry of the Earth, Parts A/B/C, 27, 471 – 476, doi:10.1016/S1474-7065(02)00028-1, 2002.

Krivolutsky, A. A., Kuminov, A. A., Kukoleva, A. A., Repnev, A. I., Pereyaslova, N. K., and Nazarova, M. N.: Solar proton activity during cycle 23 and changes in the ozonosphere: Numerical simulation and analysis of observational data, Geomagnetism and Aeronomy, 48, 432–445, doi:10.1134/S0016793208040038, 2008.

Krivova, N. A., Solanki, S. K., Fligge, M., and Unruh, Y. C.: Reconstruction of solar irradiance variations in cycle 23: Is solar surface magnetism the cause?, Astronomy & Astrophysics, 399, L1–L4, doi:10.1051/0004-6361:20030029, 2003.

Krivova, N. A., Vieira, L. E. A., and Solanki, S. K.: Reconstruction of solar spectral irradiance since the Maunder minimum, Journal of Geophysical Research (Space Physics), 115, doi:10.1029/2010JA015431, 2010.

Krivova, N. A., Solanki, S. K., and Unruh, Y. C.: Towards a long-term record of solar total and spectral irradiance, Journal of Atmospheric and Solar-Terrestrial Physics, 73, 223–234, doi:10.1016/j.jastp.2009.11.013, 2011.

Kunze, M., Godolt, M., Langematz, U., Grenfell, J., Hamann-Reinus, A., and Rauer, H.: Investigating the early Earth faint young Sun problem with a general circulation model, Planet. Space Sci., 98, 77–92, doi:10.1016/j.pss.2013.09.011, planetary evolution and life, 2014.

Laken, B. A. and Čalogović, J.: Composite analysis with Monte Carlo methods: an example with cosmic rays and clouds, Journal of Space Weather and Space Climate, 3, A29, doi:10.1051/swsc/2013051, 2013.

Lam, M. M., Horne, R. B., Meredith, N. P., Glauert, S. A., Moffat-Griffin, T., and Green, J. C.: Origin of energetic electron precipitation $>$30 keV into the atmosphere, J. Geophys. Res. (Space Physics), 115, A00F08, doi:10.1029/2009JA014619, 2010.

Langematz, U., Kubin, A., Brühl, C., Baumgaertner, A., Cubasch, U., and Spangehl, T.: Solar effects on chemistry and climate including ocean interactions in Climate And Weather of the Sun-Earth System (CAWSES): Highlights from a Priority Program, pp. 541–571, Springer, Dordrecht, The Netherlands, doi:10.1007/978-94-007-4348-9, 2013.

Lean, J. L.: The Sun's Variable Radiation and Its Relevance For Earth, Annual Review Astronomy Astrophysics, 35, 33–67, doi:10.1146/annurev.astro.35.1.33, 1997.

Lean, J. L.: Evolution of the Sun's spectral irradiance since the Maunder Minimum, Geophysical Research Letters, 27, 2425–2428, doi:10.1029/2000GL000043, 2000.

Lean, J. L. and DeLand, M. T.: How Does the Sun's Spectrum Vary?, Journal of Climate, 25, 2555–2560, doi:10.1175/JCLI-D-11-00571.1, 2012.

Lean, J. L. and Rind, D. H.: How natural and anthropogenic influences alter global and regional surface temperatures: 1889 to 2006, Geophysical Research Letters, 35, n/a–n/a, doi:10.1029/2008GL034864, http://dx.doi.org/10.1029/2008GL034864, l18701, 2008.

Lean, J. L. and Rind, D. H.: How will Earth's surface temperature change in future decades?, Geophysical Research Letters, 36, 15 708, doi:10.1029/2009GL038932, 2009.

Lean, J. L., Cook, J., Marquette, W., and Johannesson, A.: Magnetic Sources of the Solar Irradiance Cycle, The Astronomical Journal, 492, 390–401, doi:10.1086/305015, 1998.

Lean, J. L., Woods, T. N., Eparvier, F. G., Meier, R. R., Strickland, D. J., Correira, J. T., and Evans, J. S.: Solar extreme ultraviolet irradiance: Present, past, and future, Journal of Geophysical Research (Space Physics), 116, A01 102, doi:10.1029/2010JA015901, 2011.

Lilensten, J., Dudok de Wit, T., and Matthes, K., eds.: Earth's climate response to a changing Sun, EDP Sciences, Paris, 2015.

Ljung, L.: System Identification: Theory for the User, Prentice-Hall, Englewood Cliffs, New Jersey, 2nd edn., 1997.

Lockwood, M., Harrison, R. G., Woollings, T., and Solanki, S.: Are cold winters in Europe associated with low solar activity?, Environ. Res. Lett., 5, doi:10.1088/1748-9326/5/2/024001, 2010.

Lockwood, M., Barnard, L., Nevanlinna, H., Owens, M. J., Harrison, R. G., Rouillard, A. P., and Davis, C. J.: Reconstruction of geomagnetic activity and near-Earth interplanetary conditions over the past 167 yr – Part 1: A new geomagnetic data composite, Annales Geophysicae, 31, 1957–1977, doi:10.5194/angeo-31-1957-2013, 2013.

Lockwood, M., Nevanlinna, H., Barnard, L., Owens, Harrison, R. G., Rouillard, A. P., and Scott, C. J.: Reconstruction of geomagnetic activity and near-Earth interplanetary conditions over the past 167 yr - Part 4: Near-Earth solar wind speed, IMF, and open solar flux, Annales Geophysicae, 32, 383–399, doi:10.5194/angeo-32-383-2014, 2014.

López-Puertas, M., Funke, B., Gil-López, S., von Clarmann, T., Stiller, G. P., Höpfner, M., Kellmann, S., Fischer, H., and Jackman, C. H.: Observation of NO_x Enhancement and Ozone Depletion in the Northern and Southern Hemispheres after the October–November 2003 Solar Proton Events, J. Geophys. Res., 110, A09S43, doi:10.1029/2005JA011050, 2005a.

López-Puertas, M., Funke, B., Gil-López, S., von Clarmann, T., Stiller, G. P., Höpfner, M., Kellmann, S., Mengistu Tsidu, G., Fischer, H., and Jackman, C. H.: HNO_3, N_2O_5 and $ClONO_2$ Enhancements after the October–November 2003 Solar Proton Events, J. Geophys. Res., 110, A09S44, doi:10.1029/2005JA011051, 2005b.

Maliniemi, V., Asikainen, T., and Mursula, K.: Spatial distribution of Northern Hemisphere winter temperatures during different phases of the solar cycle, J. Geophys. Res., 119, 9752–9764, doi:10.1002/2013JD021343, 2014.

Mamajek, E. E., Prsa, A., Torres, G., Harmanec, P., Asplund, M., Bennett, P. D., Capitaine, N., Christensen-Dalsgaard, J., Depagne, E., Folkner, W. M., Haberreiter, M., Hekker, S., Hilton, J. L., Kostov, V., Kurtz, D. W., Laskar, J., Mason, B. D., Milone, E. F., Montgomery, M. M., Richards, M. T., Schou, J., and Stewart, S. G.: IAU 2015 Resolution B3 on Recommended Nominal Conversion Constants for Selected Solar and Planetary Properties, Resolution b3, International Astronomical Union, 2015.

Marsh, D. R., Solomon, S. C., and Reynolds, A. E.: Empirical model of nitric oxide in the lower thermosphere, J. Geophys. Res., 109, A07301, doi:10.1029/2003JA010199, 2004.

Marsh, D. R., Garcia, R. R., Kinnison, D. E., Boville, B. A., Sassi, F., Solomon, S. C., and Matthes, K.: Modeling the whole atmosphere response to solar cycle changes in radiative and geomagnetic forcing, J. Geophys. Res., 112, D23306, doi:10.1029/2006JD008306, 2007.

Marsh, D. R., Mills, M. J., Kinnison, D. E., Lamarque, J.-F., Calvo, N., and Polvani, L. M.: Climate Change from 1850 to 2005 Simulated in CESM1(WACCM), J. Climate, 26(19), 7372–7391, doi:10.1175/JCLI-D-12-00558.1, 2013.

Matthes, K., Kodera, K., Haigh, J., Shindell, D., Shibata, K., Langematz, U., Rozanov, E., and Kuroda, Y.: GRIPS solar experiments intercomparison project: Initial results, Papers in Meteorology and Geophysics, 54, 71–90, 2003.

Matthes, K., Kuroda, Y., Kodera, K., and Langematz, U.: Transfer of the solar signal from the stratosphere to the troposphere: Northern winter, J. Geophys. Res., 111, D06108, doi:10.1029/2005JD006283, 2006.

Matthes, K., Marsh, D. R., Garcia, R. R., Kinnison, D. E., Sassi, F., and Walters, S.: Role of the QBO in modulating the influence of the 11 year solar cycle on the atmosphere using constant forcings, J. Geophys. Res., 115, D18110, doi:10.1029/2009JD013020, 2010.

Mayaud, P.: The aa indices: A 100-year series characterizing the magnetic activity, Journal of Geophysical Research, 77, 6870–6874, doi:10.1029/JA077i034p06870, 1972.

Mayaud, P.-N.: Derivation, Meaning, and Use of Geomagnetic Indices, Geophysical Monograph, 22, 1980.

Maycock, A. C., Ineson, S., Gray, L. J., Scaife, A. A., Anstey, J. A., Lockwood, M., Butchart, N., Hardiman, S. C., Mitchell, D. M., and Osprey, S. M.: Possible impacts of a future Grand Solar Minimum on climate: Stratospheric and global circulation changes, Journal of Geophysical Research: Atmospheres, 120, 9043—9058, doi:10.1002/2014JD022022, 2015.

Maycock, A. C., Matthes, K., Tegtmeier, S., Thiéblemont, R., and Hood, L. L.: The representation of solar cycles signals in stratospheric ozone. Part I: A comparison of satellite observations, Atmos. Chem. Phys. Diss., in review, doi:10.5194/acp-2015-882, 2016a.

Maycock, A. C., Matthes, K., Tegtmeier, S., Thiéblemont, R., and Hood, L. L.: The representation of solar cycles signals in stratospheric ozone. Part II: A comparison of global models, Atmos. Chem. Phys. Diss., in preparation, 2016b.

Mayer, B. and Kylling, A.: Technical note: The libRadtran software package for radiative transfer calculations - description and examples of use, Atmos. Chem. Phys., 5, 1855–1877, doi:10.5194/acp-5-1855-2005, 2005.

McClintock, W. E., Rottman, G. J., and Woods, T. N.: Solar-Stellar Irradiance Comparison Experiment II (Solstice II): Instrument Concept and Design, Solar Physics, 230, 225–258, doi:10.1007/s11207-005-7432-x, 2005.

McCracken, K. G., Beer, J., Steinhilber, F., and Abreu, J.: A Phenomenological Study of the Cosmic Ray Variations over the Past 9400 Years, and Their Implications Regarding Solar Activity and the Solar Dynamo, Solar Physics, 286, 609–627, doi:10.1007/s11207-013-0265-0, 2013.

McIlwain, C. E.: Coordinates for Mapping the Distribution of Magnetically Trapped Particles, J. Geophys. Res., 66, 3681–3691, doi:10.1029/JZ066i011p03681, 1961.

McPeters, R. D.: A nitric oxide increase observed following the July 1982 solar proton event, Geophys. Res. Lett., 13, 667–670, doi:10.1029/GL013i007p00667, 1986.

McPeters, R. D. and Jackman, C. H.: The response of ozone to solar proton events during solar cycle 21: The observations, J. Geophys. Res., 90, 7945–7954, doi:10.1029/JD090iD05p07945, 1985.

McPeters, R. D., Jackman, C. H., and Stassinopoulos, E. G.: Observations of ozone depletion associated with solar proton events, J. Geophys. Res., 86, 12 071–12 081, doi:10.1029/JC086iC12p12071, http://dx.doi.org/10.1029/JC086iC12p12071, 1981.

Meehl, G. A., Arblaster, J. M., and Marsh, D. R.: Could a future "Grand Solar Minimum" like the Maunder Minimum stop global warming?, Geophysical Research Letters, 40, 1789–1793, doi:10.1002/grl.50361, 2013.

Mewaldt, R. A., Cohen, C. M. S., Labrador, A. W., Leske, R. A., Mason, G. M., Desai, M. I., Looper, M. D., Mazur, J. E., Selesnick, R. S., and Haggerty, D. K.: Proton, helium and electron spectra during the large solar particle events of October–November 2003, J. Geophys. Res., 110, A09S18, doi:10.1029/2005JA011038, 2005.

Mironova, I. A., Aplin, K. L., Arnold, F., Bazilevskaya, G. A., Harrison, R. G., Krivolutsky, A. A., Nicoll, K. A., Rozanov, E. V., Turunen, E., and Usoskin, I. G.: Energetic Particle Influence on the Earth's Atmosphere, Space Sci Rev., 194, 1–96, doi:10.1007/s11214-015-0185-4, 2015.

Misios, S., Mitchell, D. M., Gray, L. J., Tourpali, K., Matthes, K., Hood, L. L., Schmidt, H., Chiodo, G., Thiéblemont, R., Rozanov, E., and Krivolutsky, A.: Solar signals in CMIP-5 simulations: effects of atmosphere–ocean coupling, Q. J. Roy. Meteorol. Soc., 142, 928–941, doi:10.1002/qj.2695, 2016.

Mitchell, D. M., Gray, L. J., Fujiwara, M., Hibino, T., Anstey, J., Harada, Y., Long, C., Misios, S., Stott, P. A., and Tan, D.: Signatures of naturally induced variability in the atmosphere using multiple reanalysis datasets., Q. J. Roy. Meteorol. Soc., 141, 2011–2031, doi:10.1002/qj.2492, 2015a.

Mitchell, D. M., Misios, S., Gray, L. J., Tourpali, K., Matthes, K., Hood, L. L., Schmidt, H., Chiodo, G., Thiéblemont, R., Rozanov, E., Shindell, D., and Krivolutsky, A.: Solar signals in CMIP-5 simulations: the stratospheric pathway, Q. J. Roy. Meteorol. Soc., 141, 2390–2403, doi:10.1002/qj.2530, 2015b.

Morley, S. K., Friedel, R. H. W., Cayton, T. E., and Noveroske, E.: A rapid, global and prolonged electron radiation belt dropout observed with the Global Positioning System constellation, Geophys. Res. Lett., 37, L06102, doi:10.1029/2010GL042772, 2010.

Mudelsee, M.: Climate Time Series Analysis: Classical Statistical and Bootstrap Methods, vol. 42 of *Atmospheric and Oceanographic Sciences Library*, Springer Verlag, doi:10.1007/978-90-481-9482-7, 2010.

Neal, J. J., Rodger, C. J., Clilverd, M. A., Thomson, N. R., Raita, T., and Ulich, T.: Long-term determination of energetic electron precipitation into the atmosphere from AARDDVARK subionospheric VLF observations, J. Geophys. Res. (Space Physics), 120, 2194–2211, doi:10.1002/2014JA020689, 2015.

Neale, R. B., Richter, J., Park, S., Lauritzen, P. H., Vavrus, S. J., Rasch, P. J., and Zhang, M.: The Mean Climate of the Community Atmosphere Model (CAM4) in Forced SST and Fully Coupled Experiments, J. Climate, 26, 5150–5168, doi:10.1175/jcli-d-12-00236.1, 2013.

Nevanlinna, H.: Results of the Helsinki magnetic observatory 1844-1912, Annales Geophysicae, 22, 1691–1704, doi:10.5194/angeo-22-1691-2004, 2004.

Nieder, H., Winkler, H., Marsh, D., and Sinnhuber, M.: NOx production due to energetic particle precipitation in the MLT region: Results from ion chemistry model studies, Journal of Geophysical Research, 119, 2137–2148, doi:10.1002/2013JA019044, 2014.

Nissen, K. M., Matthes, K., Langematz, U., and Mayer, B.: Towards a better representation of the solar cycle in general circulation models, Atmos. Chem. Phys., 7, 5391–5400, doi:10.5194/acp-7-5391-2007, 2007.

Passos, D., Charbonneau, P., and Beaudoin, P.: An Exploration of Non-kinematic Effects in Flux Transport Dynamos, Solar Physics, 279, 1–22, doi:10.1007/s11207-012-9971-2, 2012.

Pesnell, W. D.: Solar Cycle Predictions, Solar Physics, 281, 507–532, doi:10.1007/s11207-012-9997-5, 2012.

Petrovay, K.: Solar Cycle Prediction, Living Reviews in Solar Physics, 7, doi:10.12942/lrsp-2010-6, 2010.

Picone, J. M., Hedin, A. E., Drob, D. P., and Aikin, A. C.: NRLMSISE-00 empirical model of the atmosphere: Statistical comparisons and scientific issues, Journal of Geophysical Research (Space Physics), 107, 1468, doi:10.1029/2002JA009430, 2002.

Porter, H. S., Jackman, C. H., and Green, A. E. S.: Efficiencies for production of atomic nitrogen and oxygen by relativistic proton impact in air, J. Chem. Phys., 65, 154–167, doi:10.1063/1.432812, 1976.

Prša, A., Harmanec, P., Torres, G., Mamajek, E., Asplund, M., Capitaine, N., Christensen-Dalsgaard, J., Depagne, É., Haberreiter, M., Hekker, S., Hilton, J., Kopp, G., Kostov, V., Kurtz, D. W., Laskar, J., Mason, B. D., Milone, E. F., Montgomery, M., Richards, M., Schmutz, W., Schou, J., and Stewart, S. G.: Nominal Values for Selected Solar and Planetary Quantities: IAU 2015 Resolution B3, The Astronomical Journal, 152, 41, doi:10.3847/0004-6256/152/2/41, 2016.

Randall, C. E., Rusch, D. W., Bevilacqua, R. M., Hoppel, K. W., and Lumpe, J. D.: Polar Ozone and Aerosol Measurement (POAM) II stratospheric NO_2, 1993–1996, J. Geophys. Res., 103, 28,361–28,371, 1998.

Randall, C. E., Siskind, D. E., and Bevilacqua, R. M.: Stratospheric NO_x enhancements in the southern hemisphere vortex in winter/spring of 2000, Geophys. Res. Lett., 28, 2385–2388, 2001.

Randall, C. E., Harvey, V. L., Singleton, C. S., Bailey, S. M., Bernath, P. F., Codrescu, M., Nakajima, H., and Russell III, J. M.: Energetic particle precipitation effects on the Southern Hemisphere stratosphere in 1992-2005, J. Geophys. Res., 112, D08308, doi:10.1029/2006JD007696, 2007.

Randall, C. E., Harvey, V. L., Siskind, D. E., France, J., Bernath, P. F., Boone, C. D., and Walker, K. A.: NO_x descent in the Arctic middle atmosphere in early 2009, Geophys. Res. Lett., 36, doi:10.1029/2009GL039706, 2009.

Rayner, N. A., Parker, D. E., Horton, E. B., Folland, C. K., Alexander, L. V., Rowell, D. P., Kent, E. C., and Kaplan, A.: Global analyses of sea surface temperature, sea ice, and night marine air temperature since the late nineteenth century, J. Geophys. Res., 108, n/a–n/a, doi:10.1029/2002JD002670, 4407, 2003.

Reames, D.: Particle Acceleration at the Sun and in the Heliosphere, Space Sciences Reviews, 90, 413–491, 1999.

Reddmann, T., Ruhnke, R., Versick, S., and Kouker, W.: Modeling disturbed stratospheric chemistry during solar-induced NO_x enhancements observed with MIPAS/ENVISAT, J. Geophys. Res., 115, D00I11, doi:10.1029/2009JD012569, 2010.

Rees, M. H.: Physics and chemistry of the upper atmosphere, Cambridge University Press, http://dx.doi.org/10.1017/CBO9780511573118, 1989.

Reeves, G. D., McAdams, K. L., Friedel, R. H. W., and O'Brien, T. P.: Acceleration and loss of relativistic electrons during geomagnetic storms, Geophys. Res. Lett., 30, 1529, doi:10.1029/2002GL016513, 2003.

Richardson, I. and Cane, H.: Near-Earth Interplanetary Coronal Mass Ejections During Solar Cycle 23 (1996 – 2009): Catalog and Summary of Properties, Solar Physics, 264, 189–237, doi:10.1007/s11207-010-9568-6, 2010.

Rienecker, M. M., Suarez, M. J., Gelaro, R., Todling, R., Bacmeister, J., Liu, E., Bosilovich, M. G., Schubert, S. D., Takacs, L., Kim, G.-K., Bloom, S., Chen, J., Collins, D., Conaty, A., da Silva, A., Gu, W., Joiner, J., Koster, R. D., Lucchesi, R., Molod, A., Owens, T., Pawson, S., Pegion, P., Redder, C. R., Reichle, R., Robertson, F. R., Ruddick, A. G., Sienkiewicz, M., and Woollen, J.: MERRA: NASA's Modern-Era Retrospective Analysis for Research and Applications, J. Climate, 24, 3624–3648, doi:10.1175/jcli-d-11-00015.1, 2011.

Rind, D., Lean, J., Lerner, J., Lonergan, P., and Leboissitier, A.: Exploring the stratospheric/tropospheric response to solar forcing, J. Geophys. Res., 113, doi:10.1029/2008JD010114, 2008.

Rodger, C. J., Clilverd, M. A., Green, J. C., and Lam, M. M.: Use of POES SEM-2 observations to examine radiation belt dynamics and energetic electron precipitation into the atmosphere, J. Geophys. Res., 115, A04 202, doi:10.1029/2008JA014023, 2010a.

Rodger, C. J., Kavanagh, A. J., Clilverd, M. A., and Marple, S. R.: Comparison between POES energetic electron precipitation observations and riometer absorptions: Implications for determining true precipitation fluxes, J. Geophys. Res. (Space Physics), 118, 7810–7821, doi:10.1002/2013JA019439, 2013.

Roeckner, E., Bäuml, G., Bonaventura, L., Brokopf, R., Esch, M., Giorgetta, Hagemann, S., Kirchner, I., Kornblueh, L., Manzini, E., Rhodin, A., Schlese, U., Schulzweida, U., and Tompkins, A.: The atmospheric general circulation model ECHAM5, Part I, Tech. Rep. No. 349, Max-Planck-Institut für Meteorologie, Hamburg, 2003.

Roeckner, E., Brokopf, R., Esch, M., Giorgetta, M., Hagemann, S., Kornblueh, L., Manzini, E., Schlese, U., and Schulzweida, U.: Sensitivity of Simulated Climate to Horizontal and Vertical Resolution in the ECHAM5 Atmosphere Model, J. Climate, 19, 3771–3791, doi:10.1175/JCLI3824.1, 2006.

Rohen, G. J., von Savigny, C., Sinnhuber, M., Llewellyn, E. J., Kaiser, J. W., Jackman, C. H., Kallenrode, M.-B., Schrőter, J., Eichmann, K.-U., Bovensmann, H., and Burrows, J. P.: Ozone depletion during the solar proton events of October/November 2003 as seen by SCIAMACHY, J. Geophys. Res., 110, A09S39, doi:10.1029/2004JA010984, 2005.

Rottman, G.: The SORCE Mission, Solar Physics, 230, 7–25, doi:10.1007/s11207-005-8112-6, 2005.

Rozanov, E., Calisto, M., Egorova, T., Peter, T., and Schmutz, W.: Influence of the Precipitating Energetic Particles on Atmospheric Chemistry and Climate, Surv. Geophys., 33, 483–501, doi:10.1007/s10712-012-9192-0, 2012.

Rusch, D. W., Gérard, J.-C., Solomon, S., Crutzen, P. J., and Reid, G. C.: The effect of particle precipitation events on the neutral and ion chemistry of the middle atmosphere. I - Odd nitrogen, Planet. Space Sci., 29, 767–774, 1981.

Salmi, S.-M., Verronen, P. T., Thölix, L., Kyrölä, E., Backman, L., Karpechko, A. Y., and Seppälä, A.: Mesosphere-to-stratosphere descent of odd nitrogen in February–March 2009 after sudden stratospheric warming, Atmos. Chem. Phys., 11, 4645–4655, doi:10.5194/acp-11-4645-2011, 2011.

Sander, R., Baumgaertner, A., Gromov, S., Harder, H., Jöckel, P., Kerkweg, A., Kubistin, D., Regelin, E., Riede, H., Sandu, A., Taraborrelli, D., Tost, H., and Xie, Z.-Q.: The atmospheric chemistry box model CAABA/MECCA-3.0, Geosci. Model Dev., 4, 373–380, doi:10.5194/gmd-4-373-2011, 2011a.

Sander, R., Jöckel, P., Kirner, O., Kunert, A. T., Landgraf, J., and Pozzer, A.: The photolysis module JVAL-14, compatible with the MESSy standard, and the JVal PreProcessor (JVPP), Geosci. Model Dev., 7, 2653–2662, doi:10.5194/gmd-7-2653-2014, 2014.

Sander, S. P., Abbatt, J., Barker, J. R., Burkholder, J. B., Friedl, R. R., Golden, D. M., Huie, R. E., Kolb, C. E., Kurylo, M. J., Moortgat, G. K., Orkin, V. L., and Wine, P. H.: Chemical Kinetics and Photochemical Data for Use in Atmospheric Studies, Tech. Rep. Evaluation No. 17, JPL Publication 10-6, Jet Propulsion Laboratory, Pasadena, http://jpldataeval.jpl.nasa.gov, 2011b.

Scaife, A. A., Ineson, S., Knight, J. R., Gray, L., Kodera, K., and Smith, D. M.: A mechanism for lagged North Atlantic climate response to solar variability, Geophysical Research Letters, 40, 434–439, doi:10.1002/grl.50099, 2013.

Schmidt, H., Brasseur, G., Charron, M., Manzini, E., Giorgetta, M., Diehl, T., Formichev, V., Kinnison, D., Marsh, D., and Walters, S.: The HAMMONIA chemistry climate model: sensitivity of the mesopause region to the 11-year solar cycle and CO_2 doubling, J. Clim., 19, 3903–3931, 2006.

Schmutz, W., Fehlmann, A., Finsterle, W., Kopp, G., and Thuillier, G.: Total solar irradiance measurements with PREMOS/PICARD, in: AIP conference proceedings, vol. 1531 of *American Institute of Physics Conference Series*, p. 624, doi:10.1063/1.4804847, 2013.

Schöll, M., de Wit, T. D., Kretzschmar, M., and Haberreiter, M.: Making of a solar spectral irradiance dataset I: observations, uncertainties, and methods, Journal of Space Weather and Space Climate, 6, A14, doi:10.1051/swsc/2016007, 2016.

Semeniuk, K., Fomichev, V. I., McConnell, J. C., Fu, C., Melo, S. M. L., and Usoskin, I. G.: Middle atmosphere response to the solar cycle in irradiance and ionizing particle precipitation, Atmos. Chem. Phys., 11, 5045–5077, doi:10.5194/acp-11-5045-2011, 2011.

Seppälä, A., Randall, C. E., Clilverd, M. A., Rozanov, E., and Rodger, C. J.: Geomagnetic activity and polar surface air temperature variability, J. Geophys. Res., 114, doi:10.1029/2008JA014029, 2009.

Seppälä, A., Matthes, K., Randall, C. E., and Mironova, I. A.: What is the solar influence on climate? Overview of activities during CAWSES-II, Progress in Earth and Planetary Science, 1, 24, doi:10.1186/s40645-014-0024-3, 2014.

Seppälä, A. and Clilverd, M. A.: Energetic Particle Forcing of the Northern Hemisphere winter stratosphere: Comparison to solar irradiance forcing, Frontiers in Physics, 2, doi:10.3389/fphy.2014.00025, 2014.

Seppälä, A., Verronen, P. T., Sofieva, V. F., Tamminen, J., Kyrölä, E., Rodger, C. J., and Clilverd, M. A.: Destruction of the tertiary ozone maximum during a solar proton event, Geophys. Res. Lett., 33, n/a–n/a, doi:10.1029/2005GL025571, l07804, 2006.

Shibata, K. and Kodera, K.: Simulation of radiative and dynamical responses of the middle atmosphere to the 11-year solar cycle, J. Atmos. Sol. Terr. Phys., 67, 125–143, 2005.

Shindell, D. T., Schmidt, G. A., Mann, M. E., Rind, D., and Waple, A.: Solar Forcing of Regional Climate Change During the Maunder Minimum, Science, 294, 2149–2152, doi:10.1126/science.1064363, 2001.

Sinnhuber, M., Kazeminejad, S., and Wissing, J.-M.: Interannual variation of NOx from the lower thermosphere to the upper stratosphere in the years 1991-2005, Journal of Geophysical Research, 116, doi:10.1029/2010JA015825, 2011.

Sinnhuber, M., Nieder, H., and Wieters, N.: Energetic particle precipitation and the chemistry of the mesosphere / lower thermosphere, Surveys in Geophysics, 33, doi:10.1007/s10712-012-9201-3, 2012.

Sinnhuber, M., Friederich, F., Bender, S., and Burrows, J.: The response of mesospheric NO to geomagnetic forcing in 2002-2012 as seen by SCIAMACHY, Journal of Geophysical Research (Space Physics), 121, doi:10.1002/2015JA022284, 2016.

Siskind, D. E.: Atmospheric science across the Stratopause, vol. 123 of *Geophysical Monograph*, chap. On the coupling between middle and upper atmospheric odd nitrogen, pp. 101–116, American Geophysical Union, 2000.

Smart, D. F., Shea, M. A., and Flückiger, E. O.: Magnetospheric Models and Trajectory Computations, Space Sci. Rev., 93, 305–333, doi:10.1023/A:1026556831199, 2000.

Smith, D. M., Scaife, A. A., Boer, G. J., Caian, M., Doblas-Reyes, F. J., Guemas, V., Hawkins, E., Hazeleger, W., Hermanson, L., Ho, C. K., Ishii, M., Kharin, V., Kimoto, M., Kirtman, B., Lean, J., Matei, D., Merryfield, W. J., Müller, W. A., Pohlmann, H., Rosati, A., Wouters, B., and Wyser, K.: Real-time multi-model decadal climate predictions, Climate Dynamics, 41, 2875–2888, doi:10.1007/s00382-012-1600-0, 2013.

Solanki, S. K., Krivova, N. A., and Haigh, J. D.: Solar Irradiance Variability and Climate, Annual Review of Astronomy and Astrophysics, 51, 311–351, doi:10.1146/annurev-astro-082812-141007, 2013.

Solomon, S., Rusch, D. W., Gérard, J.-C., Reid, G. C., and Crutzen, P. J.: The effect of particle precipitation events on the neutral and ion chemistry of the middle atmosphere. II - Odd hydrogen, Planet. Space Sci., 29, 885–892, 1981.

Solomon, S., Crutzen, P. J., and Roble, R. G.: Photochemical coupling of the thermosphere and the lower atmosphere 1. Odd nitrogen from 50 to 120 km, J. Geophys. Res., 87, 7206–7220, 1982.

Solomon, S. C. and Qian, L.: Solar extreme-ultraviolet irradiance for general circulation models, J. Geophys. Res., 110, A10306, doi:10.1029/2005JA011160, 2005.

Steinhilber, F. and Beer, J.: Prediction of solar activity for the next 500 years, Journal of Geophysical Research (Space Physics), 118, 1861–1867, doi:10.1002/jgra.50210, 2013.

Steinhilber, F., Abreu, J. A., Beer, J., Brunner, I., Christl, M., Fischer, H., Heikkilä, U., Kubik, P. W., Mann, M., McCracken, K. G., Miller, H., Miyahara, H., Oerter, H., and Wilhelms, F.: 9,400 years of cosmic radiation and solar activity from ice cores and tree rings, Proceedings of the National Academy of Sciences, 109, 5967–5971, doi:10.1073/pnas.1118965109, 2012.

Stott, P., Jones, G. S., and Mitchell, J. F. B.: Do Models Underestimate the Solar Contribution to Recent Climate Change?, J. Climate, 16, 4070–4093, http://dx.doi.org/10.1175/1520-0442(2003)016<4079:DMUTSC>2.0.CO;2, 2003.

Summers, D., Ni, B., and Meredith, N. P.: Timescales for radiation belt electron acceleration and loss due to resonant wave-particle interactions: 1. Theory, J. Geophys. Res. (Space Physics), 112, A04206, doi:10.1029/2006JA011801, 2007.

Swider, W. and Keneshea, T.: Decrease of ozone and atomic oxygen in the lower mesosphere during a PCA event, Planetary and Space Science, 21, 1969 – 1973, doi:http://dx.doi.org/10.1016/0032-0633(73)90126-8, 1973.

Tapping, K. F.: The 10.7 cm solar radio flux (F10.7), Space Weather, 11, 394–406, doi:10.1002/swe.20064, 2013.

Thébault, E.: International Geomagnetic Reference Field: the 12th generation, Earth, Planets and Space, 67, 1–19, doi:10.1186/s40623-015-0228-9, 2015.

Thieblemont, R., Matthes, K., Omrani, N.-E., Kodera, K., and Hansen, F.: Solar forcing synchronizes decadal North Atlantic climate variability, Nature Commun., 6, 8268, doi:10.1038/ncomms9268, 2015.

Thomas, R. J., Barth, C. A., Rottman, G. J., Rusch, D. W., Mount, G. H., Lawrence, G. M., Sanders, R. W., Thomas, G. E., and Clemens, L. E.: Mesospheric ozone depletion during the Solar Proton Event of July 13, 1982 Part I Measurement, Geophys. Res. Lett., 10, 253–255, doi:10.1029/GL010i004p00253, 1983.

Tummon, F., Hassler, B., Harris, N. R. P., Staehelin, J., Steinbrecht, W., Anderson, J., Bodeker, G. E., Bourassa, A., Davis, S. M., Degenstein, D., Frith, S. M., Froidevaux, L., Kyrölä, E., Laine, M., Long, C., Penckwitt, A. A., Sioris, C. E., Rosenlof, K. H., Roth, C., Wang, H. J., and Wild, J.: Intercomparison of vertically resolved merged satellite ozone data sets: interannual variability and long-term trends, Atmos. Chem. Phys., 15, 3021–3043, 2015.

Turunen, E., Verronen, P. T., Seppälä, A., Rodger, C. J., Clilverd, M. A., Tamminen, J., Enell, C.-F., and Ulich, T.: Impact of different precipitation energies on NO_x generation during geomagnetic storms, J. Atmos. Sol.-Terr. Phys., 71, 1176–1189, doi:10.1016/j.jastp.2008.07.005, 2009.

Unruh, Y. C., Solanki, S. K., and Fligge, M.: The spectral dependence of facular contrast and solar irradiance variations, Astronomy & Astrophysics, 345, 635–642, 1999.

Usoskin, I. G.: A History of Solar Activity over Millennia, Living Reviews in Solar Physics, 5, 3–67, doi:10.12942/lrsp-2008-3, 2008.

Usoskin, I. G. and Kovaltsov, G. A.: Cosmic ray induced ionization in the atmosphere: Full modeling and practical applications, J. Geophys. Res., 111, D21206, doi:10.1029/2006JD007150, 2006.

Usoskin, I. G., Alanko-Huotari, K., Kovaltsov, G. A., and Mursula, K.: Heliospheric modulation of cosmic rays: Monthly reconstruction for 1951–2004, J. Geophys. Res., 110, A12108, doi:10.1029/2005JA011250, 2005.

Usoskin, I. G., Desorgher, L., Velinov, P., Storini, M., Flückiger, E. O., Bütikofer, R., and Kovaltsov, G. A.: Ionization of the earth's atmosphere by solar and galactic cosmic rays, Acta Geophys., 57, 88–101, doi:10.2478/s11600-008-0019-9, 2009.

Usoskin, I. G., Kovaltsov, G. A., and Mironova, I. A.: Cosmic ray induced ionization model CRAC:CRII: An extension to the upper atmosphere, J. Geophys. Res., 115, D10302, 2010.

Usoskin, I. G., Bazilevskaya, G. A., and Kovaltsov, G. A.: Solar modulation parameter for cosmic rays since 1936 reconstructed from ground-based neutron monitors and ionization chambers, J. Geophys. Res., 116, A02104, doi:10.1029/2010JA016105, 2011.

Usoskin, I. G., Hulot, G., Gallet, Y., Roth, R., Licht, A., Joos, F., Kovaltsov, G. A., Thébault, E., and Khokhlov, A.: Evidence for distinct modes of solar activity, Astronomy & Astrophysics, 562, L10, doi:10.1051/0004-6361/201423391, 2014.

Van Allen, J. A. and Frank, L. A.: Radiation Around the Earth to a Radial Distance of 107,400 km, Nature, 183, 430–434, doi:10.1038/183430a0, 1959.

van de Kamp, M., Seppälä, A., Clilverd, M. A., Rodger, C. J., Verronen, P. T., and Whittaker, I. C.: A model providing long-term datasets of energetic electron precipitation during geomagnetic storms, J. Geophys. Res. Atmos., in press, 2015JD024212, 2016.

Verronen, P. T. and Lehmann, R.: Analysis and parameterisation of ionic reactions affecting middle atmospheric HO_x and NO_y during solar proton events, Ann. Geophys., 31, 909–956, doi:10.5194/angeo-31-909-2013, 2013.

Verronen, P. T., Seppälä, A., Kyrölä, E., Tamminen, J., Pickett, H. M., and Turunen, E.: Production of odd hydrogen in the mesosphere during the January 2005 solar proton event, Geophys. Res. Lett., 33, L24811, doi:10.1029/2006GL028115, 2006.

Verronen, P. T., Funke, B., López-Puertas, M., Stiller, G. P., von Clarmann, T., Enell, C.-F., Turunen, E., and Tamminen, J.: About the Increase of HNO_3 in the Stratopause Region During the Halloween 2003 Solar Proton Event, Geophys. Res. Lett., 35, L20809, doi:10.1029/2008GL035312, 2008.

Verronen, P. T., Santee, M. L., Manney, G. L., Lehmann, R., Salmi, S.-M., and Seppälä, A.: Nitric acid enhancements in the mesosphere during the January 2005 and December 2006 solar proton events, J. Geophys. Res., 116, D17 301, doi:10.1029/2011JD016075, 2011a.

Verronen, P. T., Rodger, C. J., Clilverd, M. A., and Wang, S.: First evidence of mesospheric hydroxyl response to electron precipitation from the radiation belts, J. Geophys. Res., 116, D07 307, doi:10.1029/2010JD014965, 2011b.

Vieira, L. E. A. and Solanki, S. K.: Evolution of the solar magnetic flux on time scales of years to millenia, Astronomy & Astrophysics, 509, A100, doi:10.1051/0004-6361/200913276, 2010.

Vieira, L. E. A., Solanki, S. K., Krivova, N. A., and Usoskin, I.: Evolution of the solar irradiance during the Holocene, Astronomy & Astrophysics, 531, A6, doi:10.1051/0004-6361/201015843, 2011.

Viereck, R., Puga, L., McMullin, D., Judge, D., Weber, M., and Tobiska, W. K.: The Mg II index: A proxy for solar EUV, Geophysical Research Letters, 28, 1343–1346, doi:10.1029/2000GL012551, 2001.

Vitt, F. M. and Jackman, C. H.: A comparison of sources of odd nitrogen production from 1974 through 1993 in the Earth's middle atmosphere as calculated using a two-dimensional model, J. Geophys. Res., 101, 6729–6739, 1996.

von Clarmann, T., Glatthor, N., Höpfner, M., Kellmann, S., Ruhnke, R., Stiller, G. P., Fischer, H., Funke, B., Gil-López, S., and López-Puertas, M.: Experimental Evidence of Perturbed Odd Hydrogen and Chlorine Chemistry After the October 2003 Solar Proton Events, J. Geophys. Res., 110, A09S45, doi:10.1029/2005JA011053, 2005.

von Clarmann, T., Funke, B., López-Puertas, M., Kellmann, S., Linden, A., Stiller, G. P., Jackman, C. H., and Harvey, V. L.: The Solar Proton Events in 2012 as Observed by MIPAS, Geophys. Res. Lett., 40, 1–5, doi:10.1002/grl.50119, 2013.

Wang, Y.-M., Lean, J. L., and Sheeley, Jr., N. R.: Modeling the Sun's Magnetic Field and Irradiance since 1713, The Astrophysical Journal, 625, 522–538, doi:10.1086/429689, 2005.

Watkins, N. W., Credgington, D., Hnat, B., Chapman, S. C., Freeman, M. P., and Greenhough, J.: Towards Synthesis of Solar Wind and Geomagnetic Scaling Exponents: A Fractional Lévy Motion Model, Space Science Reviews, 121, 271–284, doi:10.1007/s11214-006-4578-2, 2005.

Weeks, L. H., Cuikay, R. S., and Corbin, J. R.: Ozone Measurements in the Mesosphere During The Solar Proton Event of 2 November 1969., Journal of Atmospheric Sciences, 29, 1138–1142, doi:10.1175/1520-0469(1972)029<1138:OMITMD>2.0.CO;2, 1972.

Wenzler, T., Solanki, S. K., and Krivova, N. A.: Can surface magnetic fields reproduce solar irradiance variations in cycles 22 and 23?, Astronomy & Astrophysics, 432, 1057–1061, doi:10.1051/0004-6361:20041956, 2005.

Whittaker, I. C., Gamble, R. J., Rodger, C. J., Clilverd, M. A., and Sauvaud, J.-A.: Determining the spectra of radiation belt electron losses: Fitting DEMETER electron flux observations for typical and storm times, J. Geophys. Res. (Space Physics), 118, 7611–7623, doi:10.1002/2013JA019228, 2013.

Whittaker, I. C., Clilverd, M. A., and Rodger, C. J.: Characteristics of precipitating energetic electron fluxes relative to the plasmapause during geomagnetic storms, J. Geophys. Res. (Space Physics), 119, 8784–8800, doi:10.1002/2014JA020446, 2014a.

Whittaker, I. C., Rodger, C. J., Clilverd, M. A., and Sauvaud, J.-A.: The effects and correction of the geometric factor for the POES/MEPED electron flux instrument using a multisatellite comparison, J. Geophys. Res. (Space Physics), 119, 6386–6404, doi:10.1002/2014JA020021, 2014b.

Winkler, H., Kazeminejad, S., Sinnhuber, M., Kallenrode, M.-B., and Notholt, J.: Conversion of mesospheric HCl into active chlorine during the solar proton event in July 2000 in the northern polar region, J. Geophys. Res., 114, D00I03, doi:10.1029/2008JD011587, 2009.

Woods, T. N., Tobiska, W. K., Rottman, G. J., and Worden, J. R.: Improved solar Lyman α irradiance modeling from 1947 through 1999 based on UARS observations, J. Geophys. Res., 105, 27 195–27 216, doi:10.1029/2000JA000051, 2000.

Woods, T. N., Eparvier, F. G., Bailey, S. M., Chamberlin, P. C., Lean, J., Rottman, G. J., Solomon, S. C., Tobiska, W. K., and Woodraska, D. L.: Solar EUV Experiment (SEE): Mission overview and first results, Journal of Geophysical Research (Space Physics), 110, A01 312, doi:10.1029/2004JA010765, 2005.

Woollings, T., Lockwood, M., Masato, G., Bell, C., and Gray, L.: Enhanced signature of solar variability in Eurasian winter climate, Geophys. Res. Lett., 37, doi:10.1029/2010GL044601, 2010.

Yando, K., Millan, R. M., Green, J. C., and Evans, D. S.: A Monte Carlo simulation of the NOAA POES Medium Energy Proton and Electron Detector instrument, J. Geophys. Res., 116, A10 231, doi:10.1029/2011JA016671, 2011.

Yeo, K. L., Krivova, N. A., Solanki, S. K., and Glassmeier, K. H.: Reconstruction of total and spectral solar irradiance from 1974 to 2013 based on KPVT, SoHO/MDI and SDO/HMI observations, Astronomy & Astrophysics, 570, doi:10.1051/0004-6361/201423628, 2014.

Yeo, K. L., Ball, W. T., Krivova, N. A., Solanki, S. K., Unruh, Y. C., and Morrill, J.: UV solar irradiance in observations and the NRLSSI and SATIRE-S models, J. Geophys. Res., 120, 6055–6070, doi:10.1002/2015JA021277, 2015.

Zadorozhny, A., Tuchkov, G., Kikhtenko, V., Laštovička, J., Boška, J., and Novák, A.: Nitric oxide and lower ionosphere quantities during solar particle events of October 1989 after rocket and ground-based measurements, Journal of Atmospheric and Terrestrial Physics, 54, 183 – 192, doi:http://dx.doi.org/10.1016/0021-9169(92)90127-7, 1992.

Zadorozhny, A. M., Kikhtenko, V. N., Kokin, G. A., Tuchkov, G. A., Tyutin, A. A., Chizhov, A. F., and Shtirkov, O. V.: Middle atmosphere response to the solar proton events of October 1989 using the results of rocket measurements, J. Geophys. Res., 99, 21 059–21 069, doi:10.1029/93JD03194, 1994.